Alma Mater Studiorum – Università di Bologna

DOTTORATO DI RICERCA IN

SCIENZE BIOMEDICHE

PROGETTO FORMATIVO IN NEUROFISIOLOGIA

Ciclo XXV

Settore Concorsuale di afferenza: 05/D1

Settore Scientifico disciplinare: BIO/09

INFLUENCE OF ELECTROMAGNETIC FIELDS ON BIOLOGICAL SIGNALLING: AN EXPERIMENTAL AND THEORETICAL APPROACH

Presentata da: David John Muehsam

Coordinatore **Relatore**

Prof. Claudio Galletti **Prof. Giorgio Aicardi**

Esame finale anno 2013

ACKNOWLEDGMENTS

I would like to offer my heartfelt thanks to all who assisted me in this project. To Arthur Pilla, for believing in me, and for the constant support he has selflessly given, I am forever indebted. I offer a debt of thanks to Parviz Lalezari, Rukmani Lekhraj, and Diana Casper, who gave me invaluable instruction in many laboratory techniques, and provided guidance and inspiration throughout this study. I wish to express my gratitude to my professors at the University of Bologna, Marina Marini, Ferdinando Bersani and Giorgio Aicardi, for their wisdom, kindness, friendship and support throughout this study, and to Camille Roche, Provvidenza Abruzzo, Alessandra Bolotta, Christine Grossjohan and Rosaria Russo, for assistance without which I could not have completed this study. I also wish to express my deepest thanks to Diana Casper, Joel Friedman, Astrid Sasse, Marina Marini, Michele Samaja, Luca Sangiorgio, and Alessandro Parra, for opening their laboratories for my use, and for their continued interest in the research we performed. I also wish to acknowledge the late Alessandro Chiabrera, whose works on the Lorentz Model are the shoulders upon which I stand, and to give thanks to him for many lively conversations which provided direction and inspiration as I set out upon this path.

My deepest gratitude goes out to my mother, Diana, and my sister, Trish for their continual support and unconditional love, which has always given me a sense of home.

TABLE OF CONTENTS

1. SUMMARY OF THE STUDY

Biological interactions due to electromagnetic fields (EMF) have been reported over nearly the entire range of frequencies, field strengths and amplitudes occurring in the natural and man-made environments, and it is certain that the wide range of biological effects observed is governed by a variety of distinct mechanisms [Funk et al., 2009]. Environmental exposure to a wide range of EMFs has increased substantially in recent years, motivating a large and growing body of research. Questions regarding the health effects of power line fields oscillating at 50-60 Hz with amplitudes in the mT range were raised more than 30 years ago [Wertheimer et al., 1979]. Although the present controversy over GSM mobile phone exposure and cancer is ongoing [Kundi, 2009], public health concerns are reflected by the recent classification (31 May, 2011) by the International Agency for Research on Cancer of radiofrequency EMFs from mobile phone use as possibly carcinogenic to humans. Of particular interest to neuroscience is the possibility of EMF effects on neural functioning and neurodegenerative diseases [Cook et al., 2002, 2006; Consales et al, 2012], and a recent conference, *Neurodegenerative Diseases and ELF & RF EMF Exposure,* hosted by the Italian National Agency for New Technologies, Energy and Sustainable Economic Development (Berlin, 20th-21st September 2011), helped to establish strategies for *in vitro* and *in vivo* research. Ongoing concerns regarding health risks of EMF exposure led to the release of the *BioInitiative Report, A Rationale for a Biologically-based Public Exposure Standard for Electromagnetic Fields (ELF and RF)* [published online: www.bioinitiative.org, 31 August, 2007]. This 610-page report was written by 14 prominent scientists, public health and public policy experts to document the scientific evidence on health effects of electromagnetic fields and subjected to review by another dozen outside reviewers. The BioInititative Report provides a review of bioeffects and reports of health risks occurring at very low exposure levels (non-thermal levels of extremely low frequency (ELF) and radiofrequency EMF and has made several recommendations urging the immediate reduction of current public exposure limits. However, in contrast to public alarm regarding long-term hazards, a body

of double-blind placebo-controlled studies report therapeutic effects for a variety of types of short-term EMF exposures [Pilla, 2006] and these modalities are approved for clinical use to reduce pain and edema, and enhance bone and wound repair. Also, recent studies have reported GSM treatment to be neuroprotective and to reverse cognitive impairment in an Alzheimer's disease mouse model [Arendash et al., 2010, 2012].

Although the discussion regarding health risks and benefits is ongoing, it is clear that neurological effects due to a wide range of subthreshold EMFs do in fact occur [Cook et al., 2002, 2006], and that further research is required to establish the mechanisms of action, and to assess safety and potential harm. Reports of EMFs bioeffects of particular interest to the neurosciences include brain cancers [Repacholi et al., 2012], oxidative stress and neurodegeneration [Consales et al., 2012], the effects of radiofrequency fields [van Rongen et al., 2009], cognitive effects [Cook et al., 2002, 2006] and psychotherapeutic potential [Pooley, 2010]. While reports of both injurious and therapeutic EMF bioefects continues to accrue, uncertainty remains regarding the basic mechanism of many of the above observed effects. Some bioeffects due to microwave and radiofrequency exposures can be directly attributed to EMF-induced heating of biological tissues [Lin, 2004, Chou, 2006], and a large body of evidence has conclusively demonstrated that also nonthermal EMFs, which can be shown to produce no heating of the biological target, have a variety of biological effects [Funk et al., 2009]. One promising line of research has been motivated by *in vitro* evidence suggesting pathways mediated by ion binding as common targets using nonthermal EMF signals. Nonthermal bioeffects on ion binding systems have been demonstrated using a variety of EMF configurations. Among these are: static (DC) and extremely low frequency (ELF) alternating (AC) magnetic fields, configured such that heating due to the induced electric field is negligible, and radiofrequency fields configured using pulse-modulation techniques to yield with low duty cycles and negligible levels of heating. The first speculations that ion and ligand binding may serve as the primary transduction pathways for DC and

ELF magnetic field effects were suggested by observations of effects on Ca^{2+} binding and efflux [Bawin et al., 1975, 1976; Blackman et al. 1982]. Subsequent studies on Ca^{2+}-calmodulin (CaM)-dependent phosphodiesterase [Bull et al., 1993, Liboff et al., 2003] and myosin phosphorylation [Shuvalova et al., 1991; Markov et al., 1992, 1994, 1997] suggested sensitivity to static and time-varying magnetic fields and also to pulse-modulated radiofrequency (PRF) signals. A report of Ca^{2+}-dependence of these effects further suggested Ca^{2+}/CaM binding as a possible primary EMF transduction pathway [Markov et al., 1997]. In the light of this experimental evidence, several of my previous biophysical models [Muehsam et al., 1994, 1996, 1999, 2009a, 2009b] and collaborations [Pilla et al., 2011] were concerned primarily with the mechanisms of action of EMFs on ion binding pathways.

The primary goals of this study were to develop a neurologically-relevant cell-free in vitro assay for the assessment of nonthermal EMF bioeffects and to develop theoretical models in accord with current experimental observations. A Ca^{2+}/CaM-dependent nitric oxide (NO) synthesis assay was developed to assess the effects of a pulsed radiofrequency (PRF) signal [Muehsam et al., 2012a], based upon previous the hypotheses [Muehsam et al., 1994, 1996, 1999, 2009a, 2009b; Pilla et al., 2006] that EMF effects operate by modulating Ca^{2+} binding to CaM, and thus are observable only when the free cytosolic Ca^{2+} concentration is rate determining. NO synthesis was quantified using the Hb assay [Hevel et al., 1994]. The effects of PRF on Ca^{2+}/CaM binding were also assessed directly, using a Ca^{2+}-selective electrode. No effects of PRF were observed in either of these studies. The results of the NO assay do not support the hypothesis that EMF acts directly upon Ca^{2+}/CaM binding to modulate the activity of the NOS enzyme. Trials using a Ca^{2+}-sensitive electrode do not support the notion that EMF acts upon Ca^{2+}/CaM binding under equilibrium conditions. However, in the former trials, the observation of a PRF effect on the interaction of Hb with tetrahydrobiopterin led to the development of an *in vitro* cell-free human Hb deoxygenation assay [Muehsam et al., 2012b, 2012c, 2012d] that showed a

reduction in the rate of Hb deoxygenation for exposures to both PRF and a static magnetic field (SMF), occurring from several minutes to hours after fields were removed. Structural studies were conducted to assess the effects of EMF on Hb using pyranine fluorescence, Gd^{3+} vibronic sideband luminescence and attenuated total reflectance Fourier transform infrared (ATR-FTIR) spectroscopy. Structural studies showed no definitive changes in protein structure, suggesting the necessity of developing a real-time instrumentation to assess the submolecular causes for the EMF effects observed. Also, the effect of SMF on Hb oxygen saturation (SO2) was assessed under gas-controlled conditions, with results suggesting that the SMF does not directly remove oxygen under equilibrium conditions. Theoretical models were developed treating EMF primary transduction and effects on ion binding, protein hydration, neuronal spike timing, membrane potential, and molecular dynamics of Hb deoxygenation.

The EMF sensitivity and biochemical simplicity of the Hb deoxygenation assay developed here suggest a new tool that may help to further establish basic biophysical EMF transduction mechanisms. The EMF effects observed are robust and were repeated in NY and Bologna using human Hb from different stocks. To my knowledge, this is the first report showing that a PRF signal, and independently, a SMF could affect similar outcomes in the same *in vitro* biological system, in the same study. Enhanced delivery of oxygen has been shown to reduce inflammation [Bitterman, 2007] and enhance tissue repair [Tandara et al., 2004] and at least one trial has reported an EMF-induced increase in deoxyHb in an *in vivo* animal model [Milweski, 2006]. Allosteric modification of Hb has been suggested as a clinically useful means of enhancing oxygen delivery [Papassotiriou et al., 1998], and is in development for *in vivo* treatment of ischemia from stroke, cardiac disease and diabetic ulcers [Najjar et al., 2005]. Well-known interactions of NO with hemoprotein transition metals [Ignarro et al., 1986; Thomas et al., 2003; Bonaventura et al., 2001] and recent results clearly demonstrating regulation by endothelial Hb alpha of the action of NO on vascular reactivity at the myeloendothelial junction [Straub et al., 2012] and the *in vivo*

modulation of Hb oxygen affinity by NO synthase activity [Zinchuk, 1999] may also suggest that the molecular dynamics exhibited by neuroglobin and other hemoproteins [Frauenfelder et al., 2009] play an important role in EMF-mediated regulation and maintenance of biological growth and repair processes. Although much further work is required to ascertain the clinical relevance of the results reported here, if an EMF-induced increase in the rate of deoxygenation can be demonstrated *in vivo*, then a resulting enhancement of oxygen delivery may be an important non-invasive, non-pharmacologic therapeutic method by which clinically relevant EMF-mediated enhancement of growth and repair processes can occur.

EMF Exposures

The EMF exposures used for all the experiments described here were chosen for their reported therapeutic efficacy. PRF signals and SMFs have been employed in a variety of therapeutically relevant settings. For example, variants of the PRF signal employed in the this study, and currently in clinical use for the treatment of pain and edema, have been shown to: accelerate growth factor production in tissue repair [Aaron et al., 2004]; increase neovascularization and enhance skin flap survival [Roland et al., 2000; Weber et al., 2004]; modulate anti-CD3 binding at lymphocyte receptors [Nindl et al., 1997]; accelerate wound repair [Strauch et al., 2007]; accelerate Achilles' tendon repair [Strauch et al., 2006]; reduce inflammation and post-operative pain [Heden et al., 2008; Rhode et al., 2010]; and enhance chronic wound repair [Kloth et al., 1999]. Reports of therapeutically relevant effects of magnetic fields include modulation of calmodulin-dependent mysosin phosphorylation [Markov et la., 1997] and cyclic nucleotide phosphodiesterase activity [Liboff et al., 2003]; changes in the dielectric properties of solutions [Jones et al., 1987]; increases in neurite outgrowth in embryonic chick ganglia [McDonald 1993]; changes in morphology of rat tendon fibroblasts [Blumenthal et al., 1997]; blockage of action potentials in cultured neurons [McLean et al., 1995; Cavapol et al., 1995]; enhancement of cutaneous

microcirculation in a rabbit model [Ohkubo et al., 1997; Okano et al., 1999] and enhancement of wound healing in rats [Henry et al., 2008; Patiño et al., 1996]. SMF exposures have been shown to produce, in *in vivo*, double-blind studies: reduction in discoloration, edema and pain post suction lipectomy [Man et al., 1999]; reduction in fibromyalgia pain and sleep disorders [Colbert et al., 1999; Alfano et al., 2001]; reduction in chronic pelvic pain [Brown et al., 2002]; relief from pain, numbness and tingling due to diabetic peripheral neuropathy [Weintraub, 1999; Weintraub et al., 2003]; and reduction in post-polio pain [Valbona et al., 1997]. Other trials demonstrated no effects on foot [Caselli et al., 1997; Winemiller et al., 2003], and chronic back pain [Collacott et al., 2000], although the latter two trials employed magnets in bipolar configuration, resulting in lower amplitude inside the target as compared to unipolar configuration.

The 27.12 MHz PRF signal employed in these studies was transmitted in 4 ms bursts, repeating at 5 Hz, 10 μT peak amplitude (Ivivi Health Sciences, USA), and is currently approved by the US FDA for clinical use for treatment of pain and edema, and by reimbursed Medicare for treatment of chronic wound. The PRF signal was delivered with a 20 cm circular single turn antenna (coil). This resulted in a mean induced electric field of 3 ± 1 V/m in the sample. PRF field parameters were assessed and verified for each experiment using a calibrated field probe (model FCC-301-1-MR1, Fischer Custom Communications, Torrance, CA) connected to a calibrated 100-MHz oscilloscope (model 2358, Tektronix, Beaverton, OR). All components of this PRF transmitter were previously mapped by me at 1-2 mm resolution in order to fulfill the requirements of the US FDA for approval for clinical use. The static magnetic field employed in these studies (SMF, 150 - 186 mT) was delivered using circular permanent ceramic magnets 3.8 cm in diameter and 1.3 cm thick, intended for therapeutic applications (Magnetherapy, West Palm Beach, FL, USA). The SMF amplitude was assessed and verified for each experiment using a digital magnetometer (model TM-401, Kanatec, Tokyo, Japan). All biological samples were exposed to the ambient magnetic field, which was measured using a digital Gauss/Tesla meter (model

7010, F.W. Bell, USA) to be 40.5 ± 2 μT, 59 degrees from horizontal (vertical component = 34.7 ± 2 μT, horizontal component = 21.0 ± 2μT). Temperature variation between exposed and control samples was less than ± 0.1° C [Fisher AB15 BioBasic, USA].

REFERENCES

Aaron RK, Boyan BD, Ciombor D, Schwartz Z, Simon BJ. 2004. Stimulation of growth factor synthesis by electric and electro-magnetic fields. Clin Orthop 419:30–37.

Alfano AP, Taylor AG, Foresman PA, Dunkl PR, McConnell GG, Conaway MR, Gillies GT. 2001. Static Magnetic Fields for Treatment of Fibromyalgia: A Randomized Controlled Trial. J Altern Complement Med. 7(1):53-64.

Arendash GW, Sanchez-Ramos J, Mori T, Mamcarz M, Lin X, Runfeldt M, Wang L, Zhang G, Sava V, Tan J, Cao C. 2010. Electromagnetic field treatment protects against and reverses cognitive impairment in Alzheimer's disease mice. J Alzheimers Dis. 19(1):191-210.

Arendash GW, Mori T, Dorsey M, Gonzalez R, Tajiri N, Borlongan C. 2012. Electromagnetic treatment to old Alzheimer's mice reverses β-amyloid deposition, modifies cerebral blood flow, and provides selected cognitive benefit. PLoS One. 7(4):e35751.

Bawin SM, Adey WR 1976. Sensitivity of calcium binding in cerebral tissue to weak environmental electric fields oscillating at low frequency. Proc Natl Acad Sci USA 73:1999-2003.

Bawin SM, Kaczmarek LK, Adey WR. 1975. Effects of modulated VHF fields on the central nervous system. Ann NY Acad Sci 247: 74– 81.

Bitterman H. Oxygen: An Anti-Inflammatory Drug. Isr Med Assoc J. 9 (2007) 874-876.

Blackman CF, Benane SG, Kinney LS, Joines WT, House DE. 1982. Effects of ELF fields on calcium-ion efflux from brain tissue in vitro. Radiat Res 92: 510–520.

Blumenthal NC, Ricci J, Breger L, Zychlinsky A, Solomon H, Chen GG, Kuznetsov D, Dorfman R. 1997. Effects of low intensity AC and/or DC electromagnetic fields on cell attachment and induction of apoptosis. Bioelectromagnetics 18(3):264-272.

Bonaventura J, Lance VP. 2001. Nitric Oxide, Invertebrates and Hemoglobin. American Zoologist. 41:346–359.

Brown CS, Ling FW, Wan JY, Pilla AA, 2002. Efficacy of Static Magnetic Field Therapy in Chronic Pelvic Pain: A Double-Blind Pilot Study. Am J Obs Gyn, 187:1581-7.

Bull AW, Chemg KA, Jenrow KA, Liboff AR. 1993. Weak magnetostatic fields alter calmodulin-dependent cyclic nucleotide phosphodiesterase activity. In Electricity and Magnetism in Biology and Medicine. M. Blank, editor. San Francisco Press, Inc., San Francisco. 319-322.

Caselli MA, Clark N, Lazarus S, Velez Z, Venegas L. 1997. Evaluation of magnetic foil and PPT Insoles in the treatment of heel pain. Journal of the American Podiatric Medical Association 87:11-16.

Cavapol AV, Wamil AW, Holcomb RR, McLean MJ.1995. Measurement and analysis of static magnetic fields that block action potentials in cultured neurons. Bioelectromagnetics 16(3):197-206.

Chou C. 2006. Therapeutic Heating Applications of Radio Frequency Energy. in: Barnes F, Greenebaum B editors. Biological and Medical Aspects of Electromagnetic Fields. Boca Raton, CRC Press. pp. 414-425.

Colbert AP, Markov MS, Banerij M, Pilla AA. 1999. Magnetic mattress pad use in patients with fibromyalgia: A randomized double-blind pilot study. J Back Musculoskeletal Rehab. 13:19-31.

Collacott EA, Zimmerman JT, White DW, Rindone JP. 2000. Bipolar permanent magnets for the treatment of chronic low back pain. JAMA 283:1322-1325.

Consales C, Merla C, Marino C, Benassi B. 2012. Electromagnetic fields, oxidative stress, and neurodegeneration. Int J Cell Biol. 683897. Epub 2012 Sep 9.

Cook CM, Thomas AW, Prato FS. 2002. Human electrophysiological and cognitive effects of exposure to ELF magnetic and ELF modulated RF and microwave fields: a review of recent studies. Bioelectromagnetics. 23(2):144-57.

Cook CM, Saucier DM, Thomas AW, Prato FS. 2006. Exposure to ELF magnetic and ELF-modulated radiofrequency fields: the time course of physiological and cognitive effects observed in recent studies (2001-2005). Bioelectromagnetics. 27(8):613-27.

Frauenfelder H, Chen G, Berendzen J, Fenimore PW, Jansson H, McMahon BH, Stroe IR, Swenson J, Young RD. 2009. A unified model of protein dynamics. Proc Natl Acad Sci USA. 106(13):5129-34.

Heden P, Pilla A. 2008. Effects of Pulsed Electromagnetic Fields on Postoperative Pain: A Double-Blind Randomized Pilot Study in Breast Augmentation Patients. Aesthetic Plast Surg. 32(4):660-666.

Henry SL, Concannon MJ, Yee GJ. 2008. The effect of magnetic fields on wound healing: experimental study and review of the literature. Eplasty 8:393-399.

Hevel JM, Marletta MA. 1994. Nitric-oxide synthase assays. Methods Enzymol. 233:250-258.

Ignarro LJ, Adams JB, Horwitz PM, Wood KS. 1986. Activation of soluble guanylate cyclase by NO-hemoproteins involves NO-heme exchange. Comparison of heme-containing and heme-deficient enzyme forms. J Biol Chem. 261(11):4997-5002.

Jones DB, Ryaby JT. 1987. Low energy time varying electromagnetic field interactions with cellular control mechanisms. In: Blank M, Findl E, editors. Mechanistic approaches to interactions of electric and electromagnetic fields with living systems. New York: Plenum Press. pp. 389-97.

Kloth LC, Berman JE, Sutton CH, Jeutter DC, Pilla AA, Epner ME. 1999. Effect of Pulsed Radio Frequency Stimulation on Wound Healing: A Double-Blind Pilot Clinical Study. In Bersani F, editor. Electricity and Magnetism in Biology and Medicine. New York: Plenum. pp. 875-878.

Kundi M. 2009. The controversy about a possible relationship between mobile phone use and cancer. Environ Health Perspect. 117(3):316-24.

Liboff AR, Cherng S, Jenrow KA, Bull A. 2003. Calmodulin-Dependent Cyclic Nucleotide Phosphodiesterase Activity is Altered by 20 μT Magnetostatic Fields. Bioelectromagnetics, 24(1):32-38.

Lin JC. 2004. Studies on microwaves in medicine and biology: From snails to humans. Bioelectromagnetics 25:146-159.

Man D, Man B, Plosker H. 1999. The influence of permanent magnetic field therapy on wound healing in suction lipectomy patients: A double-blind study. Plastic and Reconstructive Surgery 104: 2261-2296.

Markov MS, Muehsam DJ, Pilla AA. 1994. Modulation of Cell-Free Myosin Phosphorylation with Pulsed Radio Frequency Electromagnetic Fields, In: Allen MJ, Cleary SF, Sowers AE, (Eds.) Charge and Field Effects in Biosystems 4. NJ: World Scientific, pp. 274-88.

Markov MS, Pilla AA. 1997. Weak static magnetic field modulation of myosin phosphorylation in a cell-free preparation: Calcium dependence. Bioelectrochem Bioenerg 43: 235–240.

Markov MS, Ryaby JT, Kaufman JJ, Pilla AA. 1992. Extremely weak AC and DC magnetic fields significantly affect myosin phosphorylation. In: Allen MJ, Cleary SF, Sowers AE, Shillady DD (Eds.) Charge and Field effects in biosystems 3, Boston: Birkhauser, pp. 225-230.

Markov MS, Wang S, Pilla AA. 1993. Effects of weak low frequency sinusoidal and DC magnetic fields on myosin phosphorylation in a cell-free preparation. Bioelectrochem Bioenergetics 30:119-125.

McDonald F. 1993. Effect of static magnetic fields on osteoblasts and fibroblasts in-vitro. Bioelectomagnetics, 14(3):187-96.

McLean MJ, Holcomb RR, Wamil AW, Pickett JD, Cavapol AV. 1995. Blockade of sensory neuron action potentials by a static magnetic field in the 10 mT range. Bioelectromagnetics 16(1):20-32.

Milweski S, Szczepański W. Effects of electromagnetic fields on the meat performance and wool performance of sheep Arch. Tierz., Dummerstorf 49(Special Issue) (2006) 219-225.

Muehsam D, Pilla A. 1994. Weak Magnetic Field Modulation of Ion Dynamics in a Potential Well: Mechanistic and Thermal Noise Considerations. Bioelectrochemistry and Bioenergetics 35:71-79.

Muehsam DJ, Pilla AA. 1996. Lorentz Approach to Static Magnetic Field Effects on Bound Ion Dynamics and Binding Kinetics: Thermal Noise Considerations. Bioelectromagnetics 17:89-99.

Muehsam DJ et al., Pilla AA. 1999. The Sensitivity of Cells and Tissues to Exogenous Fields: Dependence Upon Target System Initial State, in "Electricity and Magnetism in Biology and Medicine", Bersani F, ed, Plenum, New York, pp. 405-408.

Muehsam DJ, Pilla AA. 2009a. A Lorentz Model for Weak Magnetic Field Bioeffects: Part I -Thermal Noise Is an Essential Component of AC/DC Effects on Bound Ion Trajectory. Bioelectromagnetics. 30:462-475.

Muehsam DJ, Pilla AA. 2009b. A Lorentz Model for Weak Magnetic Field Bioeffects: Part II – Secondary Transduction Mechanisms and Measures of Reactivity. Bioelectromagnetics. 30:476-488.

Muehsam D, Lalezari P, Lekhraj R, Aicardi G, Casper D. 2012a. Effect of a pulsed radiofrequency electromagnetic field on in vitro cell-free nitric oxide synthesis. Proceedings, National Conference ICEmB, Bologna, Italy, 27-29 June.

Muehsam D, Lalezari P, Lekhraj R, Aicardi G, Casper D. 2012b. Non-thermal electromagnetic fields increase rate of hemoglobin deoxygenation in a cell-free preparation. Proceedings, National Conference ICEmB, Bologna, Italy, 27-29 June.

Muehsam D, Lalezari P, Lekhraj R, Aicardi G, Pilla A, Diana Casper. 2012c. Non-thermal electromagnetic fields increase rate of hemoglobin deoxygenation in a cell-free preparation. Proceedings, Bioelectromagnetics Society 34th Annual Meeting, Brisbane, Australia, 17-22 June.

Muehsam D, Lalezari P, Lekhraj R, Abruzzo P, Bolotta A, Marini M, Bersani F, Aicardi G, Pilla A, Diana Casper. 2013. Non-thermal radio frequency and static magnetic fields increase rate of hemoglobin deoxygenation in a cell-free preparation. PLoS ONE 8(4): e61752. doi:10.1371/journal.pone.0061752.

Najjar SS, Bottomley PA, Schulman SP, Waldron MM, Steffen RP, Gerstenblith G, Weiss RG. Effects of a pharmacologically-induced shift of hemoglobin-oxygen dissociation on myocardial energetics during ischemia in patients with coronary artery disease. J Cardiovasc Magn Reson. 7 2005 657-666.

Nindl G, Swezb JA, Millera JM, Balcavage WX. 1997. Growth stage dependent effects of electromagnetic fields on DNA synthesis of Jurkat cells. FEBS Lett. 414:501–506.

Ohkubo C, Xu S. 1997. Acute effects of static magnetic fields on cutaneous microcirculation in rabbits. In Vivo 11(3):221-226.

Okano H, Gmitrov J, Ohkubo C. 1999. Biphasic effects of static magnetic fields on cutaneous microcirculation in rabbits. Bioelectromagnetics 20(3):161-171.

Papassotiriou I, Kister J, Griffon N, Stamoulakatou A, Abraham DJ Modulating the oxygen affinity of human fetal haemoglobin with synthetic allosteric modulators. Br J Haematol. 102 (1998) 1165-1171.

Patiño O, Grana D, Bolgiani A, Prezzavento G, Merlo A. 1996. Effect of magnetic fields on skin wound healing. Experimental study. Medicina (B Aires) 56(1):41-4.

Pilla AA. 2006. Mechanisms and therapeutic applications of time varying and static magnetic fields, in: Barnes F, Greenebaum B editors. Biological and Medical Aspects of Electromagnetic Fields. Boca Raton, CRC Press. pp. 351–411.

Pilla AA, Fitzsimmons R, Muehsam DJ, Wu J, Rohde C, Casper D. 2011. Electromagnetic fields as first messenger in biological signaling: application to calmodulin-dependent signaling in tissue repair. Biochimica et Biophysica Acta 1810:1236–1245.

Repacholi MH, Lerchl A, Röösli M, Sienkiewicz Z, Auvinen A, Breckenkamp J, d'Inzeo G, Elliott P, Frei P, Heinrich S, Lagroye I, Lahkola A, McCormick DL, Thomas S, Vecchia P. 2012. Systematic review of wireless phone use and brain cancer and other head tumors. Bioelectromagnetics. 2012 33(3):187-206.

Rhode C, Chiang A, Adipoju O, Casper D, Pilla AA. 2010. Effects of pulsed electromagnetic fields on interleukin-1 beta and postoperative pain: a double-blind, placebo-controlled, pilot study in breast reduction patients. Plast Reconstr Surg 125(6):1620-1629.

Roland D, Ferder M, Kothuru R, Faierman T, Strauch B. 2000. Effects of pulsed magnetic energy on a microsurgically transferred vessel. Plast Reconstr Surg 105:1371–1374.

Shuvalova LA, Ostrovskaia MV, Sosunov EA, Lednev VV. 1991. Influence of a weak magnetic field under conditions of parametric resonance on the rate of calmodulin-dependent phosphorylation of myosin in solution. Proc Natl Acad Sci USSR (Biophysics) 317: 227–230 (in Russian).

Straub AC, Lohman AW, Billaud M, Johnstone SR, Dwyer ST, Lee MY, Bortz PS, Best AK, Columbus L, Gaston B, Isakson BE. 2012. Endothelial cell expression of haemoglobin α regulates nitric oxide signalling. Nature 491:473–477.

Strauch B, Patel MK, Navarro A, Berdischevsky M, Pilla AA. 2007. Pulsed magnetic fields accelerate wound repair in a cutaneous wound model in the rat. Plast Reconstr Surg 120:425–430.

Strauch B, Patel MK, Rosen DJ, Mahadevia S, Brindzei N, Pilla AA. 2006. Pulsed magnetic field therapy increases tensile strength in a rat Achilles' tendon repair model. J Hand Surg Am. 31:1131–1135.

Tandara AA, Mustoe TA. Oxygen in wound healing--more than a nutrient. World J Surg. 28 (2004) 294-300.

Thomas DD, Miranda KM, Colton CA, Citrin D, Espey MG, Wink DA. 2003. Heme proteins and nitric oxide (NO): the neglected, eloquent chemistry in NO redox signaling and regulation. Antioxid Redox Signal. 5(3)307-17.

Valbona, C., Hazlewood, C.F., Jurida, G., 1997. Response of pain to static magnetic fields in post-polio patients: A double-blind pilot study. Arch. Phys. Med. Rehabil., 78: 1200.

Van Rongen E, Croft R, Juutilainen J, Lagroye I, Miyakoshi J, Saunders R, de Seze R, Tenforde T, Verschaeve L, Veyret B, Xu Z. 2009. Effects of radiofrequency electromagnetic fields on the human nervous system. J Toxicol Environ Health B Crit Rev. 2009 Oct;12(8):572-97.

Weber RV, Navarro A, Wu JK, Yu HL, Strauch B. 2004. Pulsed magnetic fields applied to a transferred arterial loop support the rat groin composite flap. Plast Reconstr Surg 114:1185–1189

Weintraub MI, Wolfe GI, Barohn RA, Cole SP, Parry GJ, Hayat G, Cohen JA, Page JC, Bromberg MB, Schwartz SL; Magnetic Research Group. 2003. Static magnetic field therapy for symptomatic diabetic neuropathy: a randomized, double-blind, placebo-controlled trial. Arch Phys Med Rehabil 84(5):736-46.

Weintraub, MI. 1999. Magnetic bio-stimulation in painful diabetic peripheral neuropathy: a novel intervention – a randomized double-placebo crossover study. Am J Pain Manag. 9:8-17.

Wertheimer N, Leeper E. 1979. Electrical wiring configurations and childhood cancer. Am J Epidemiol. 109(3):273-84.

Winemiller MH, Billow RG, Laskowski ER, Harmsen WS. 2003. Effect of magnetic vs sham-magnetic insoles on plantar heel pain: a randomized controlled trial. JAMA 290:1474-1478.

Zinchuk V. 1999. Effect of nitric oxide synthase inhibition on hemoglobin-oxygen affinity and lipid peroxidation in rabbits during fever. Respiration. 66(5):448-54.

2. EFFECT OF A PULSED RADIOFREQUENCY ELECTROMAGNETIC FIELD ON ION BINDING SYSTEMS

INTRODUCTION

In the light of the above reports describing EMF effects on Ca^{2+}/CaM-dependent enzyme syntheses, we considered Ca^{2+}/CaM-dependent NO synthesis to be a reasonable candidate for another EMF sensitive signaling pathway. The NO pathway, which plays a role in a variety of growth and repair processes, responds rapidly to departures from intracellular Ca^{2+} homeostasis and plays a role in a variety activities of therapeutic interest. For example, NO signaling plays a role in tissue maintenance [Madhusoodanan et al., 2007] and in the production of heat shock proteins relevant to the inflammatory, repair, and regenerative phases of healing [Kim et al., 1997; Steensberg et al., 2007; Li et al., 2008]. Transient changes in cytosolic Ca^{2+} due to external stimuli such as changes in temperature and mechanical forces or injury, activate CaM [Colomer et al., 2007], thus activating the constitutive nitric oxide synthase (cNOS) enzymes, i.e., endothelial and neuronal NOS, or eNOS and nNOS, respectively. Studies have shown that both forms are inactive at basal intracellular levels of Ca^{2+}, however, their activity increases with elevated Ca^{2+}, reaching half-maximal activity at about 300 nM [Bredt et al., 1990; Schmidt et al., 1991]. The importance of NO signalling in therapeutic and repair processes have been the subject of a large body of research [Hill et al., 2010]. As a gaseous free radical with a half-life of about 5 s [Ignarro et al., 1993], NO diffuses locally through membranes and organelles, acts on molecular targets at a distance up to 200 μm from the location of synthesis [Malinski et al., 1993; Wood et al., 1994; Tsoukias, 2008], and has been shown to exhibit a high affinity for transition metal centers, in particular ferrous heme and for hemoproteins such as soluble guanylyl cyclase (sGC) and hemoglobin [Ignarro et al., 1986; Thomas et al., 2003]. NO has also been recently demonstrated to be regulated by Hb-alpha in the myeloendothelial junction, suggesting a role for globular proteins in the availability of NO [Straub et al, 2012].

Small changes in the basal concentrations of NO from cNOS can activate the hemoprotein sGC, which catalyzes the synthesis of cyclic guanosine monophosphate (cGMP) [Cho et al., 1992]. This CaM-activated NO/cGC/cGMP signaling pathway is a rapid response cascade, mediated by NO binding to the ferrous heme [Ignarro et al., 1986] which modulates peripheral and cardiac blood flow in response to normal physiologic demands, as well as to inflammation [Bredt, 2003]. This same pathway also modulates the release growth factors such as basic fibroblast growth factor (FGF-2) and vascular endothelial growth factor (VEGF) [Madhusoodanan et al., 2007; Werner et al., 2003] involved in tissue repair and maintenance. Evidence for NO control of Ca^{2+}-activated K^{+} channels also suggests that attempts to observe of EMF effects in patch-clamped ion channels [Højevik et al., 1995; Tonini et al., 2001; Obo et al., 2002] might be informed by accounting for NO signaling and Ca^{2+}/CaM binding [Bolotina et al., 1994; Lu et al, 1998]. NO signalling also acts in a variety of pathways in the nervous system, and a brief glance at the literature suggests: control of CREB-mediated gene expression in neurons [Riccio, et al., 2006], in conjuction with histone deacetylases [Watson et al., 2009], epigenetic changes associated with cell cycle arrest and differentiation [Nott et al., 2009], human chondrocyte proliferation [Fitzsimmons et al., 2008], regulation of transcription factors [Contestabile 2008], survivability of neurons [Ciani et al., 2002], and recycling of BDNF by hippocampal neurons [Aicardi et al., 2004; Santi et al., 2008].

Nonthermal EMF Bioeffects Relevant to the Ca^{2+}/CaM/NO Pathway

The growing interest in pulsed EMF (PEMF) therapeutics has resulted large body of evidence demonstrating effects of nonthermal fields on a variety of biological systems. For example, a variety of bioeffects have been reported for nonthermal PRF fields, for time-averaged heating is negligible [Foley-Nolan et al., 1990; 1992; Kloth et al., 1999; Mayrovitz et al., 1992; 1995; Mayrovitz et al., 2002; Salzberg et al., 1995; Pennington et al., 1993; Pilla et al., 1996]. Of particular

interest due to their relevance to CaM/NO signaling, are studies reporting: nonthermal PEMF enhancement of nNOS expression and phospholipase C-gamma1 in regenerating murine neuronal cells [Kim et al., 2002]; NO-mediated effects of pulsed electromagnetic field stimulation on osteoblast proliferation and differentiation [Diniz et al., 2002]; increased rat osteoblast differentiation and maturation via activation of NO-cGMP-PKG pathway [Cheng et al., 2011]; increase in NO transient expression in MN9D cells [Pilla, 2012]; modulation of release of both growth factors and cytokines [Seegers et al., 2001; Brighton et al., 2001; Aaron et al., 2004; Li et al., 2007; Callaghan et al., 2008; Fitzsimmons et al., 2008; Rohde et al., 2009]; down-regulation of the inducible isoform of NOS, iNOS, in monocytes [Reale et al., 2006]; reduction in pro-inflammatory cytokines in human keratinocytes [Vianale et al., 2008]; modulation of the sequential expression of iNOS, eNOS and cyclooxygenase-2 (COX-2) in human keratinocytes, although in this study this is likely to be magnetic field effect [Patruno et al., 2010]; protective effect on dopaminergic neurons from several types of toxicity [Casper et al., 2006]; increase in cGMP in endothelial cells [Tepper et al., 2004; Callaghan et al., 2008]; increase in cGMP in MN9D dopaminergic neurons [Casper et al., 2008]; increase in articular chondrocyte proliferation [Fitzsimmons et al., 2008]. While the above bioeffects suggest a link to EMF modulation of NO signaling pathways, these effects also cannot be attributed to EMF heating of the target tissues, thus suggesting that nonthermal mechanisms exist.

The experiments conducted here considered *in vitro* cell-free Ca^{2+}-CaM-dependent NO synthesis. Our working hypothesis for EMF effects on NO synthesis was that EMF acts upon Ca^{2+}/CaM binding, thus resulting in a modulation of NO synthesis according to Figure 1. Schematically, transient changes in free cytosolic Ca^{2+} are rapidly detected by CaM [Blumenthal et al., 1982], resulting in concomitant changes in the concentration of activated CaM*, which then binds to and activates the constitutive enzyme cNOS, i.e. neuronal nNOS or endothelial eNOS. The activated enzyme cNOS* then, in conjunction

with the necessary redox cofactors nicotinamide adenine dinucleotide phosphate (NADPH), tetrahydrobiopterin (H4B), flavin mononucleotide (FMN), flavin adenine dinucleotide (FAD), converts L-arginine to citrulline, in the process releasing one mole of both NO and citrulline for each mole of L-arginine. The vertical arrow represents the recycling of the enzyme and subsequent release of CaM from cNOS* which is required for the release of Ca^{2+} from CaM [Cox, 1988; Daff, 2003].

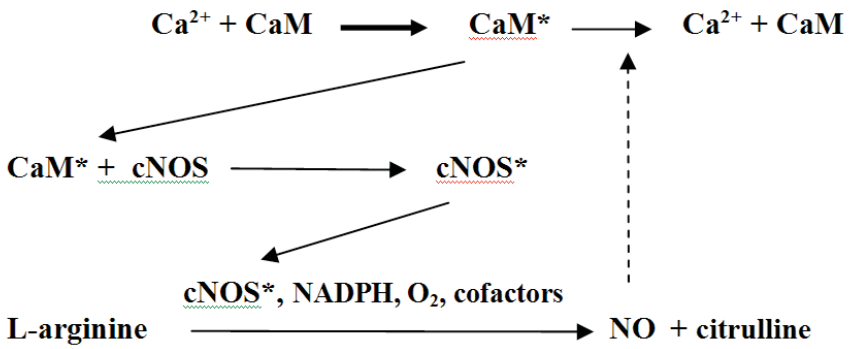

Figure 1. Schematic representation of the NO synthesis pathway. EMF was assumed to act upon Ca^{2+}/CaM binding, thus resulting in a modulation of NO synthesis.

MATERIALS AND METHODS

In order to assess the possibility that this enzymatic synthesis could be a sensitive detector to changes in CaM activation due to EMFs, we chose to perform EMF exposures under conditions for which Ca^{2+}/CaM binding was rate-limiting. Thus, if the effect of the EMF was to enhance the binding of Ca^{2+} to CaM, and thus concentration of CaM*, this would result in an increased rate of NO synthesis. This required the control of free Ca^{2+} using EGTA, and the use of purified preparations of CaM and the NOS enzyme, to minimize interference due to

residual Ca^{2+} and/or CaM. After initial unsuccessful attempts to measure NO synthesis using the Griess assay (due to NADPH interference) [Griess, 1879; Weissman et al., 2001] and a NO-selective electrode (due to problems with stirring, temperature control, and the rapid rate of NO conversion to nitrite) [See Appendix to this Chapter], we chose to quantify NO synthesis using the hemoglobin assay [Hevel et al., 1994; Murphy et al., 1994]. This method takes advantage of the rapid scavenging of NO ($k \approx 10^7\ M^{-1}\cdot s^{-1}$)[Doyle et al., 1981; Eich et al., 1996; Herold et al. 2001] by oxygenated Hb (oxyHb), and the resulting conversion of oxyHb to metHb which may then be quantified using visible light spectroscopy to yield the molar concentration of NO synthesis [Hevel et al., 1994].

Reaction mixtures consisted of 50 mM HEPES buffer, pH 7.4; 50 μM L-arginine; 170 μM DTT; 0.2-4 μM CaM; 0–2 mM CaCl2; 0-2 mM EGTA, pH 8.0; 50 μM NADPH; 10 μM H4B; nNOS or eNOS 0.25-1 U/mL. All reagents except CaM and some cNOS stocks were obtained from Sigma, USA. Purified Ca^{2+}- and CaM-free nNOS and eNOS (Sigma, USA; Cayman, USA) were used. Calibration experiments showed that additional FAD and FMN was not required for synthesis and conversation with Cayman indicated that these were likely residually bound to the NOS enzyme. Free calcium concentrations were controlled in the 0.1–1.0 μM range via EGTA [Schoenmakers et al., 1992] and NO synthesis was quantified at 401, 411 and 421 nm [Hevel et al., 1994] using a Molecular Devices 190 spectrophotometer. Over the course of at least 48 independent experiments, reactions were initiated with nNOS or eNOS 0.25-1 U/mL + 10 μM H4B, or 50 μM NADPH + 10 μM H4B. Trials were also conducted wherein the reaction was initiated using Ca^{2+} + H4B or CaM + H4B, all other reagents being in the reaction stock mixture. Enzymatic synthesis was halted through the addition of 5 mM EGTA in 50 mM Hepes buffer. For all calibration experiments, negative controls were performed by adding the appropriate volume of Hepes + H4B rather than the above initiating reagents. Purified Ca^{2+}-free CaM used here was shown to yield negligible NO synthesis, confirming the Ca^{2+}-dependence of CaM activity.

Similar results were produced for the purified Ca^{2+}/CaM-free NOS employed for these experiments. In the absence of enzymatic NO donation, no effects of PRF were observed on the location of the Hb peak in the 406-415 nm range, corresponding to met-Hb conversion due to NO. In order to obviate errors due to the interactions of H4B with HB [Hevel et al., 1994], H4B was left out of the stock solutions until the final step of reaction initiation. In order to insure that experiments were performed in the linear region (R^2 = .998) of NO synthesis, for which Ca^{2+}-CaM binding is rate-limiting [Wrighton et al., 1993.], time series of the NO synthesis were obtained for all experiments using PRF exposure, and also for all new combinations of reagents, and when new stocks of critical ingredients such as cNOS, CaM, Hb, etc., were obtained. Trials were performed either in batches of 3-10 tubes for each EMF exposure condition, or an alternating design with PRF coil active or inactive for successive tubes, reacted independently, with n = 10 tubes for each EMF exposure condition. Stock solutions were aliquoted into individual 1.5 mL Eppendorf tubes which were kept on ice until immediately prior to reaction. In order to obviate artifacts due to H4B interactions with Hb [Hevel et al., 1994], visible light spectra were read for each tube immediately after EGTA quenching. Calibration experiments confirmed a reduction in Hb optical density with increasing H4B concentration. Titrations were performed for each experimental condition to record the location relative to saturation on Ca^{2+} activation curve. A wide range of ratios of enzyme to substrate was tested, and EGTA titration was performed for each in order to establish specific Ca^{2+} dependence. EGTA titrations were also performed for each new batch or reagents or upon freeze-thawing the NOS enzyme. Hb concentrations were optimized in the low μM-range for each experiment to yield sufficient sensitivity, dependent upon the current enzyme activity and number of units of NOS used in specific experiments. Times series were performed for each exposure condition and final reaction times between 1-10 minutes were chosen in order to insure that all experiments were conducted within the linear range of synthesis. NO synthesis was carried out at 37° C and quantified spectrophotometrically by measuring visible light absorbance at 401, 411 and 421 nm. The PRF signal was as described

in Chapter 1, and generated by a 20 cm coil surrounding the plastic water bath housing containing samples, as shown in figure 2. In order to maximize the electric field induced in the tubes, the coil was placed parallel to the long axis of the tubes. For each experiment, five 1.5 mL microfuge tubes containing the NOS preparation were exposed to PRF + ambient of ambient alone (PRF coil inactive) for the 1-10 min duration of enzymatic synthesis.

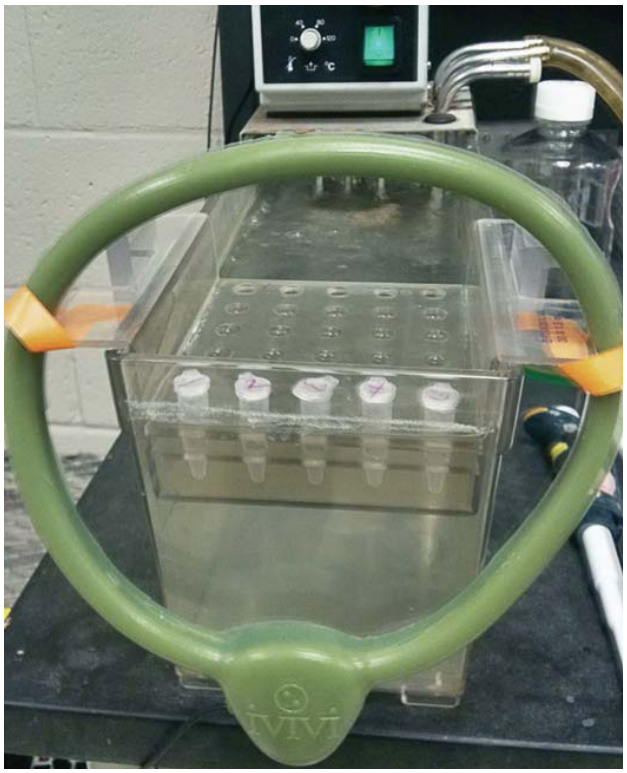

Figure 2. PRF exposure system for NO synthesis. Samples undergo NO synthesis in water bath at 37° C during exposure to 10 μT 27.12 MHz PRF field.

Further experiments were carried out using a Ca^{2+}-selective electrode (Fisher 9720BNWP) to measure the equilibrium binding of Ca^{2+}/CaM [Iida et al., 1986; Iida 1988; McGuigan et al., 2006] under PRF+ambient and ambient-only EMF exposure conditions. The electrode was rated by the manufacturer to provide a

500 nM sensitivity to Ca^{2+} concentration. Experiments were carried in 50 mM Hepes buffer, pH 7.2, at 22° C, using purified Ca^{2+}-free CaM (Ocean Biologics, USA). In one set of experiments, total $CaCl_2$ concentration was raised in 10 μM steps in a solution of 12.5 μM Ca^{2+}-free CaM in 10 mL volume. A second series of trials, consisted of adding 62.5 μM CaM in 200 μL aliquots to 10 mL of 30 μM $CaCl_2$ solution, allowing for direct observation in electrode potential due to uptake of Ca^{2+} by CaM. Electrode potentials were recorded after a time period sufficient to produce a stable electrode potential, usually approximately 40-60 seconds, allowing a direct observation of the change in Ca^{2+} concentration due to Ca^{2+} uptake by CaM. Both series of trials were repeated 5 times at 22° C for PRF+ambient and ambient-only exposure conditions. No changes in electrode potential were observed when buffer solution was substituted for Ca^{2+} or CaM.

RESULTS

The NO synthesis assay developed here was able to detect in the enzymatic activity, small nm-range changes in free Ca^{2+} concentrations. Through the use of purified Ca^{2+}-free CaM and purified Ca^{2+}-CaM-free cNOS, EGTA titration allowed repeatable control of the enzymatic synthesis through adjustment of free Ca^{2+} concentration. Figure 3, left hand plot, shows the Hb optical density (OD) spectra data from the visible light spectrophotometer for a typical EGTA titration in our assay, using a 10 min reaction time, ¼ U nNOS and 1 mM total Ca^{2+}. The production of NO and resulting conversion of oxyHb to metHb is evidenced by the passage with decreasing EGTA (i.e. more free Ca^{2+} and thus greater NO synthesis) of the characteristic Hb peak to 415 nm to the left, finally settling at approximately 406 nm for full oxy-met conversion [Hevel et al., 1994]. The isosbestic point at approximately 411 nm yields an indication of the pipetting accuracy for a given experiment. Figure 3, right hand plot, shows NO via the method of Hevel et al., 1994, using the OD at 401, 411 and 421 nm to compute the molar concentration of NO from the linear relation given by Hevel et al., 1994: $NO(\mu M) = 10^3(\Delta 401-\Delta 411)/p\varepsilon$, where p = path length (cm) and $\varepsilon = 38$

$mM^{-1}cm^{-1}$. Error bars are given by SEM for triplicate samples taken from each microfuge tube. Thus, we developed an assay which allowed, by varying free Ca2+ using EGTA, for the control of NO synthesis from zero synthesis (as given by the resolution of the Hb assay) into the μM range. Similarly, greater accuracy was obtained by keeping the EGTA concentration constant and adjusting the total Ca^{2+} concentration, as shown here in figure 4, left hand plot, using a 4 min incubation, ½ U eNOS (Cayman), 400 nM CaM, and 1 mM EGTA. Again, synthesis may be measured from the lower limit of the assay to the μM range, and exhibits saturation in this experiment at approximately 1 mM total added Ca^{2+}. Interestingly, as the total Ca^{2+} concentration increased above saturation, a small but marked inhibition of NO synthesis was observed, in accord with previous observations suggesting the existence of additional weak affinity sites on Calmodulin [Bredt et al., 1990; Weissman et al., 2002]. Making use of EGTA titration data [Schoenmakers et al., 1992], the dependence of NO synthesis upon free Ca^{2+} concentration may be estimated, as shown in Figure 4, right hand plot. Also, the time series of the NO synthesis was obtained for all experiments with PRF, new combinations of reagents, and when new stocks of critical ingredients such as cNOS, CaM, Hb, etc., were obtained. A typical time series is shown in Figure 5, using the above combination of reagents with ¼ U nNOS. Time series data was essential in order to insure that experiments were performed in the linear region (R^2 = .998) of NO synthesis, for which Ca^{2+}-CaM binding is rate-limiting. The results show that the assay developed here exhibits a low-nm-range sensitivity to changes in the concentration of free Ca^{2+}, thus suggesting the application of this cell-free system to our hypothesis that EMF may modulate NO synthesis by affecting Ca^{2+}/CaM binding in the 300 nm range of half-maximal basal concentrations observed to modulate in vivo NO synthesis [Bredt et al., 1990; Schmidt et al., 1991].

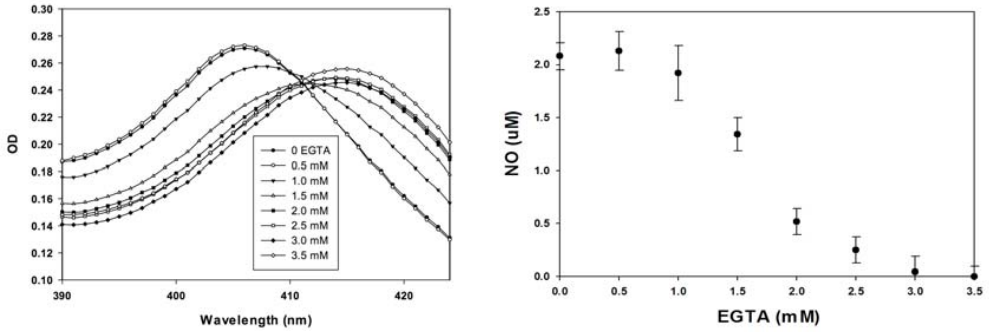

Figure 3. Left: Change in optical density (OD) of spectra of Hb in NOS synthesis assay corresponding to oxy-met Hb conversion due to NO uptake. Data from visible light spectrophotometer for a typical titration of EGTA from 0 – 3.5 mM. Peak at 415 nm characteristic of oxyHb moves to the left with decreasing EGTA (i.e. more free Ca^{2+}, and thus greater NO synthesis). **Right:** Concentration of NO in reaction mixture, from data on left, using the method of Hevel et al., 1994. Results show that NO synthesis is controlled from the lower limit of resolution of the assay to the μM range.

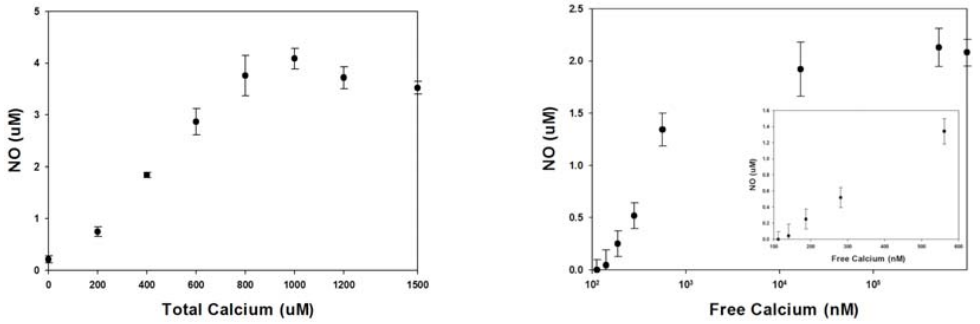

Figure 4. Left: NO synthesis as a function of total added Ca^{2+} concentration, keeping EGTA constant = 1 mM. Rate of synthesis reaches saturation at approximately 1 mM total Ca^{2+} concentration, defining range over which NO is dependent upon added Ca^{2+}. **Right:** Free Ca^{2+} concentration for a similar

experiment, using EGTA chelation data banks. The results show that the assay developed here exhibits a physiologically relevant low-nm sensitivity to free Ca^{2+} concentration, thus suggesting application to our hypothesis of Ca^{2+}/CaM binding as the EMF-sensitive step in NO synthesis.

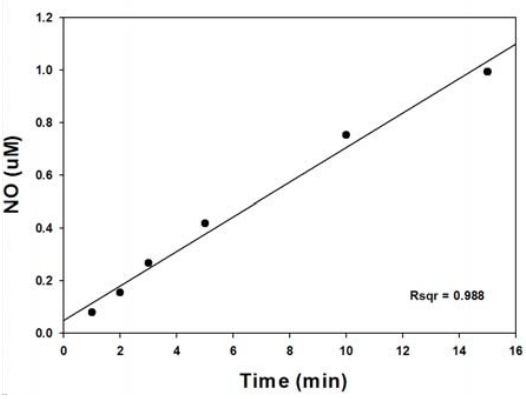

Figure 5. Typical time series for NO synthesis, using ¼ U nNOS, 400 nM CaM, and 1 mM EGTA. Time series were performed for all experiments in order to ensure that reaction was in the linear portion of synthesis for which Ca^{2+}-CaM binding is rate-limiting.

For preliminary trials, similar titrations were performed for several combination of ratios of enzyme/substrate, and PRF exposure of NO synthesis was performed at 2 or more points in the range of free Ca^{2+} concentrations for which Ca^{2+}-CaM binding was rate-limiting. For these trials, PRF and ambient only exposures were performed in batches of 5 tubes for each condition, in an experimental design that alternated the order of PRF and ambient (control) exposures. After these initial trials revealed a promising combination of reagents which exhibited a non statistically significant trend towards an increase in NO synthesis with PRF exposure, it was decided to perform a lengthy series of trials using one combination of reagents, in hopes of establishing significance. Using a 5 min incubation time, ½ U/mL nNOS, 1 mM CaM, 1 mM Total Ca^{2+}, 2 mM EGTA and all other reagents as described in the Methods section above. For these conditions,

free Ca^{2+} may be estimated at approximately 281 nM [Schoenmakers et al., 1992], corresponding to approximately 28% of saturation NO activation in our assay. In other words, we chose a location on the Ca^{2+} binding curve, well below saturation, yet high enough to allow reliable detection of NO via Hb oxy-met conversion. For these conditions, we found a statistically significant increase in NO synthesis, such that NO synthesis for PRF/null = 1.22, P = 0.02, n = 25. However, these results were obtained by an accumulation of data over 7 experiments, each using 3-4 tubes per exposure condition. The results required n = 25 tubes in order to achieve statistical significance, and individual experiments within this data set yielded both increases and decreases in NO, suggesting that the effect observed was due to the accumulation of variability within the assay itself. Thus, these data were not considered to be a reliable assessment of the EMF sensitivity of the NO assay. In hopes of producing a more effective assay for EMF sensitivity, a final group of trials employed an alternating exposure design, wherein each tube was individually reacted and assessed spectrophotometrically for NO synthesis, and PRF and control exposures were alternated for each tube. Several extensive conversations were conducted with Dr. Marko Markov, the author of several papers reporting EMF effects on Ca^{2+}/CaM-dependent myosin phosphorylation [Markov et al., 1992, 1993, 1994, 1997], in hopes of obtaining better knowledge of the conditions for which Ca^{2+}/CaM binding exhibits EMF sensitivity. The Ca^{2+}/CaM/EGTA concentrations employed by Markov were used for several of these trials, and several different means of initiating the reaction were also employed, such as initiation using $CaCl_2$, nNOS, CaM, and NADPH. None of these trials yielded significant changes in NO synthesis for PRF as compared to ambient exposures, with a metanalysis over the last 10 trials showing NO synthesis for PRF/null = 0.99, P =0.72, n = 100 tubes, 10 individual experiments, as summarized in Figure 6. One trial, 'PRF 3,' appeared promising, however the results were not repeatable in the successive trial. If this experiment is removed as an outlier from the metanalysis shown below, then the final result for NO synthesis for PRF/null = 1.00 (0.998669), P = 0.78, n = 90 tubes, 9 experiments. However, subsequent analysis of the Hb spectra showed that some trials exhibited

showed a statistically significant increase in the optical density of the 411 nm isosbestic point 2.8% higher OD than untreated, (P = 0.04, n = 3), suggesting the possibility of a PRF effect on Hb itself.

expt	EGTA (mM)	Ca total (uM)	Ca free (M)	CaM (nM)	NO +PMF/-PMF	T test P =
PRF 1	1	250	3.93e-8	1500	1.03	0.31
PRF 2	1	900	1.05e-6	200	1.02	0.80
PRF 3	**1**	900	1.05e-6	200	0.86	0.15
PRF 4	**1**	900	1.05e-6	200	0.97	0.38
PRF 5	1	900	1.05e-6	800	0.97	0.88
PRF 6	1	900	1.05e-6	800	1.00	0.99
PRF 7	**1**	900	1.05e-6	800	0.99	0.87
PRF 8	1	400	7.87e-8	200	1.00	0.97
PRF 9	2	500	3.93e-8	5000	1.00	0.97
PRF 10	2	500	3.93e-8	5000	1.01	0.89
				mean	**0.99**	**0.72**

Figure 6. Summary of the final 10 trials, for which the NO synthesis assay employed an alternating design of PRF and control exposures with each microfuge tube reacted and assessed individually. Results show no effects of PRF on NO synthesis for any of the individual experiments. The overall average ratio of NO synthesis for PRF/null = 0.99, P =0.72. Each experiment consisted of n = 10 tubes for each exposure condition.

Trials performed allowed direct observation of the uptake of Ca^{2+} by CaM. The addition of successive 10 μM aliquots of $CaCl_2$ to 12.5 μM Ca^{2+}-free CaM in a 10 mL reaction volume produced no significant difference in equilibrium electrode potential for PRF vs ambient exposures, as shown in Figure 7, left hand plot. No significant differences were found for trials in PRF field, $0.38 < P < 0.86$ for all

points in curve, n = 5. Also, addition of calmodulin to $CaCl_2$ solution offered a unique opportunity to directly observe the decrease in free Ca^{2+} concentration with the addition of 62.5 μM CaM in 200 μL aliquots. Again, no significant differences were found for trials in PRF field, $0.23 < P < 0.91$ for all points in curve, n = 5. Thus, Ca^{2+}/CaM binding, measured using the Ca^{2+}-selective electrode employed here, yielded no significant changes in Ca^{2+}/CaM equilibrium binding across the range of concentrations measured here. The size of the SEM error bars shown here provides an indication of the electrode stability and the repeatability of these results.

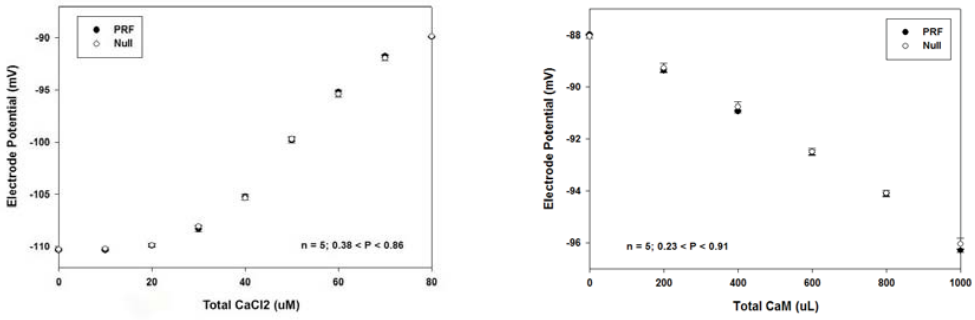

Figure 7. Left: addition of $CaCl_2$ to calmodulin solution: $CaCl_2$ concentration was raised in 10 μM steps in a solution of 12.5 μM Ca^{2+}-free CaM in 10 mL volume. No significant differences were found for trials in PRF field, $0.38 < P < 0.86$ for all points in curve. **Right:** addition of calmodulin to $CaCl_2$ solution: 62.5 μM CaM was added in 200 μL aliquots to 10 mL of 30 μM $CaCl_2$ solution, which allowed for direct observation of the uptake of Ca^{2+} for each aliquot of CaM. No significant differences were found for trials in PRF field, $0.23 < P < 0.91$.

DISCUSSION AND CONCLUSIONS

The enzymatic synthesis of NO performed here was able to detect changes in free Ca^{2+} concentrations on the order of 100 nM, corresponding to the basal changes known to activate NO synthesis *in vivo* [Bredt et al., 1990; Schmidt et al., 1991]. Over the course of at least 48 independent experiments with PRF exposures, no significant differences in NO synthesis were found for PRF vs. null exposures. Although a trend was observed for one set of trials, a large number (25) of trials were required to yield statistical significance, and we thus attributed this result to variability in the assay itself, rather than a PRF effect. Further trials, carefully controlling conditions by reacting and assaying each tube individually in an alternating design for EMF exposures yielded no PRF significant effects, with the ratio of NO synthesis for PRF/null being very close to unity.

Over the course of at least 48 independent experiments with PRF exposure for which Ca^{2+}-CaM binding was rate-limiting, no significant differences in NO synthesis were found. Thus, the results reported here do not support that hypothesis that PRF acts upon Ca^{2+}/CaM binding to yield an effect observable using this *in vitro* cell-free assay, i.e. within the approximately 100 nM resolution of the assay. Although a body of literature exists concerning NO/NOS/Hb interactions, including the inhibition of NOS by Hb and even NO itself [Griscavage et al., 1994; Kopincová et al., 2011], which could conceivably mask or counterbalance a PRF effect on Ca^{2+}/CaM binding, the assay performed here exhibits a clear, quantifiable dependence upon Ca^{2+}/CaM binding, so that PRF induced changes in CaM activation should be observable if greater than the resolution of the assay. It is highly unlikely that a putative PRF effect directly on Hb or NO/NOS/Hb interactions acted in an exactly equal and opposite direction as the hypothesized effect on Ca^{2+}/CaM binding, thus masking precisely the action of the PRF on Ca^{2+}/CaM. However, changes in Ca^{2+}/CaM binding below the resolving power of this assay could have occurred, and one means assaying NO with a potential for pM-range resolution is the citrulline assay which measures directly the radioactively labelled product of the enzyme reaction [Hevel et al.,

1994; Bredt et al., 1989; Ward et al., 1999]. Indeed, such a sensitivity may be necessary in order for the results to be relevant to the function of NO signalling in guanylyl cyclase receptors [Batchelor et al., 2010]. Trials reported here employing a Ca^{2+}-selective electrode further lend support to the notion that the equilibrium concentration of activated CaM is not altered by the PRF signal utilized in this study, within the 500 nM electrode resolution. A real-time assay using a Ca^{2+}-selective electrode might enable a study of the binding kinetics Ca^{2+} with CaM, but was obviated here by the high cost of Ca^{2+}-free CaM.

These results are in contrast to reports of a PRF effect on Ca^{2+}/CaM dependent myosin phosphorylation [Markov et al., 1994], wherein a nearly twofold increase in phosphorylation was reported for a PRF signal with waveform parameters (0.05 G, 2 ms, 1 Hz) similar to those employed here (5 μT, 2 ms, 1 Hz). For these experiments, Ca^{2+} and CaM were placed together in the reaction mixture with myosin light chain kinase before initiating the reaction with ATP and were thus at equilibrium. Assuming Ca^{2+}/CaM as the EMF-sensitive target, such an effect would have required a concomitant increase (i.e. a doubling) in activated CaM, due to PRF. As several of the trials on NO synthesis reported here employed the same Ca^{2+}/CaM combination as the experiments of Markov et al., such a doubling would have lain clearly within the resolution of our assay. Trials reported here employing a Ca^{2+}-selective electrode further lend support to the notion that the equilibrium concentration of activated CaM is not altered by the PRF signal utilized in this study, within the 500 nM electrode resolution. One possible interpretation is that the data presented here suggest that earlier reports of EMF effects may have acted upon transient non-equilibrium concentrations during synthesis and re-cycling of the enzyme, or were due to effects on enzyme/substrate/cofactor interactions. This may shed light on unsuccessful attempts at replication of EMF effects in Ca^{2+}/CaM dependent systems [Bruckner-Lea et al., 1992; Hendee et al., 1996; Coulton et al., 2000;]. Several trials with low values of free Ca^{2+} showed a statistically significant 2.8% ($P < 0.04$, $n = 3$) increase in absorbance at the Hb isosbestic point at 411nm, suggesting the

possibility of a PRF effect on Hb itself. Calibration experiments showed a reduction in Hb optical density with increasing H4B concentration, and this effect was partially mitigated by the PRF signal, perhaps suggesting an EMF effect on the action of H4B on Hb. However, because of the episodic nature of this result and the absence of a clinically relevant literature detailing direct Hb-H4B interactions, we chose not to study the effect of EMFs on these interactions.

APPENDIX
QUANTIFYING NO SYNTHESIS USING AN NO-SELECTIVE ELECTRODE

"Any newcomer to the NO field is confronted with a bewildering nomenclature that uses very similar sounding names to describe very distinct molecules, e.g. nitrous oxide (laughing gas) and nitric oxide (sometimes called crying gas by those working on it!)." [Hill et al., 2010]

The difficulties encountered in the accurate measurement of NO are familiar to many researchers, and stem from NO being a highly gregarious free radical with a high reactivity for transition metals and other radicals [Tsoukias et al., 2003], and also the natural oxidation of NO to nitrite [Ignarro et al., 1993]. This oxidation to nitrite, which occurs with a half-life of approximately 5 seconds, occurs *in vitro*, and is one source of difficulty in use of NO-selective electrodes to accurately quantify NO synthesis [Boo et al, 2007]. Our trials with an NO-selective electrode (Model ISO-NOP3020, World Precision Instruments, Sarasota, FL, USA) confirmed NO's dubious properties as a 'crying gas,' as we found electrode readings to be unreliable for quantifying enzymatic synthesis, and chose to abandoned plans to assay NO synthesis with this method. A brief analysis of the dynamics of NO synthesis and decay (in the absence of a scavenging agent such

as Hb) helps to clarify why detection of NO synthesis using an electrode is difficult.

Given a constant linear enzymatic synthesis of NO, as observed here and used by manufacturers to define the activity of cNOS enzymes, the rate of change of the NO concentration is given by

$$\frac{dN(t)}{dt} = \alpha - \beta N(t) \tag{1}$$

where α = 1 nmol/min [Cayman Chemical Item Number 60880, Cayman, USA], and the decay constant β for a half-life of 5 second is ln(2)/5.

Eqn. (1) is of the general form

$$\frac{dN(t)}{dt} + \beta N(t) = \alpha \tag{2}$$

which admits a solution of the form

$$N(t) = \frac{\alpha \int e^{\beta t}\, dt}{\int \beta\, dt}, \tag{3}$$

so that N(t) is given by

$$N(t) = \frac{\alpha \int_0^t e^{\beta t}\, dt}{\int_0^t \beta\, dt} = \left[\frac{\frac{\alpha}{\beta} e^{\beta t} - \alpha t}{e^{\beta t}} \right]_0^t = \frac{\frac{\alpha}{\beta} e^{\beta t} - \alpha t}{e^{\beta t}} - \frac{\alpha}{\beta}. \tag{4}$$

Thus, for the conditions we employed, using 1 U NOS in a 5 mL reaction volume, with stirring provided by air bubbling through the mixture, the time course of the

NO concentration is expected to be as shown in Figure A1. After approximately 7 seconds, we reach a maximal concentration of of about 44 nM, which is within the resolution of the electrode [from World Precision Instruments specsheet]. However, after 20-30 seconds, N(t) is in the 10-20 nM range, which is approaching the noise level we observed in our electrode. Thus, the window of detectability for *in vitro* synthesis is very short, on the order of 10-15 seconds, and accurate measurements cannot be made by hand/eye most likely due to stirring artifacts present immediately after initiating the reaction. Figure A2 shows the time course of NO concentration for 5, 25 and 50 U nNOS in a 5 mL reaction volume. Due to the linear dependence of equation (3) on α, the maximal concentration increases linearly with the amount of enzyme used. However, for all amounts of the NOS enzyme shown here, the maximal concentration is always reached after approximately 7 seconds, and decays rapidly thereafter. The 20 nM upper limit of detectability of our electrode is indicated by the horizontal dotted line, which shows that even using 5-10 times as much NOS results in only approximately a doubling of the time for which the NO concentration lies above the electrode resolution. However, in the absence of an automated method for data acquisition, considering the high cost of the NOS enzyme (approximately 100 USD for 5 U at the time of these experiments), we found the electrode inaccurate for the quantitative detection on NO.

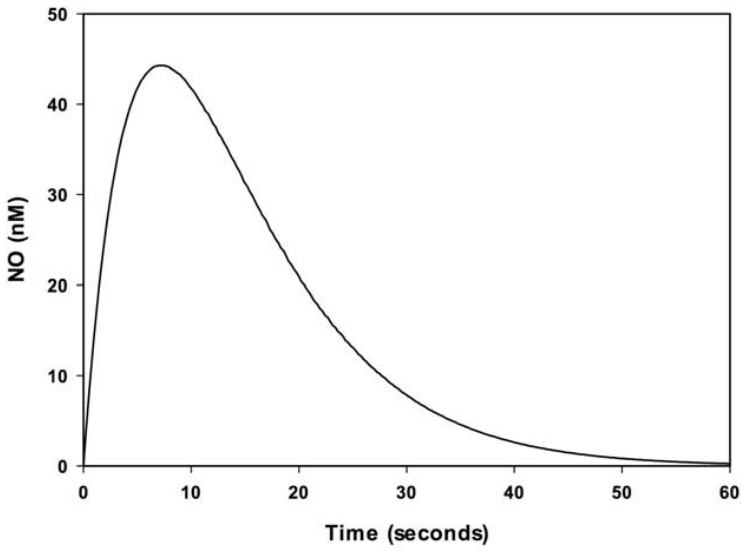

Figure A1. Time course of NO concentration *in vitro*, accounting for rate of enzymatic synthesis and decay to nitrite using 5 U nNOS in a 5 mL reaction volume. Maximal concentration of approximately 44 nM is reach after approximately 7 seconds. The limit of detectability with our electrode was in the 10-20 nM range, indicating that after 20-30 seconds the electrode signal is embedded in noise.

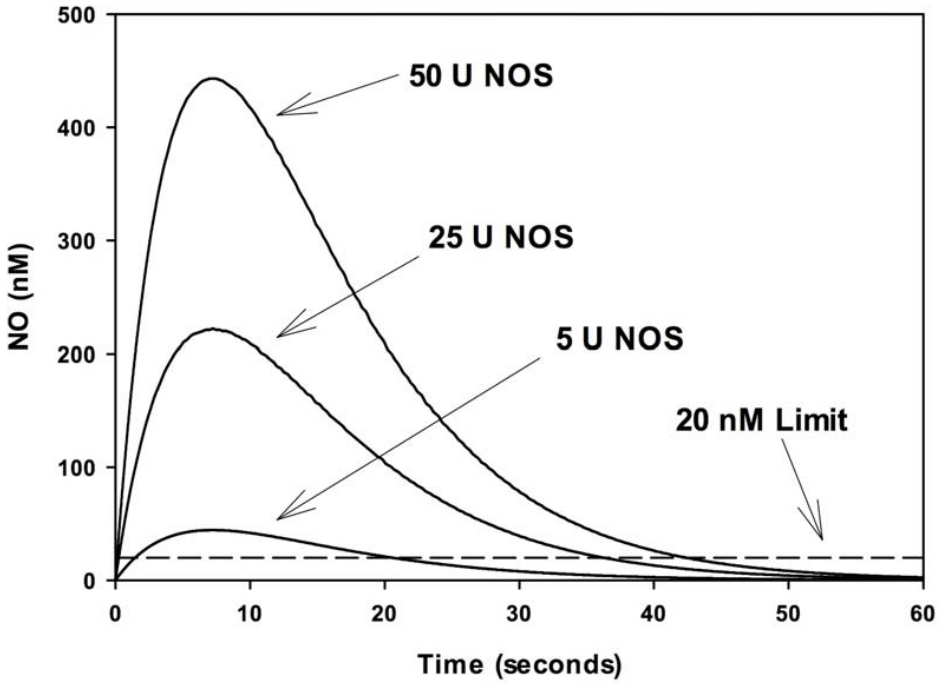

Figure A2. Time course of NO concentration *in vitro*, accounting for rate of enzymatic synthesis and decay to nitrite using 5, 25 and 50 U nNOS in a 5 mL reaction volume. Note that for all the amounts of the NOS enzyme shown here, the maximal concentration is always reached after approximately 7 seconds. The horizontal dotted line shows the 20 nM upper limit of detectability of our electrode, thus indicating that even using 5-10 times as much NOS results in only approximately a doubling of the time for which the NO concentration lies above the electrode resolution.

REFERENCES

Aaron RK, Boyan BD, Ciombor DMcK, Schwartz Z, Simon BJ. 2004. Stimulation of Growth Factor Synthesis by Electric and Electromagnetic Fields. Clin Orthop 419:30–37.

Aicardi G, Argilli E, Cappello S, Santi S, Riccio M, Thoenen H, Canossa M. 2004. Induction of long-term potentiation and depression is reflected by corresponding changes in secretion of endogenous brain-derived neurotrophic factor. PNAS 101:15788–15792.

Batchelor AM, Bartus K, Reynell C, Constantinou S, Halvey EJ, Held KF, Dostmann WR, Vernon J, Garthwaite J. 2010. Exquisite sensitivity to subsecond, picomolar nitric oxide transients conferred on cells by guanylyl cyclase-coupled receptors. Proc Natl Acad Sci U S A. 107(51):22060-5.

Blumenthal DK, Stull JT. 1982. Effects of pH, ionic strength, and temperature on activation by calmodulin an catalytic activity of myosin light chain kinase. Biochemistry. 21(10):2386-91.

Bolotina VM, Najibi S, Palacino JJ, Pagano PJ, Cohen RA. 1994. Nitric oxide directly activates calcium-dependent potassium channels in vascular smooth muscle. Nature. 368:850-3.

Boo YC, Tressel SL, Jo H. 2007. An improved method to measure nitrate/nitrite with an NO-selective electrochemical sensor. Nitric Oxide. 16(2):306-12.

Bredt DS, Snyder SH. 1989. Nitric oxide mediates glutamate-linked enhancement of cGMP levels in the cerebellum. Proc Natl Acad Sci USA. 86(22):9030-3.

Bredt DS, Snyder SH. 1990. Isolation of nitric oxide synthetase, a calmodulin-requiring enzyme. Proc Natl Acad Sci USA 87:682-5.

Bredt DS. 2003. Nitric oxide signaling specificity--the heart of the problem. J Cell Sci 116:9-15.

Brighton CT, Wang W, Seldes R, Zhang G, Pollack SR. 2001. Signal Transduction in Electrically Stimulated Bone Cells. J Bone Joint Surg 83A:1514-1523.

Bruckner-Lea C, Durney CH, Janata J, Rappaport C, Kaminski M. 1992. Calcium binding to metallochromic dyes and calmodulin in the presence of combined, AC-DC magnetic fields. Bioelectromagnetics. 13(2):147-62.

Callaghan MJ, Chang EI, Seiser N, Aarabi S, Ghali S, Kinnucan ER, Simon BJ, Gurtner GC. 2008. Pulsed Electromagnetic Fields Accelerate Normal and Diabetic Wound Healing by Increasing Endogenous FGF-2 Release. Plastic and Reconstructive Surgery. 121:130-141.

Casper D, Lekhraj R, Pidel A, Pilla AA. 2008. Transient induction of nitric oxide by PEMF in the dopaminergic MN9D neuronal cell line. Proceedings of the 30th Annual Meeting of the Bioelectromagnetics Society, San Diego, CA; June 8-12, p 155.

Casper D, Taub E, Alammar L, Pidel A, Pilla AA. 2006. Pulsed electromagnetic fields have neuroprotective effects on cultured dopaminergic neurons. Experimental Neurology 198 (2006) 558– 597.

Cheng G, Zhai Y, Chen K, Zhou J, Han G, Zhu R, Ming L, Song P, Wang J. 2011. Sinusoidal electromagnetic field stimulates rat osteoblast differentiation and maturation via activation of NO-cGMP-PKG pathway. Nitric Oxide. 25:316-325.

Cho HJ, Xie QW, Calaycay J, Mumford RA, Swiderek KM, Lee TD, Nathan C. 1992. Calmodulin is a subunit of nitric oxide synthase from macrophages. J Exp Med 176:599-604.

Ciani E, Virgili M, Contestabile A. 2002. Akt pathway mediates a cGMP-dependent survival role of nitric oxide in cerebellar granule neurones. Journal of Neurochemistry 81:218–228.

Colomer J, Means AR. 2007. Physiological roles of the Ca2+/CaM-dependent protein kinase cascade in health and disease. Subcell Biochem 45:169-214.

Contestabile A. 2008. Regulation of transcription factors by nitric oxide in neurons and in neural-derived tumor cells. Progress in Neurobiology 84:317–328.

Coulton LA, Barker AT, Van Lierop JE, Walsh MP. 2000. The effect of static magnetic fields on the rate of calcium/calmodulin-dependent phosphorylation of myosin light chain. Bioelectromagnetics. 21(3):189-96.

Cox JA. 1988. Interactive properties of calmodulin. Biochem. J. 249:621-629.

Daff S. 2003. Calmodulin-dependent regulation of mammalian nitric oxide synthase. Biochem Soc Trans 31(3):502-505.

Diniz P, Soejima K, Ito G. 2002. Nitric oxide mediates the effects of pulsed electromagnetic field stimulation on the osteoblast proliferation and differentiation. Nitric Oxide. 7. 18-23.

Doyle MP, Hoekstra JW. 1981. Oxidation of nitrogen oxides by bound dioxygen in hemoproteins. J Inorg Biochem. 14(4):351-8.

Eich RF, Li T, Lemon DD, Doherty DH, Curry SR, Aitken JF, Mathews AJ, Johnson KA, Smith RD, Phillips GN Jr, Olson JS. 1996. Mechanism of NO-induced oxidation of myoglobin and hemoglobin. Biochemistry. 35(22):6976-83.

Fitzsimmons RJ, Gordon SL, Kronberg J, Ganey T, Pilla AA. 2008. A pulsing electric field (PEF) increases human chondrocyte proliferation through a transduction pathway involving nitric oxide signaling. J Orthop Res 26:854-9.

Foley-Nolan D, Barry C, Coughlan RJ, O'Connor P, Roden D. 1990. Pulsed high frequency (27MHz) electromagnetic therapy for persistent neck pain: a double blind placebo-controlled study of 20 patients. Orthopedics 13:445-451.

Foley-Nolan D, Moore K, Codd M, et al. 1992. Low energy high frequency pulsed electromagnetic therapy for acute whiplash injuries: a double blind randomized controlled study. Scan J Rehab Med 24:51-59.

Griess JP. 1879. Ber. Deutsch Chem. Ges. 12, 426.

Griscavage JM, Fukuto JM, Komori Y, Ignarro LJ. 1994. Nitric oxide inhibits neuronal nitric oxide synthase by interacting with the heme prosthetic group. Role of tetrahydrobiopterin in modulating the inhibitory action of nitric oxide. J Biol Chem. 269(34):21644-9.

Hendee SP, Faour FA, Christensen DA, Patrick B, Durney CH, Blumenthal DK. 1996. The effects of weak extremely low frequency magnetic fields on calcium/calmodulin interactions. Biophys J. 70(6):2915-23.

Herold S, Exner M, Nauser T. 2001. Kinetic and mechanistic studies of the NO*-mediated oxidation of oxymyoglobin and oxyhemoglobin. Biochemistry. 40(11):3385-95.

Hevel JM, Marletta MA. 1994. Nitric-oxide synthase assays. Methods Enzymol. 233:250-258.

Hill BG, Dranka BP, Bailey SM, Lancaster JR Jr, Darley-Usmar VM. 2010. What part of NO don't you understand? Some answers to the cardinal questions in nitric oxide biology. J Biol Chem. 285(26):19699-704.

Höjevik P, Sandblom J, Galt S, Hamnerius Y. 1995. Ca2+ ion transport through patch-clamped cells exposed to magnetic fields. Bioelectromagnetics 16:33-40.

Ignarro LJ, Adams JB, Horwitz PM, Wood KS. 1986. Activation of soluble guanylate cyclase by NO-hemoproteins involves NO-heme exchange. Comparison of heme-containing and heme-deficient enzyme forms. J Biol Chem. 261(11):4997-5002.

Ignarro LJ, Fukuto JM, Griscavage JM, Rogers NE, Byrns RE. 1993. Oxidation of nitric oxide in aqueous solution to nitrite but not nitrate: comparison with enzymatically formed nitric oxide from L-arginine. Proc Natl Acad Sci USA 90:8103-7.

Iida S, Potter JD. 1986. Calcium binding to calmodulin. Cooperativity of the calcium-binding sites. J Biochem. (6):1765-72.

Iida S. 1988. Calcium binding to troponin C. II. A Ca2+ ion titration study with a Ca2+ ion sensitive electrode. J Biochem. 103(3):482-6.

Kim SS, Shin HJ, Eom DW, Huh JR, Woo Y, Kim H, Ryu SH, Suh PG, Kim MJ, Kim JY, Koo TW, Cho YH, Chung SM. 2002. Enhanced expression of neuronal nitric oxide synthase and phospholipase C-gamma1 in regenerating murine neuronal cells by pulsed electromagnetic field. Exp Mol Med 34:53-9.

Kim YM, de Vera ME, Watkins SC, Billiar TR. 1997. Nitric oxide protects cultured rat hepatocytes from tumor necrosis factor-alpha-induced apoptosis by inducing heat shock protein 70 expression. J Biol Chem 272:1402-11.

Kloth LC, Berman JE, Sutton CH, Jeutter DC, Pilla AA, Epner ME. 1999. Effect of Pulsed Radio Frequency Stimulation on Wound Healing: A Double-Blind Pilot Clinical Study, in "Electricity and Magnetism in Biology and Medicine", Bersani F, ed, Plenum, New York pp. 875-878.

Kopincová J, Púzserová A, Bernátová I. 2011. Biochemical aspects of nitric oxide synthase feedback regulation by nitric oxide. Interdiscip Toxicol. 4(2):63-8.

Li JK, Lin JC, Liu HC, Chang WH. 2007. Cytokine release from osteoblasts in response to different intensities of pulsed electromagnetic field stimulation. Electromagn Biol Med 26:153-65.

Li WJ, Zhao ZJ, Liu B, Zhang DX, Li F, Wang HC, Guo WY, Jia GL, Kitakaze M, Hori M. 2008. Nitric oxide induces heat shock protein 72 production and delayed protection against myocardial ischemia in rabbits via activating protein kinase C. Chin Med J (Engl) 121:1109-13.

Lu G, Mazet B, Sarr MG, Szurszewski JH. 1998. Effect of nitric oxide on calcium-activated potassium channels in colonic smooth muscle of rabbits. Am J Physiol Gastrointest Liver Physiol 274:G848-G856.

Madhusoodanan KS, Murad F. 2007. NO-cGMP signaling and regenerative medicine involving stem cells. Neurochem Res 32:681-94.

Malinski T, Taha Z, Grunfeld S, Patton S, Kapturczak M, Tomboulian P. 1993. Diffusion of nitric oxide in the aorta wall monitored in situ by porphyrinic

microsensors. Biochemical and biophysical research communications 193:1076-82.

Manucha W, Vallés PG. 2008. Cytoprotective role of nitric oxide associated with Hsp70 expression in neonatal obstructive nephropathy. Nitric Oxide 204-15.

Markov MS, Ryaby JT, Kaufman JJ, Pilla AA. 1992. Extremely weak AC and DC magnetic fields significantly affect myosin phosphorylation. In: Allen MJ, Cleary SF, Sowers AE, Shillady DD (Eds.) Charge and Field effects in biosystems 3, Boston: Birkhauser, pp. 225-230.

Markov MS, Wang S, Pilla AA. 1993. Effects of weak low frequency sinusoidal and DC magnetic fields on myosin phosphorylation in a cell-free preparation. Bioelectrochem Bioenergetics 30:119-125.

Markov MS, Muehsam DJ, Pilla AA. 1994. Modulation of Cell-Free Myosin Phosphorylation with Pulsed Radio Frequency Electromagnetic Fields, In: Allen MJ, Cleary SF, Sowers AE, (Eds.) Charge and Field Effects in Biosystems 4. NJ: World Scientific, pp. 274-88.

Markov MS, Pilla AA. 1997. Weak Static Magnetic Field Modulation of Myosin Phosphorylation in a Cell-Free Preparation: Calcium Dependence, Bioelectrochem Bioenergetics 43:235-240.

Mayrovitz HN, Larsen PB. 1992. Effects of Pulsed Magnetic Fields on Skin Microvascular Blood Perfusion. Wounds: A Compendium of Clinical Research and Practice 4:192-202.

Mayrovitz HN, Larsen PB. 1995. A Preliminary Study to Evaluate the Effect of Pulsed Radio Frequency Field Treatment on Lower Extremity Peri-Ulcer Skin

Microcirculation of Diabetic Patients. Wounds: A Compendium of Clinical Research and Practice 7:90-93.

Mayrovitz HN, Macdonald J, Sims N. 2002. Effects of pulsed radio frequency diathermy on postmastectomy arm lymphedema and skin blood flow: A pilot investigation. Lymphology 35(suppl):353-356.

McGuigan JA, Kay JW, Elder HY. 2006. Critical review of the methods used to measure the apparent dissociation constant and ligand purity in Ca2+ and Mg2+ buffer solutions. Prog Biophys Mol Biol. 92(3):333-70.

Murphy ME, Noack E. 1994. Nitric oxide assay using hemoglobin method. Methods Enzymol. 233:240-50.

Nott A, Riccio A. 2009. Nitric oxide-mediated epigenetic mechanisms in developing neurons. Cell Cycle 8:725-730.

Obo M, Konishi S, Otaka Y, Kitamura S. 2002. Effect of Magnetic Field Exposure on Calcium Channel Currents Using Patch Clamp Technique. Bioelectromagnetics 23:306-314.

Patruno A, Amerio P, Pesce M, Vianale G, Di Luzio S, Tulli A, Franceschelli S, Grilli A, Muraro R, Reale M. 2010. Extremely low frequency electromagnetic fields modulate expression of inducible nitric oxide synthase, endothelial nitric oxide synthase and cyclooxygenase-2 in the human keratinocyte cell line HaCat: potential therapeutic effects in wound healing. Br J Dermatol. 162:258-66.

Pennington GM, Danley DL, Sumko MH, et al. 1993. Pulsed, non-thermal, high frequency electromagnetic energy (Diapulse) in the treatment of grade I and grade II ankle sprains. Military Med 158:101-104.

Pilla AA, Martin DE, Schuett AM, et al. 1996. Effect of pulsed radiofrequency therapy on edema from grades I and II ankle sprains: a placebo controlled, randomized, multi-site, double-blind clinical study. J Athl Train S31:53.

Pilla AA. 2012. Electromagnetic fields instantaneously modulate nitric oxide signaling in challenged biological systems. Biochem Biophys Res Commun. 426(3):330-3.

Reale M, De Lutiis MA, Patruno A, et al. 2006. Modulation of MCP-1 and iNOS by 50-Hz sinusoidal electromagnetic field. Nitric Oxide 15:50-7.

Reale M. 2010. Extremely low frequency electromagnetic fields modulate expression of inducible nitric oxide synthase, endothelial nitric oxide synthase and cyclooxygenase-2 in the human keratinocyte cell line HaCat: potential therapeutic effects in wound healing. Br J Dermatol. 162:258-66.

Riccio A, Alvania RS, Lonze BE, Ramanan N, Kim T, Huang Y, Dawson TM, Snyder SH, Ginty DD. 2006. A Nitric Oxide Signaling Pathway Controls CREB-Mediated Gene Expression in Neurons. Molecular Cell 21:1–12.

Rohde C, Chiang A, Adipoju O, Casper D, Pilla AA. 2009. Effects of Pulsed Electromagnetic Fields on IL-1β and Post Operative Pain: A Double-Blind, Placebo-Controlled Pilot Study in Breast Reduction Patients. Plast Reconstr Surg.125(6):1620-9.

Salzberg CA, Cooper SA, Perez P, Viehbeck MG, Byrne DW. 1995. The effects of non-thermal pulsed electromagnetic energy on wound healing of pressure ulcers in spinal cord-injured patients: a randomized, double-blind study. Ostomy Wound Management. 41:42-51.

Santi S, Cappello S, Riccio M, Bergami M, Aicardi G, Schenk U, Matteoli M, Canossa M. 2006. Hippocampal neurons recycle BDNF for activitydependent secretion and LTP maintenance. The EMBO Journal 25:4372–4380.

Schmidt HH, Pollock JS, Nakane M, Gorsky LD, Förstermann U, Murad F. 1991. Purification of a soluble isoform of guanylyl cyclase-activating-factor synthase. Proc Natl Acad Sci USA 88:365-9.

Schoenmakers TJ, Visser GJ, Flik G, Theuvenet AP. 1992. Chelator: An Improved Method for Computing Metal Ion Concentrations in Physiological Solutions. BioTechniques 12:870-879.

Seegers JC, Engelbrecht CA, van Papendorp DH. 2001. Activation of signal-transduction mechanisms may underlie the therapeutic effects of an applied electric field. Med Hypotheses 57:224-30.

Shuvalova LA, Ostrovskaia MV, Sosunov EA, Lednev VV. 1991. Influence of a weak magnetic field under conditions of parametric resonance on the rate of calmodulin-dependent phosphorylation of myosin in solution. Proc Natl Acad Sci USSR (Biophysics) 317: 227–230 (in Russian).

Steensberg A, Keller C, Hillig T, Frøsig C, Wojtaszewski JF, Pedersen BK, Pilegaard H, Sander M. 2007. Nitric oxide production is a proximal signaling event controlling exercise-induced mRNA expression in human skeletal muscle. FASEB J 21:2683-94.

Straub AC, Lohman AW, Billaud M, Johnstone SR, Dwyer ST, Lee MY, Bortz PS, Best AK, Columbus L, Gaston B, Isakson BE. 2012. Endothelial cell expression of haemoglobin α regulates nitric oxide signalling. Nature 491:473–477.

Tepper OM, Callaghan MJ, Chang EI, Galiano RD, Bhatt KA, Baharestani S, Gan J, Simon B, Hopper RA, Levine JP, Gurtner GC. 2004. Electromagnetic fields increase in vitro and in vivo angiogenesis through endothelial release of FGF-2. FASEB J 18:1231-1233.

Thomas DD, Miranda KM, Colton CA, Citrin D, Espey MG, Wink DA. 2003. Heme proteins and nitric oxide (NO): the neglected, eloquent chemistry in NO redox signaling and regulation. Antioxid Redox Signal. 5(3)307-17.

Tonini R, Baroni MD, Masala E, Micheletti M, Ferroni A, Mazzanti M. 2001. Calcium protects differentiating neuroblastoma cells during 50 Hz electromagnetic radiation. Biophys J. 81(5):2580-9.

Tsoukias NM, Kavdia M, Popel AS. 2004. A theoretical model of nitric oxide transport in arterioles: frequency- vs. amplitude-dependent control of cGMP formation. Am J Physiol Heart Circ Physiol 286:H1043–H1056.

Vianale G, Reale M, Amerio P, Stefanachi M, Di Luzio S, Muraro R. 2008. Extremely low frequency electromagnetic field enhances human keratinocyte cell growth and decreases proinflammatory chemokine production. Br J Dermatol 158:1189-96.

Ward TR, Mundy WR. 1999. Measurement of the nitric oxide synthase activity using the citrulline assay. Methods Mol Med. 22:157-62.

Watson D, Antonella Riccio A. 2009. Nitric oxide and histone deacetylases: A new relationship between old molecules. Communicative & Integrative Biology 2: 11-13.

Weissman BA, Gross SS. 2001. Measurement of NO and NO synthase. Curr Protoc Neurosci. Chapter 7:Unit7.13.

Weissman BA, Jones CL, Liu Q, Gross SS. 2002. Activation and inactivation of neuronal nitric oxide synthase: characterization of Ca^{2+}-dependent [^{125}I]Calmodulin binding. Eur J Pharmacol. 435(1):9-18.

Werner S, Grose R. 2003. Regulation of wound healing by growth factors and cytokines. Physiol Rev 83:835-70.

Wood J, Garthwaite J. 1994. Models of the diffusional spread of nitric oxide: implications for neural nitric oxide signalling and its pharmacological properties. Neuropharmacology 33:1235–1244.

Wrighton, MS, Ebbing DD. 1993. General chemistry (4th ed.). Boston: Houghton Mifflin.

3. EFFECTS OF NONTHERMAL EMF ON HUMAN HEMOGLOBIN

a. NONTHERMAL RADIO FREQUENCY AND STATIC MAGNETIC FIELDS INCREASE RATE OF HEMOGLOBIN DEOXYGENATION IN A CELL-FREE PREPARATION

INTRODUCTION

The development of the Hb assay presented here stemmed from the observation reported above that the NO synthesis assay we developed exhibited in some experiments a small, statistically significant 2.8% ($P < 0.04$, $n= 3$) increase in optical density at the Hb isosbestic point at 411nm. This result suggested the possibility of a PRF effect on directly on Hb and inspired confidence in the possibility of developing an *in vitro* assay based upon Hb as a detector of EMFs. A survey of recent literature lent further support to the possibility, with report of a variety of EMF effects on human Hb in solution and erythrocyte suspensions, including decreases in viscosity [Tao et al., 2011.] and changes in impedance [Sosa et al., 2005], dielectric properties [Shalaby et al., 2006], dia- and para-magnetic properties [Sakhnini et al., 2001], optical absorption [Iwasaka et al., 2001] and *in vivo* deoxygenation [Milweski et al., 2006]. In addition, radiofrequency mobile telephone signals have been shown to decrease Hb oxygen affinity *in vitro* [Mousavy et al., 2009] and changes in infrared absorption have been reported for low-frequency EMF [Magazù et al., 2010]. Also, enhanced oxygen delivery by Hb is under investigation as a therapeutic strategy for the treatment of pathologies such as ischemia from stroke, cardiac disease and diabetic ulcers [Najjar et al., 2005]. Thus, the present study was aimed at characterizing the effect of a pulse-modulated radiofrequency (PRF) signal currently in clinical use for treatment of pain, edema and chronic wounds [Pilla, 2006; Pilla et al., 2011], and, applied independently, a static magnetic field (SMF), from permanent ceramic magnets intended for therapeutic applications and reported to reduce pain [Pilla et al., 2006], on the rate of oxygen release from

human hemoglobin (Hb) in an *in vitro* cell-free assay. These non-thermal EMF modalities were chosen for this study due to their demonstrated efficacy in a variety of therapeutically relevant settings [Pilla et al., 2006]. The reducing agent dithiothreitol (DTT) was chosen for the ability to easily control the time course of Hb deoxygenation via the ratio of DTT/Hb [Herzfeld et al., 1990]. This study will show that exposure to both PRF and SMF, applied independently, yields similarly significant increases in the rate of oxyHb → deoxyHb conversion in the presence of the reducing agent DTT, observable several minutes to several hours after EMF exposure had ended.

MATERIALS AND METHODS

Hemoglobin Preparation

Fresh human blood was obtained with written donor consent from, and approved for research by the Blood Bank at S.Orsola-Malpighi Hospital, Bologna according to the rules established by Legislative Decree 03-03-2005, article 9, paragraph 3, published in G.U. n. 85, 13.04.2005. Blood samples were also obtained from one author (DM) in accord with New York State Consolidated Law, Public Health Article 24-A, Section 2442, without written approval of the Institutional Review Board of the Albert Einstein College of Medicine. Blood was drawn in EDTA anticoagulant tubes, centrifuged at 1000 x g for 10 min and plasma removed. The packed erythrocyte suspension was then washed in normal saline and centrifuged at 1000 x g for 10 min, 3 times. Erythrocytes were then hemolyzed using distilled water, the resulting solution centrifuged at 1000 x g for 10 min, and the Hb-containing supernatant recovered using a Pasteur pipette. Red cell ghosts were sedimented by additional centrifugation, and the resulting solution containing 2-2.5 mM oxyHb (measured by visible light spectroscopy [Benesch et al., 1973]), was stored in 1.5 mL aliquots at -80° C until used for each experiment. Ten mL reaction mixtures were prepared using 100-120 μM oxyHb in 50 mM Hepes buffer (pH 7.2, Sigma-Aldrich, USA), and oxyHb → deoxyHb conversion initiated with 10-30 mM DTT at 22 ± 0.1° C. Trials were also performed with 100

mM $MgCl_2$ to the deoxygenation solution [Guo et al., 2009]. Due to the moderate volatility of DTT, fresh stock solutions were made immediately prior to each experiment. pH was checked with a digital pH meter (Fisher AB15 BioBasic, USA) and maintained at 7.2 for all hemoglobin samples used in this experiment. Immediately upon addition of DTT, the 10 mL reaction mixture volume was divided into 1 mL aliquots in sealed 1.5 mL microfuge tubes. No attempt was made to alter the gaseous environment within the tubes.

EMF Exposure

All hemoglobin samples were exposed to the ambient magnetic field, which was measured using a digital Gauss/Tesla meter (model 7010, F.W. Bell, USA) to be 40.5 ± 2 μT, 59 degrees from horizontal (vertical component = 34.7 ± 2 μT, horizontal component = 21.0 ± 2μT). The PRF signal is approved by the US FDA for post-operative pain and edema. The signal consisted of a 27.12 MHz sinusoidal carrier (derived from the carrier frequency reserved and cleared worldwide for short wave diathermy) configured to operate nonthermally through pulse modulation in 4 ms bursts, repeating at 5 Hz and peak magnetic field amplitude of 10 ± 1 μT (Roma3, Ivivi Health Sciences, San Francisco, CA, USA). These pulse modulation parameters were chosen on the bases of theoretical modelling and published reports of bioeffects at the cellular level, and healing at the animal and clinical levels [1-3, 18-24]. The PRF signal was delivered with a 20 cm circular single-turn antenna (coil) oriented vertically, creating a 10 x 10 x 5 cm region of field homogeneity in the central area of the plane of the coil within which a plastic carrier held five upright 1.5 mL microfuge tubes, each containing 1 mL reaction volume. Each Hb sample was contained in a cylindrical volume of 2.5 cm in height and 0.8 cm diameter. For this target size, using Faraday's Law of Induction, the mean peak induced electric field is 3 ± 1 V/m. PRF field parameters were assessed and verified for each experiment using a National Institute of Standards and Testing traceable electrostatically shielded loop probe 1 cm in diameter (model 100A, Beehive Electronics, Sebastopol, CA, USA) connected to a calibrated 100-MHz oscilloscope (model 2012B, Tektronix, Beaverton, OR,

USA). The output of the loop probe was calibrated at 27.12 MHz by measurement of output power using a spectrum analyser (model 8567A, Hewlett Packard, New York, NY, USA) and the probe calibration factor for conversion to magnetic field amplitude at 27.12 MHz was certified and given by the manufacturer. SMF exposure was delivered using circular permanent ceramic magnets of 3.8 cm diameter and 1.3 cm thickness, constructed for therapeutic applications (Magnetherapy, West Palm Beach, FL, USA), and composed of compacted and sintered strontium ferrite ($SrO\text{-}6(Fe_2O_3)$), encased in plastic. These magnets are axially magnetized to have a single north (N) and a single south (S) pole on each circular face, and manufactured to produce highly uniform field strength across each face. For all experiments, magnets were arranged with circular faces oriented vertically with 1.1 cm gaps between the parallel surfaces. In order to simultaneously expose five 1.5 mL microfuge tubes, two 1.1 cm-wide treatment regions were formed using a central magnet flanked by pairs of magnets on either side. This (NS)(NS)-gap-(NS)-gap-(NS)(NS) configuration produced two cylindrical treatment regions of 1.1 cm width and 3.3 cm in diameter with uniform magnetic field (to ± 3%), in which the Hb samples were exposed. Within each treatment region the horizontal component of the magnetic field (perpendicular to the magnet surface) was 186 ± 6 mT, a field strength similar to those commonly employed in therapeutic applications [Eccles, 2005]. The maximal value of the horizontal and vertical components (both parallel to the magnet surface) was 4.0 ± 0.6 mT. SMF components were measured using a digital magnetometer (Model 450, gaussmeter with MMT-6J02-VG transverse Hall effect probe with 1 mm resolution, Lake Shore Cryotronics, Westerville, OH, USA). For each experiment, five 1.5 mL microfuge tubes containing the hemoglobin preparation were exposed to PRF or SMF for 10-30 min, and 5 tubes were simultaneously exposed to ambient geomagnetic conditions (control) on the laboratory bench, approximately 3 meters away from exposed samples. At this distance contributions from either PRF or SMF to the control condition were undetectable. Temperature variations between exposed and control samples were less than ± 0.1° C [Fisher AB15 BioBasic, Waltham, MA, USA].

Spectrophotometric Analysis

After control and EMF exposure, triplicate 300 μL samples were taken from each 1.5 mL microfuge sample tube, pipetted into an open 96-well flat-bottom plate (Fisher Scientific, USA) and the concentrations of oxy, deoxy and metHb were measured spectrophotometrically (SpectraMax 190, Molecular Devices, Sunnyvale, CA, USA). The plate remained in the spectrophotometer at 22°C during the reaction, and the time course of deoxygenation was determined using the method of Benesch et al. 1973, which employs a weighted linear combination of optical densities at 560, 576 and 630 nm to determine oxyHb, deoxyHb and metHb concentrations. Stock Hb solutions (in Hepes, pH 7.2) and spectra from Hb/DTT data at t = 0 (i.e. after 30 min EMF/Control exposures) were assayed for oxy, deoxy and metHb at 560, 576 and 630 nm [Benesch et al., 1973]. The mean ratio of deoxy/oxy for Hb stock solutions was 3.9% ± 0.8%. For the Hb/DTT data at t = 0, the mean deox/oxy was 3.3% ± 0.6%. The two datasets do not differ significantly (P = 0.44, n = 5). The mean ratio of metHb/oxyHb was 21.8% ± 3.8% for stock solutions and 25.6% ± 3.7% for Hb/DTT data at t = 0, indicating no significant differences (P = 0.33, n = 5). Optical densities at 540, 560, 576 and 630 nm were measured immediately after EMF exposure and at successive 1 to 30 min intervals, until maximal deoxygenation was observed. Calibration studies confirmed that the kinetics of deoxygenation could be controlled by adjusting the ratio of DTT/Hb concentrations [[Herzfeld et al., 1990]]. Under the conditions stated above, deoxygenation occurred between 140 and 160 min after EMF exposure. Deoxygenation time was reduced by the addition of 5 M of urea to between 60-85 min after EMF exposure. In the absence of DTT, no significant deoxygenation of Hb occurred up to 3 hours (data not shown). Changes in oxyHB concentration with time are summarized in the figures, and maximal differences between deoxy and metHb for EMF exposures vs controls are reported in the text. All figures and data shown are the results of single experiments that have been repeated 2-10 times.

RESULTS

Our early observations of changes in visible light spectra with EMF exposures suggested the possibility of a quantitative Hb assay for EMF effect. For example, Immediately after 30 min of exposure (PRF: 27.12 MHz carrier, 4 ms bursts at 5 Hz, 10 μT; SMF: 186 mT), examination of visible light spectra showed that PRF, SMF and control (ambient magnetic field only) samples all consisted of approximately deoxyHb/oxyHb = 0.03 (see Table 1 for summary). Figure 1, left hand plot shows representative visible light spectra for PRF, SMF and control exposure conditions, immediately after EMF exposure was removed. Spectra are drawn from a single exposure tube for each EMF condition and exhibit the twin-peaked form characteristic of a low ratio of deoxyHb/oxyHb [Benesch et al., 1973]. In contrast, changes in visible light spectra were observed in the 540-580 nm region during the time of most rapid deoxygenation, which occurred in this experiment at 140-160 min after EMF exposure, resulting in ratios of deoxyHb/oxyHb of about 1.51-1.52 for EMF-exposed samples, as compared to 0.92 for the control sample (see Table 1). Figure 1, right hand plot shows that the spectra corresponding to the PRF-, SMF-treated samples exhibit the characteristic spectra corresponding to a higher ratio of deoxyHb/oxyHb, and thus indicative of greater oxyHb → deoxyHb conversion for the EMF-treated samples. The molar concentrations of oxyHb and deoxyHb are summarized in Table 1 for the spectra shown in Figure 1. The results suggest that the PRF and SMF exposures employed here could yield a change in the deoxygenation behaviour of the Hb, visible several hours after EMF exposures had ended.

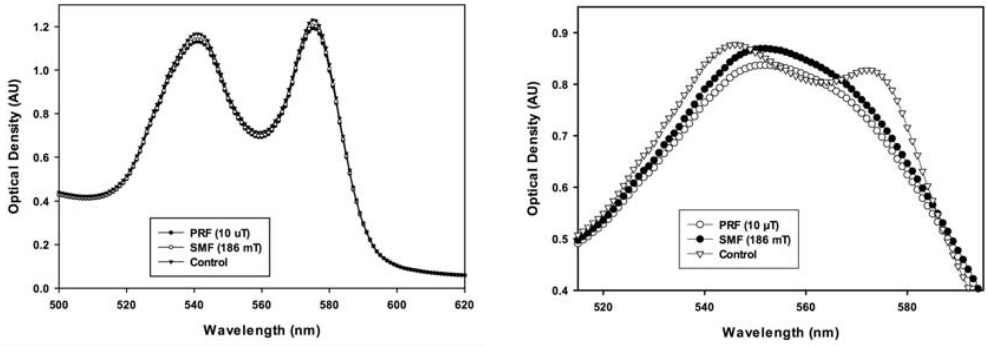

Figure 1. EMF effect on hemoglobin (Hb) visible light spectra. Spectra representative of the effect of pulsed radiofrequency (PRF) signal and 186 mT static magnetic field (SMF) on Hb visible light spectra during deoxygenation. Data shown are typical of samples drawn from a single tube for each EMF exposure condition, shown here at 150 min after a single 30 min EMF exposure. Deoxygenation of 100 μM Hb is characterized here by the passage of the spectrum from a two-peaked to one-peaked form. **Left:** At t = 0 min (immediately after EMF exposure) the ratio of deoxy/oxy Hb = 0.026 is approximately equal for all samples, and indicates nearly complete oxygenation immediately after a 30 minute exposure to either PRF, SMF or Control = ambient conditions only. **Right:** Deoxygenation occurs at an earlier time for EMF exposed samples (traces with one peak), as compared to control samples exposed only to the ambient geomagnetic laboratory environment (trace with two peaks). The EMF effect is observable at the time of most rapid deoxygenation. The results are summarized in Table 1.

0 min post exposure	PRF	SMF	Control
oxyHb (uM)	92.53	93.72	95.57
deoxy (uM)	3.01	3.06	2.99
ratio deoxy/oxy	**.033**	**.033**	**.031**
150 min post exposure	**PRF**	**SMF**	**Control**
oxyHb (uM)	33.49	34.76	47.45
deoxy (uM)	50.71	52.56	43.87
ratio deoxy/oxy	**1.51**	**1.52**	**0.92**

Table 1. Molar concentrations of oxyHb and deoxyHb for the spectroscopic data shown in Figure 1, using the equations of Benesch et al., 1973 to determine the molar concentration of oxy- and deoxyHb. These early trials suggested that PRF and SMF exposure could result in an increase in the rate of oxyHb → deoxyHb conversion, observable several hours after EMF exposure had ended.

In trials employing PRF exposure with multiple tubes (n = 5 tubes for each EMF exposure condition) using 20 mM DTT, 150 min after a single 30 min exposure, PRF-treated samples exhibited a 30.8 ± 10.3% reduction in oxyHb as compared to controls (14.6 ± 1.3 μM vs. 21.1 ± 2.5 μM, $P < 0.03$) (Figure 2). Concomitant, significant increases in deoxy Hb (86.9 ± 1.1 μM vs. 82.8 ± 1.8 μM, $P < 0.05$) and metHb (42.2 ± 1.4 μM vs. 37.1 ± 1.4 μM, $P < 0.02$) also occurred. (Figure 2). For the ratio of DTT/oxyHb concentrations employed in this trial (20 mM DTT; 120 μM oxyHb), 150 min corresponded to the time of most rapid deoxygenation. Addition of 5 M urea to the reagent solution decreased the time to deoxygenate to approximately 65-75 min after reaction initiation. For these conditions, the maximal difference between PRF-treated and control samples occurred at 73 min, with PRF-treated samples showing a 70.5 ± 9.7% reduction in oxyHb as compared to controls (8.5 ± 2.1 μM vs. 28.8 ± 6.3 μM, $P < 0.03$) (Figure 3). Concomitantly, there were significant increases in deoxy Hb (54.4 ± 2.2 μM vs.

40.9 ± 5.2 μM, $P < 0.04$) and metHb (73.4 ± 1.4 μM vs. 61.0 ± 2.3 μM, $P < 0.02$) (Figure 3). Under similar conditions (30 mM DTT, 5 M urea, n = 5) SMF treated samples (10-30 min exposure) underwent nearly complete deoxygenation before the untreated (control) samples began to deoxygenate. For these SMF treated samples, the time of most rapid deoxygenation occurred approximately 10 min earlier than for control samples (Figure 4), resulting in a 10.7-fold increase in the ratio of deoxyHb(PRF)/ deoxyHb(control) ($P < 0.002$, n = 5). Under these conditions, SMF-treated samples have substantially completed DTT-induced deoxygenation before untreated samples begin to lose O_2, rendering the magnetic field effect visibly observable in the 96-well spectrophotometer plate, as shown the photo in Figure 5, taken approximately 46 min after the reaction was initiated (P-values for these conditions have minima on the order of $P = 10^{-28}$). Experiments were also carried out for which: 1) Hb was treated with PRF or SMF for 30 min prior to introduction into the deoxygenation solution (20 mM DTT + 5M urea in 50 mM Hepes); 2) the deoxygenation solution was treated with PRF or SMF for 30 min prior to introduction of Hb. In both cases the difference between PRF or SMF treated and control samples was not significant. Also, 10 min vs. 30 min PRF and SMF treatment durations were compared in 5 M urea, with no significant difference observed in the time course of deoxygenation. Trials adding 100 mM $MgCl_2$ to the deoxygenation solution yielded rapid, 5-7 min deoxygenation for SMF-treated samples, as observed visually while samples were undergoing SMF exposure. All figures shown here are results of single experiments that have been repeated 2-10 times. In the absence of DTT, no PRF or SMF effects were observed on the Hb oxidation state. The SMF sensitivity of this Hb deoxygenation assay was reconfirmed at the Department of Histology, Embryology and Applied Biology, University of Bologna. Initial experiments were performed in New York with Hb from a single donor, and subsequent trials in Bologna used Hb from 3 different donors, with similar results.

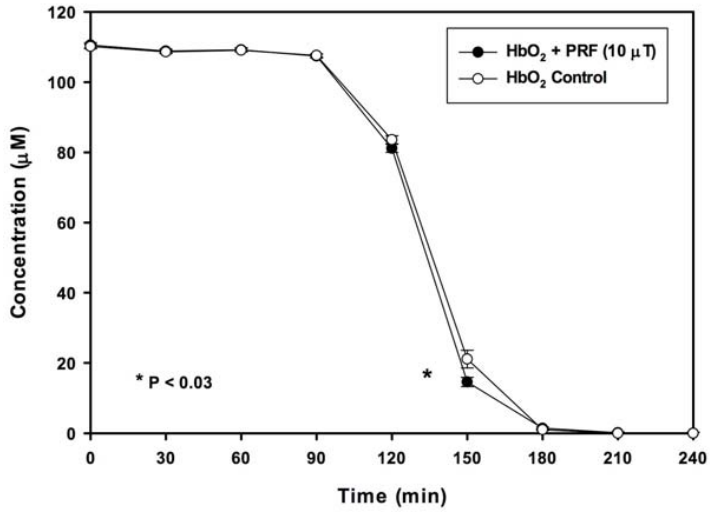

Figure 2. Effect of the pulsed radiofrequency field on time course of hemoglobin deoxygenation. Time course of oxy hemoglobin (HbO_2) concentration, after a single 30 min pulsed radiofrequency electromagnetic field (PRF) exposure of Hb, under deoxygenating conditions. Concentration was determined by visible light spectroscopy at 560, 576, 630 nm. PRF exposure resulted in a significant (30.8 ± 10.3)% reduction in oxyHb concentration, as compared to controls (14.6 ± 1.3 μM vs. 21.1 ± 2.5 μM, $P < 0.03$, $n = 5$), suggesting an alteration in Hb solution properties that persisted after PRF signal was removed.

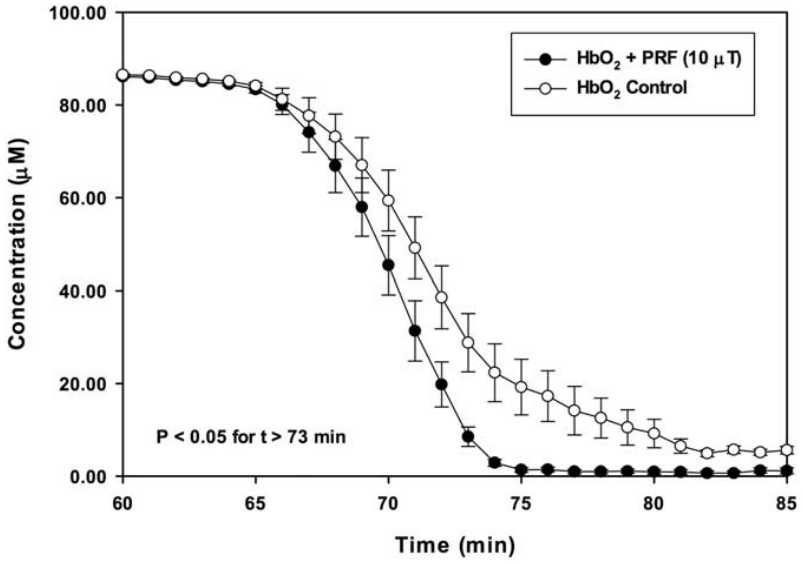

Figure 3. Addition of 5 M urea to reaction mixture. Addition of 5 M urea to the deoxygenation assay reduces the time required for deoxygenation and render the PRF effect more apparent. The maximal difference between PRF-treated and control samples occurred at 73 min, with PRF-treated samples showing a significant (70.4 ± 9.7)% reduction in oxyHb concentration, as compared to controls (8.5 ± 2.1 μM vs. 28.8 ± 6.3 μM, $P < 0.03$, $n = 5$), in contrast to the 30.8% reduction observed in the absence of urea (cf. Figure 2).

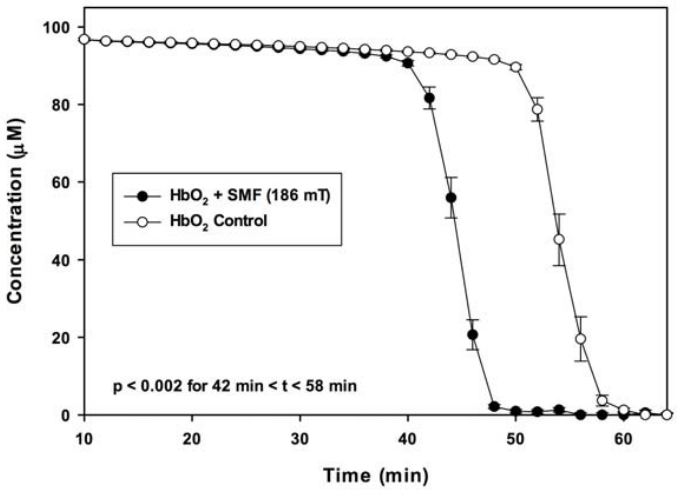

Figure 4. Effect of the static magnetic field on time course of hemoglobin deoxygenation. Hb deoxygenation after 10 min exposure to 186 mT static magnetic field (SMF) in 5M urea. No significant change in oxy/deoxy ratio was visible until the time of rapid deoxygenation, at approximately 40 min. The time of most rapid deoxygenation occurred approximately 10 min earlier for SMF treated samples ($P < 0.002$ for 42 min $< t <$ 58 min, $n = 5$).

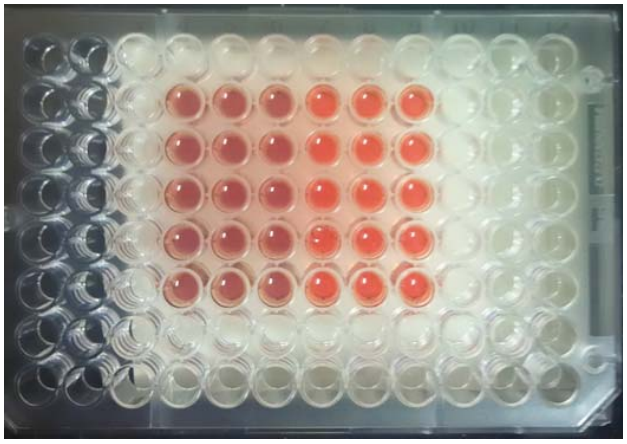

Figure 5. Reaction plate showing that addition of 5M urea to reaction solution renders magnetic field effect more apparent. 96-well spectrophotometer plate shown at 46 min after initiation of reaction of hemoglobin with dithiothreitol (DTT). Samples treated for 10 min with 186 mT static magnetic field (3 left-hand columns in plate) substantially completed (see Figure 4) DTT-induced deoxygenation before untreated samples began to lose O_2, rendering the magnetic field effect visibly apparent.

DISCUSSION AND CONCLUSIONS

The results from this study indicate that exposure to either PRF or SMF, applied independently, can alter the rate of DTT-induced deoxygenation of human Hb in an *in vitro* cell-free preparation, resulting in more rapid conversion of oxyHb → deoxyHb. To the author's knowledge, this is the first report showing that a PRF signal, or independently, a SMF could affect similar outcomes in the same biological system, in the same study. The rate of oxyHb → deoxyHb conversion is non-linear in time and is dependent upon the ratio of DTT/HbO_2. For this assay, the use of DTT as a reducing agent is preferable to other reducing agents, due to the ease with which the time to deoxygenation can be controlled [Herzfeld et al., 1990]. It is interesting to note that a similar EMF sensitivity, for Hb exposed to a GSM mobile phone signal, was observed using sodium dithionite [Mousavy et al., 2009]. This suggests that the action of the EMF is upon a functional aspect of the Hb deoxygenation process itself, and not specific to the reducing agent employed in this study. The observation that EMF pre-treatment of Hb alone, or the deoxygenation solution itself, failed to yield a significant PRF or SMF effect suggests that both the electric and magnetic fields act upon the interaction of Hb with the deoxygenating solution. The addition of 5 M urea reduced the time to deoxygenate and rendered the both the PRF and SMF effects more easily observable. Urea creates an extended cloud of waters that only weakly participates in the hydrogen bonding network of bulk water, facilitating the loosening of the protein structure [Roche et al., 2006] and destabilizing the water-oxyHb structures that act as key allosteric mediators of the Hb T-R transition [Royer et al., 1996], thus reducing the energy required to deoxygenate. However, it is unclear whether the addition of urea affected the primary PRF or SMF transduction or merely renders the EMF effects more easily observable. No differences were observed between 10 and 30 min SMF and PRF treatment durations. Effects were observable several min to several hours after PRF or SMF exposure was removed, suggesting that the induced electric field and/or static magnetic field modifies

protein/solvation structure in a manner that alters the energy required for the oxy-deoxy conformational change.

This study does not provide sufficient evidence to allow details of the EMF mechanisms of action to be elucidated, or to determine if SMF and PRF act upon the same submolecular targets to produce the effects observed here. However, the sensitivity and biochemical simplicity of the assay developed here suggest a new tool that may help to further establish basic biophysical EMF transduction mechanisms. Several models have been proposed for weak, μT-range magnetic field bioeffects [Binhi et al., 2007], and a recent model has been proposed for the interaction of the PRF signal employed here with ion binding sites at a protein's aqueous interfaces via the induced electric field [Pilla et al., 2011]. PRF transduction via the induced electric field is distinct from the transduction pathway involved in SMF effects, for which no electric field is present, suggesting that more than one mechanism may be responsible for the results reported here. Although direct action on the ferrous heme site [Pauling, 1977] and free radical lifetimes may contribute to the SMF effects observed here [Closs 1969; Timmel et al., 1998], we have previously shown via the Lorentz-Langevin model that μT-range magnetic fields may have an effect on the orientation of ionic oscillators and waters bound at the protein surface [Muehsam et al., 2009a, 2009b] and that the minimum magnetic field required to directly compete with thermal forces to affect dissociation of a bound ion or ligand from a protein binding site is in the 1-10 mT-range [Muehsam et al., 1996]. Thus, the effect of the mT-range magnetic field employed in this study could occur via the direct action of the Lorentz force on charges bound at the protein/water interface. Functionally important hemoprotein molecular motions are slaved to the thermal fluctuations of the bulk solvent [Frauenfelder et al., 2009] and protein hydration plays a fundamental role in the stability of dynamics between Hb T-R conformations [Salvay et al., 2003], so that the PRF and SMF interactions described above, acting at the protein/water interface, may suggest a means by which EMF could modulate protein function.

The deoxygenating conditions employed here, using the reducing agent DTT in an *in vitro* cell-free model, differ substantially from those found *in vivo*. However, the EMF-induced changes in structure and function of Hb and erythrocyte suspensions listed above [Tao et al., 2011; Sosa et al., 2005; Shalaby et al., 2006; Sakhnini et al., 2001; Iwasaka et al., 2001; Milweski et al., 2006; Magazù et al., 2009] occurred either *in vivo* or in aqueous solution, in the absence of deoxygenating agents, thus demonstrating an EMF sensitivity under physiological conditions and in the absence of reducing agents. Enhanced delivery of oxygen has been shown to reduce inflammation [Bitterman, 2007] and enhance tissue repair [Tandara et al., 2004] and at least one trial has reported an EMF-induced increase in deoxyHb in an *in vivo* animal model [Milweski et al., 2006]. Allosteric modification of Hb has been suggested as a clinically useful means of enhancing oxygen delivery [Papassotiriou et al., 1998], and is in development for *in vivo* treatment of ischemia from stroke, cardiac disease and diabetic ulcers [Najjar et al., 2005]. Well-known interactions of NO with hemoprotein transition metals [Ignarro et al., 1986; Thomas et al., 2003; Bonaventura et al., 2001] and recent results clearly demonstrating regulation by endothelial Hb alpha of the action of NO on vascular reactivity at the myeloendothelial junction [Straub et al., 2012] and the *in vivo* modulation of Hb oxygen affinity by NO synthase [Zinchuk, 1999] may also suggest that the molecular dynamics exhibited by hemoproteins [Frauenfelder et al., 2009] play an important role in EMF-mediated regulation and maintenance of biological growth and repair processes. Although much further work is required to ascertain the clinical relevance of the results reported here, if an EMF-induced increase in the rate of deoxygenation can be demonstrated *in vivo*, then a resulting enhancement of oxygen delivery may be an important non-invasive, non-pharmacologic therapeutic method by which clinically relevant EMF-mediated enhancement of growth and repair processes can occur.

REFERENCES

Benesch RE, Benesch R, Yung S. 1973. Equations for the spectrophotometric analysis of hemoglobin mixtures. Anal Biochem. 55:245-248.

Bonaventura J, Lance VP. 2001. Nitric Oxide, Invertebrates and Hemoglobin. American Zoologist. 41:346–359.

Binhi VN, Rubin AB. 2007. Magnetobiology: the kT paradox and possible solutions. Electromagn Biol Med. 26:45-62.

Bitterman H. 2007. Oxygen: An Anti-Inflammatory Drug. Isr Med Assoc J. 9:874-876.

Closs GL. 1969. Mechanism explaining nuclear spin polarizations in radical combination reactions. J Am Chem Soc. 91(1969) pp 4552–4554.

Guo F, Friedman JM. 2009. Osmolyte-Induced Perturbations of Hydrogen Bonding between Hydration Layer Waters: Correlation with Protein Conformational Changes. J. Phys. Chem. B 113:16632–16642.

Eccles NK. 2005. A critical review of randomized controlled trials of static magnets for pain relief. J Altern Complement Med 11(3): 495-509.

Fitzsimmons RJ, Gordon SL, Kronberg J, Ganey T, Pilla AA. 2008. A pulsing electric field (PEF) increases human chondrocyte proliferation through a transduction pathway involving nitric oxide signaling. J Orthop Res. 26:854-859.

Frauenfelder H, Chen G, Berendzen J, Fenimore PW, Jansson H, McMahon BH, Stroe IR, Swenson J, Young RD. 2009. A unified model of protein dynamics. Proc Natl Acad Sci USA. 106(13):5129-34.

Herzfeld J, Seidel NE, Taylor MP, Droupadi PR, Wang NE. 1990. Gentle chemical deoxygenation of hemoglobin solutions. Hemoglobin. 14:399-411.

Ignarro LJ, Adams JB, Horwitz PM, Wood KS. 1986. Activation of soluble guanylate cyclase by NO-hemoproteins involves NO-heme exchange. Comparison of heme-containing and heme-deficient enzyme forms. J Biol Chem. 261(11):4997-5002.

Iwasaka M, Miyakoshi J, Ueno S. 2001. Optical absorbance of hemoglobin and red blood cell suspensions under magnetic fields. IEEE Trans Magnetics 37:2906-2908.

Magazù S, Calabrò E, Campo S. 2010. FTIR spectroscopy studies on the bioprotective effectiveness of trehalose on human hemoglobin aqueous solutions under 50 Hz electromagnetic field exposure. J Phys Chem. 114:12144-12149.

Milweski S, Szczepański W. 2006. Effects of electromagnetic fields on the meat performance and wool performance of sheep Arch. Tierz., Dummerstorf 49(Special Issue):219-225.

Mousavy SJ, Riazi GH, Kamarei M, Aliakbarian H, Sattarahmady N, Sharifizadeh A, Safarian S, Ahmad F, Moosavi-Movahedi AA. 2009. Effects of mobile phone radiofrequency on the structure and function of the normal human hemoglobin. Int J Bio Macromolecules 44:278–285.

Muehsam DJ, Pilla AA. 1996. Lorentz Approach to Static Magnetic Field Effects on Bound Ion Dynamics and Binding Kinetics: Thermal Noise Considerations. Bioelectromagnetics 17:89-99.

Muehsam DJ, Pilla AA. 2009b. A Lorentz Model for Weak Magnetic Field Bioeffects: Part II – Secondary Transduction Mechanisms and Measures of Reactivity. Bioelectromagnetics. 30:476-488.

Muehsam DJ, Pilla AA. 2009a. A Lorentz Model for Weak Magnetic Field Bioeffects: Part I -Thermal Noise Is an Essential Component of AC/DC Effects on Bound Ion Trajectory. Bioelectromagnetics. 30:462-475.

Najjar SS, Bottomley PA, Schulman SP, Waldron MM, Steffen RP, Gerstenblith G, Weiss RG. 2005. Effects of a pharmacologically-induced shift of hemoglobin-oxygen dissociation on myocardial energetics during ischemia in patients with coronary artery disease. J Cardiovasc Magn Reson. 7:657-666.

Papassotiriou I, Kister J, Griffon N, Stamoulakatou A, Abraham DJ. 1998. Modulating the oxygen affinity of human fetal haemoglobin with synthetic allosteric modulators. Br J Haematol. 102:1165-1171.

Pauling L. 1977. Magnetic properties and structure of oxyhemoglobin. Proc Natl Acad Sci USA. 74:2612-2613.

Pilla A, Fitzsimmons R, Muehsam D, Wu J, Rohde C, Casper D. 2011. Electromagnetic fields as first messenger in biological signaling: Application to calmodulin-dependent signaling in tissue repair. Biochim Biophys Acta. 1810 1236-1245.

Pilla AA. 2006. Mechanisms and therapeutic applications of time varying and static magnetic fields, in: Barnes F, Greenebaum B editors. Biological and Medical Aspects of Electromagnetic Fields. Boca Raton, CRC Press. pp. 351–411.

Roche CJ, Guo F, Friedman JM. 2006. Molecular level probing of preferential hydration and its modulation by Nosmolytes through the use of pyranine complexed to hemoglobin. J Biol Chem. 281:38757-38768.

Royer WE Jr, Pardanani A, Gibson QH, Peterson ES, Friedman JM (1996) Ordered water molecules as key allosteric mediators in a cooperative dimeric hemoglobin. Proc Natl Acad Sci U S A. 93(25): 14526-31.

Sakhnini L, Khuzaie R. 2001. Magnetic behavior of human erythrocytes at different hemoglobin states. Eur Biophys J. 30:467-470.

Salvay AG, Grigera JR, Colombo MF. 2003. The role of hydration on the mechanism of allosteric regulation: in situ measurements of the oxygen-linked kinetics of water binding to hemoglobin. Biophys J 84(1): 564-70.

Shalaby TE, Shawki MM. 2006. Biophysical and biochemical changes in the characteristics of rat blood exposed to combined alternating and static magnetic fields. Rom. J. Biophys. 16:169-180.

Sosa M, Bernal-Alvarado J, Jiménez-Moreno M, Hernández JC, Gutiérrez-Juárez G, Vargas-Luna M, Huerta R, Villagómez-Castro JC, Palomares P. 2005. Magnetic field influence on electrical properties of human blood measured by impedance spectroscopy. Bioelectromagnetics 26:564-570.

Straub AC, Lohman AW, Billaud M, Johnstone SR, Dwyer ST, Lee MY, Bortz PS, Best AK, Columbus L, Gaston B, Isakson BE. 2012. Endothelial cell expression of haemoglobin α regulates nitric oxide signalling. Nature 491:473–477.

Tandara AA, Mustoe TA. 2004. Oxygen in wound healing--more than a nutrient. World J Surg. 28:294-300.

Tao R, Huang K. 2011. Reducing blood viscosity with magnetic fields. Phys Rev E Stat Nonlin Soft Matter Phys. 84(1):011905.

Thomas DD, Miranda KM, Colton CA, Citrin D, Espey MG, Wink DA. 2003. Heme proteins and nitric oxide (NO): the neglected, eloquent chemistry in NO redox signaling and regulation. Antioxid Redox Signal. 5(3)307-17.

Timmel CR, Till U, Brocklehurst B, McLauchlan KA, Hore PJ. 1998. Effects of weak magnetic fields on free radical recombination reactions. Molecular Physics 95:71-89.

Zinchuk V. 1999. Effect of nitric oxide synthase inhibition on hemoglobin-oxygen affinity and lipid peroxidation in rabbits during fever. Respiration. 66(5):448-54.

b. EMF EFFECTS ON HEMOGLOBIN STRUCTURE AND FUNCTION: PYRANINE FLUORESCENCE AND GADALINIUM^{3+} VIBRONIC SIDEBAND SPECTROSCOPY, INFRARED SPECTROSCOPY, HEMOGLOBIN OXYGEN SATURATION

INTRODUCTION

Upon discovery of the EMF sensitivity of the Hb deoxygenation assay, collaborations were sought in order increase the understanding of the underlying mechanisms. I had the good fortune to be invited to work in three laboratories with expertise and instrumentation in protein structure and function.

Pyranine fluorescence and gadolinium vibrionic sideband luminescence spectroscopy was conducted at the Department of Physiology and Biophysics, Division of Cardiovascular Physiology, Albert Einstein College of Medicine, Bronx, NY, under the direction of Drs. Joel Friedman and Camille Roche. Drs. Friedman and Roche are expert in the biophysics of Hb and protein/solvent interactions. Discussions with Dr Friedman led to the introduction of 5M urea to the Hb deoxygenation assay, resulting in the marked increase in the repeatability and observability of EMF described in the previous Chapter. We hypothesized that the structuring of water, as evidenced by the effect of solvent structure on the stability of proteins in solution [Fonseca et al., 2006; Roche et al., 2006] could play a role in the mediation of EMF effects on Hb. Under excitation at 355 nm, 8-hydroxy-1,3,6-pyrene trisulfonate (HPT) manifests a characteristic fluorescence spectrum in the 400 – 600 nm region, providing information regarding the relative amount of mobile and immobile waters (ns time scale) [Royer et al., 1996; Gow et al., 2005]. The Gd^{3+} vibronic sideband luminescence spectra, in the 342 nm region under 273 nm excitation, reflects hydrogen bond strength between 1st and 2nd shell waters relevant to protein stability [Guo et al., 2009]. Thus, both of these techniques yield information regarding the structuring of waters acting as key allosteric mediators of Hb function [Royer et al., 1996; Salvay et al., 2003].

A second collaboration was initiated at the School of Pharmacy and Pharmaceutical Sciences, Trinity College, Dublin, Ireland, under the supervision of Dr. Astrid Sasse, using attenuated total reflection (ATR) Fourier transform infrared (FTIR) spectroscopy to study the changes in protein structure on Hb structure [Jung, 2000] due to EMF exposure. Dr. Sasse and her staff have expertise in the FTIR spectroscopy and its use in the identification of protein structure and characterization of pharmacological compounds. ATR-FTIR spectroscopy is recently developed set of techniques that obviates some of the difficulties inherent in the short path lengths required transmission FTIR for aqueous samples, and allows for the analysis of a wide range of materials in liquid, solid and powdered forms [Smith et al., 2002]. Previous effects reported due to EMF exposures of Hb and human serum albumin [Magazu et al., 2010, 2011] suggested that EMF-induced changes in Hb structure could be observable using ATR-FTIR methods.

In addition, the effect of a SMF on Hb equilibrium oxygenation saturation (SO_2) was assessed at the Laboratory of Biochemistry and Molecular Biology, Ospedale San Paolo, Milano, under the direction of Drs. Michele Samaja and Rosaria Russo. Dr. Samaja's expertise is in biochemistry and physiology and is recognized as a leading expert in Hb biochemistry and hematology. This study addressed the issue of the clinical relevance of the EMF effect found in our deoxygenation assay by using a partial pressure method [Bohr et al., 1904] to determine if a SMF could directly alter SO_2. We hypothesized, based upon observations of changes of Hb oxygen affinity due to EMF exposures [Shigina, 2002; Mousavy et al., 2009], that a SMF might alter the oxygen saturation SO_2 of Hb in a solution held at partial saturation in a gas-controlled environment.

MATERIALS AND METHODS

HPT Fluorimetry and Gd^{3+} Vibronic Sideband Spectroscopy: Stock solutions of the HPT probe were prepared according to the methods of [Roche et al., 1996].

Buffer solutions were degassed with nitrogen for 30 min, then deoxy-Hb was prepared from a 100 μM (heme) solution of oxy-Hb (in degassed buffer: 0.05 M BisTris OAc or 50 mM Hepes, pH 7.2) by adding sodium dithionite (2X heme) to deoxygenate. HPT was then added to the resulting deoxy-HbA solution in a ratio of 1:1 (per molecule, in Hb tetramer, 0.25 heme concentration, per volume = 3:1000, resultant Hb concentration = 100 μM due to mM-range concentration of HPT probe). All solution preparation was performed in a nitrogen atmosphere, and cuvettes were sealed throughout all experiments. Fluorescence spectra were obtained at 1 nm resolution using a modular PTI Fluorescence system (Photon Technology Inc., Lawrenceville, NJ). Spectra were generated using the following experimental settings: an excitation wavelength of 355 nm, 1-mm slit width for excitation and emission slits, and an integration time of 0.5 or 1 s at ambient temperature = 22° C. Samples were placed in an optical cuvette with 1-mm path length, with the instrument configured for front face emission [Hirsch et al., 1994]. The integrity of the protein was verified by visible light spectroscopy before, during, and after experimental procedures, to ensure that the ligation state of the heme did not change during the time course of the experiment. Gadolinium vibronic side band luminescence spectra were measured at 0.25 nm resolution in a QuantaMaster model QM-4/2000SE enhanced performance scanning spectrofluorometer (Photon Technology International, Lawrenceville, NJ). The Gd^{3+} concentration in all probed solutions was 100 mM. Samples were held in the quartz cuvette and placed in the sample chamber in the configuration for 90° excitation. The emission profiles were recorded with the excitation of 273 nm, and luminescence was recorded from 290 to 400 nm. The step size was set to 0.25 nm. Each spectrum measurement was repeated at 10-25 times and averaged. For experiments with EMF exposures, samples were placed into two cuvettes, and immediately subjected to spectrographic measurement. EMF treated samples were exposed for 15-30 min to either the ambient geomagnetic field, or ambient plus a SMF generated by permanent ceramic magnets to produce an amplitude of 150 mT (Magnetherapy, West Palm Beach, FL). 15-30 min exposures were also made using a 27.12 MHz PRF (Ivivi Health Sciences, LLC, San Francisco) transmitted

in 4 ms bursts, repeating at 5 Hz (PRF). Both EMF-exposed and control samples were covered with optical cloth to shield fluorescence probes from light contamination. Sample spectra were collected immediately after 15 min and measured again at subsequent 15 min intervals. In order to have the ability to observe the relative change of two spectral peaks, initial trials with the HPT probe were performed in 50% glycerol. Subsequent trials added 100 mM MgCl2 [Feng, 2009] to 50% glycerol, or used 5 M urea, in either Tris or Hepes buffers, and also observed the time series of Hb deoxygenation in 30 mM dithiothreitol (DTT) in 50 mM hepes buffer. Trials using Gd^{3+} employed only SMF exposures. All experiments were controlled at pH 7.2. *Infrared Spectroscopy:* Stock solutions of 1 mM human Hb in 50 mM Hepes (pH 7.2) or Hepes + 5M urea were divided into 1 mL aliquots in sealed 1.5 mL Eppendorf tubes. 5 tubes were designated as controls, exposed only to ambient conditions in the laboratory and 5 tubes were designated to be EMF treated for 3 – 21 hrs to either the ambient field, or ambient plus a 150 mT SMF generated by permanent ceramic magnets. All controls and samples were at the same 23° C temperature, approximately 3 m distant on the same lab bench. Exposures were also made using a 10 μT, 27.12 MHz pulse-modulated radiofrequency EMF (Ivivi Health Sciences, LLC, San Francisco) transmitted in 4 ms bursts, repeating at 5 Hz. ATR-IR spectra of samples were analysed (Perkin Elmer Spectrum One infrared spectrophotometer with ATR accessory) immediately after EMF treatment. 30 μL aliquots from each tubes were placed in the ATR assembly and spectra from each tube were recorded 10-25 times and then averaged by the spectrophotometer software. After averaging the Hb spectra, the solvent spectrum, similarly averaged, was then subtracted [Barth, 2007; Damian et al., 2005]. Spectra were compared for Hb samples exposed to the PRF and SMF conditions for durations of 3 – 21 hrs. *Hemoglobin Oxygen Saturation:* A specialized apparatus consisting of a glass chamber joined smoothly to an optical cuvette was employed for observing spectrophotometrically the oxidation state of hemoglobin (Arbore Cataldo 8NC, Milano, Italy), see Photo 1. Nitrogen gas passed through the chamber for 30 min and then the chamber was sealed. Total chamber + cuvette volume 159.19 mL. 1

mL of hemoglobin solution consisting of 0.5 mM Hb in PBS was injected into the chamber and mixed smoothly for 10 min to allow for deoxygenation. The ratio of oxyHb/deoxyHb (SO_2) was determined via the method of Benesch et al., 1973, from the optical densities optical densities at 540, 560 and 576 nm. After 10 allowing min for equilibration SO_2 was = 0.048 ± 0.01. To raise SO2, 7.5 mL of air was injected into the cuvette, resulting in a stable value of SO_2 = 0.32 ± 0.001. All changes in SO_2 required gentle manual mixing of the Hb sample within the chamber portion of the chamber/cuvette assembly. After mixing, the apparatus was held in an upright position to allow the Hb sample to flow into the optical cuvette. SMF exposure was made by sandwiching the optical cuvette between 5 ceramic magnets placed in a pole-assisting configuration, producing a SMF of approximately 150 mT inside the cuvette. The Hb solution was exposed for 10 min, then the magnets were removed and the cuvette placed as quickly as possible into the spectrophotometer. Measurements of SO_2 were made using optical densities at 540, 560 and 576 nm, immediately after placing the cuvette in the spectrophotometer (time = 0) and at 1, 2, 3, 9, and 11 min later. A second 10 min SMF exposure was made, and measurements take immediately post-exposure and 30, 90, 150, and 210 s later. Calibration experiments performed using DTT to deoxygenate Hb in an optical cuvette showed that only portion of the sample at the top of the optical column underwent deoxygenation, indicating that exposure of the sample to air was in fact necessary to initiate deoxygenation (data not shown). Assessment of the effects of handling the gas chamber/cuvette were also made by performing measurements at 2 min intervals before and after gently mixing the Hb sample in the chamber portion of the apparatus and then allowing positioning the apparatus such that the Hb sample flowed back into the cuvette.

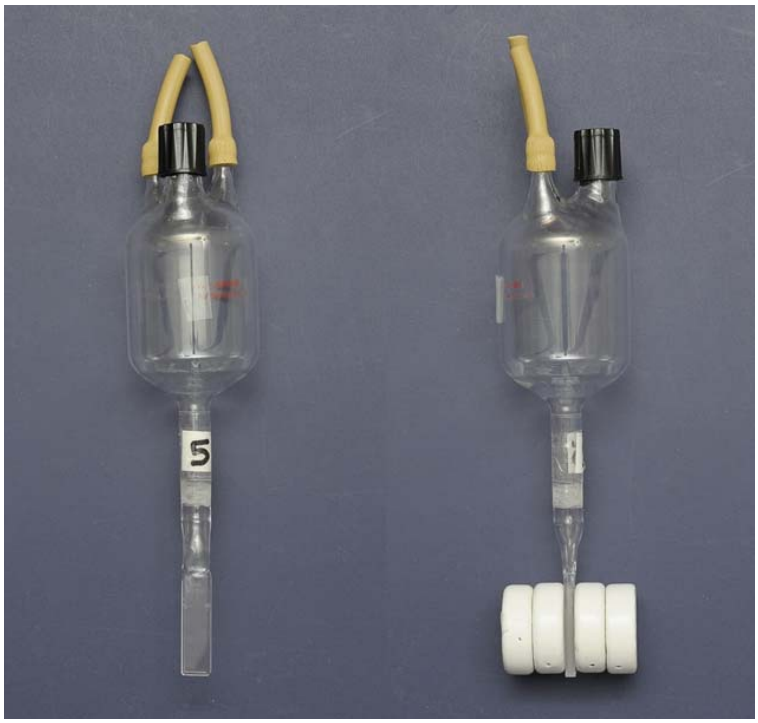

Photo 1: Specialized device for measuring Hb SO_2 under gas-controlled conditions. Chamber was evacuated and oxygen replaced with nitrogen gas, and Hb then injected into chamber and thus deoxygenated. SO_2 could be controlled by injecting aliquots of oxygen into the chamber **Left:** SO_2 assessed spectrophotometrically with liquid sample in cuvette region at bottom of device. **Right:** Magnetic field exposure was performed by placing magnets on either side of cuvette region. Magnets were held in place by pole-assisting configuration.

RESULTS

HPT Fluorimetry and Gd^{3+} Vibronic Sideband Spectroscopy: No differences in fluorescence spectra were observed between control and both SMF- and PRF-treated samples for the HPT probe in 50 mM BisTris OAc, at pH 7.2, or with the addition of 5 M urea, 50% glycerol or 10 mM $MgCl_2$, thus confirming the viability of using this method for assessing EMF effects on protein/hydration

structure. For our first trials, glycerol was chosen as a solvent due to the characteristics twin-peak spectrum in the 450 - 510 nm region, allowing for assessment of the ratio of two peaks, rather than the single 510 nm peak [Roche et al., 2006]. For 30 min SMF exposures of 100 μM deoxyHb in 50% glycerol, no changes were found in spectra for control vs. SMF exposures, as shown in Figure 1, left hand plot. Spectra shown are normalized to height of peak at 510 nm. For these conditions, the maximum difference in F/F_o for SMF exposures of 0.019 was one the same order of maximal difference of 0.021 observed for the untreated control from same stock solution. Figure 1, right hand plot shows similar results with the addition of 100 mM $MgCl_2$ [Guo et al., 2009], also in 50% glycerol, and again no differences between SMF and control exposure was observed. For these conditions, the maximum difference in F/F_o for SMF exposure of 0.018 was less again than the maximal difference of 0.045 observed for the untreated control from same stock solution. These trials were repeated a 2^{nd} time, with similar results, and the decision was made not to perform further repetitions. In order to test the hypothesis that an EMF effect might be rendered more visible through the addition of urea to the solution, trials were performed using 30 min SMF exposure of 100 μM deoxyHb in 5M urea using 50 mM Tris buffer under the same conditions as the previous experiment. The results, shown in Figure 2 let hand plot, again showed no changes in spectra between pre- and post-SMF exposures. For these conditions, the maximum difference in F/F_o for SMF exposures of 0.018 was on the same order of the maximal difference of 0.012 observed for the untreated control from same stock solution. Similar trials were performed in this reaction mixture, using a 30 min PRF exposure. The results, shown in Figure 2, right hand plot, again showed no differences between PRF exposed and control. For these conditions, the maximum difference in F/F_o for PRF exposure of 0.016 was on the same order of the maximal difference of 0.012 observed for the untreated control from same stock solution. These trials were also repeated, again with similar results, and the decision was made not to perform further repetitions. For all the trials with Hb in the HPT probe, the normalized spectra are pixel-for-pixel identical, as can be seen in Figures 1 and 2. Similar trials were performed

using 50 mM Hepes buffer, pH 7.2, but substantial variability in amplitudes of spectra were observed, which changed with time and mechanical agitation of the solutions. Difficulties encountered with Hepes buffer had been previously observed and attributed to an interaction or 'stacking' of the ring structures of Hepes and the HPT probe [Dr. Camille Roche, personal communication, 2012]. Similar experiments were performed for Gd^{3+} vibronic sideband spectra, using 100 μM deoxyHb in 5M urea, again in Tris 50 mM Tris buffer, pH 7.2. As shown in Figure 3, left hand plot, the Gd^{3+} spectra showed no differences between before and after a 30 min SMF exposure. For these conditions, the maximum difference in F/F_o for SMF exposure of 0.024 was on the same order of the maximal difference of 0.021 observed for the untreated control from same stock solution. Figure 3, right hand plot, shows the behaviour of the untreated control sample after 30 minutes, illustrating that the slight broadening of the peak occurred for controls as well as SMF treated samples (to better illustrate this, Figure 3 is presented with symbols on the data points, rather than using lines as in the previous Figures). For these conditions, the maximum difference in F/F_o of 0.024 for the untreated control from same stock solution after 30 min was on the same order of the maximal difference of 0.021 upon initial registration of the spectrum. For these experiments using Gd_{3+} spectra, the peak of the vibronic sideband spectrum always occurred either at 341.75 or 342.00 nm. These trials were repeated for 30, 60 and 90 min SMF exposures, with similar results, and the decision was made not to perform further repetitions.

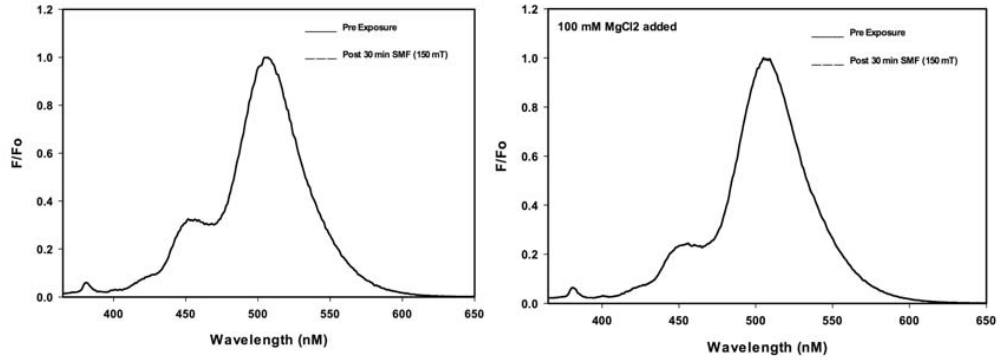

Figure 1. Left: HPT fluorescence spectra for 100 μM deoxyHb in 50% glycerol and 50 mM Tris buffer, pH 7.2, for control and SMF exposed samples, shown before and after a 30 min SMF exposure. Spectra read immediately after SMF exposure show no differences between exposed and control samples. **Right:** Similar results were found with the addition of $MgCl_2$ to the Hb solution.

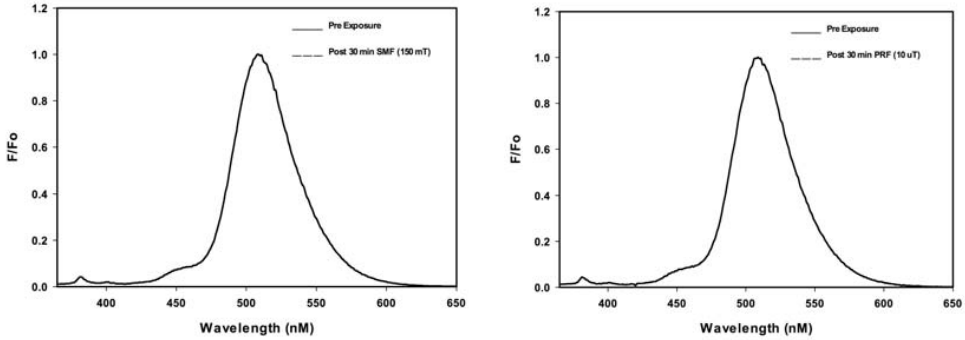

Figure 2: Left: HPT fluorescence spectra for 100 μM deoxyHb in 5 M urea and and 50 mM Tris buffer, pH 7.2, for control and SMF exposed samples, shown before and after a 30 min SMF exposure. Spectra read immediately after SMF exposure show no differences between exposed and control samples. **Right:** Similar results were found with 30 PRF exposure using the same reagent mixture.

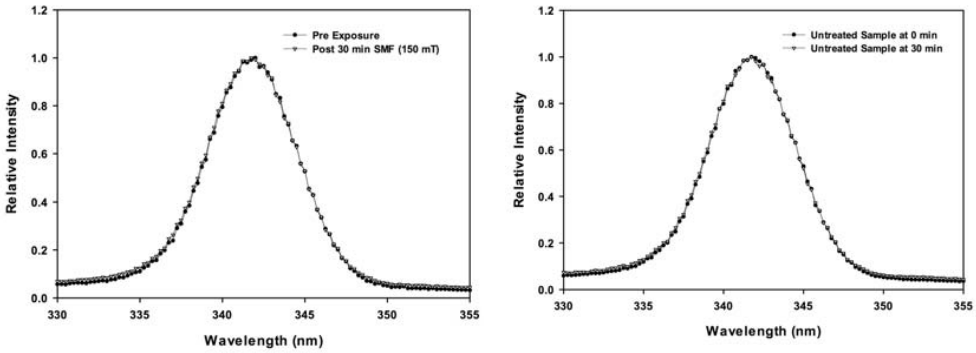

Figure 3. Left: Effect of 30 min 150 mT SMF exposure on Gd^{3+} vibronic sideband spectra, using 100 μM deoxyHb in 5M urea and Tris 50 mM Tris buffer, pH 7.2. Results show no effect of SMF exposure on vibronic sideband structure indicative of hydrogen bonding strength between 1st and 2nd shell hydration layers. **Right:** Vibronic sideband spectra of untreated sample, from same stock solution, illustrating the slight broadening with time of the sideband peak, which occurred for both SMF-treated and untreated controls. Results show no changes due to SMF exposure, after field is removed.

Infrared spectroscopy: The Perkin Elmer ATR apparatus employed here produced repeatable spectra of Hb in solution corresponding to those found previously [Magazu et al., 2010] that allowed for the discrimination Hb contribution to IR spectra above that of the solvent. For example, calibration experiments showed that the double peak in the Amide A band in the 3400 – 3200 cm^{-1} region was clearly resolved (data not shown), in accord with without requiring the use of curve-fitting or iterative methods such as concave rubberband corrections [Magazu et al., 2010]. Of particular interest are the Amide I–VI peaks in the 1700 - 1000 cm^{-1} region, used most commonly for investigating the secondary structure of proteins [Van deWeert et al., 2005]. For a 3 hr SMF exposure, in 50 mM Hepes

buffer, pH 7.2, Figure 4, left hand plot shows the IR transmittance spectra in the Amide I-II band, for the average of 5 tubes for exposed and control samples, after subtraction of the solvent contribution, normalized to the height of the Amide II peak (largest peak). An apparent difference in transmittance across the spectrum suggest an effect of the SMF exposure, and the change is significant in the 1580 – 1607 nm Amide Amide I-II region ($P < 0.05$, $n = 5$). Figure 4 right hand plot shows the data from the repetition of this same experiment, where significant changes in transmittance occurred also in the Amide I-II region ($P < 0.03$, $n = 5$). However, the change in amplitude occurs in the opposite direction for SMF-exposed and untreated samples. Also, changes in the width of the Amide I and II bands were also in opposite directions for these 1st and 2nd trials. In addition, although for each these two trials there is a change in the ratio of Amide I-II as compare to Amide III-VI, these ratios also change in opposite directions for the two trials. Both the normalized and un-normalized spectra exhibit these changes in amplitudes between the two trials. Thus, the difference spectra, a fingerprint of conformational change [Barth, 2007] have amplitudes in opposite directions for these experiments, again suggesting that any changes in amplitude that might have occurred due to SMF exposure were smaller than the variability of the assay itself. Analogous results hold for the 2nd derivative spectra of smoothed data and for the above analyses of the Amide A band in the 3400 – 3200 cm^{-1} region. In response to these data, and in hopes of magnifying EMF sensitivity, as in the Hb deoxygenation assay, we conducted further trials with 5M urea added to the Hb solution. The stability of the IR spectra was much greater with the addition of 5 M urea, allowing for repeatable measurements (Figure 5). It is of interest to note the marked smoothing of the spectrum of the protein in 5M urea, and appearance of a characteristic peak at approximately 1150 cm^{-1}, corresponding to changes in the hydrogen bonding behaviour of the solution [Barth, 2007; Roche, et al., 2006], as can be seen in Figure 5. Figure 5, left hand plot shows the Amide I–VI region for a 30 min SMF exposure, as compared to the unexposed control. No significant differences in transmittance occur throughout the Amide I-IV region ($P > 0.53$, $n = 5$). Figure 5, right hand plot show the same conditions for a 60 min PRF

exposure. Again, no significant differences in transmittance occur throughout the Amide I-IV region ($P > .21$, $n = 5$). For both SMF and PRF exposures, the transmittance varied by less than 0.5% at all points in the Amide I-VI region. Similar results held for these trials in the Amide A band.

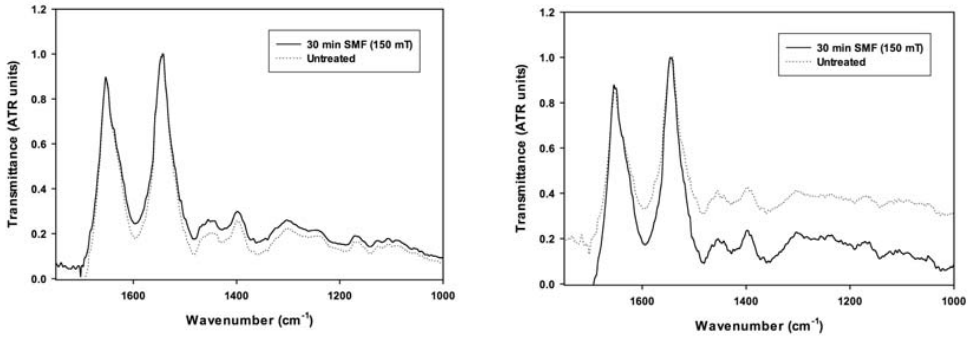

Figure 4: Repetition of experiment shows assay variability in IR transmittance spectra, for Hb in 50 mM Hepes buffer, pH 7.2, i.e., in the absence of urea. **Left:** Normalized infrared spectra of the Amide I-VI region, used most commonly for investigating the secondary structure of proteins, of Hb FTIR spectra for 30 minute SMF exposure, as compared to unexposed samples, with solvent sample subtracted. Apparent change in amplitude across the Amide I-VI region suggests an SMF effect. **Right:** Repetition of first experiment shows mean amplitude changed in opposite direction, suggesting that any putative SMF effect is smaller than the experimental error of our assay. Note that, as shown below, the addition of urea greatly stabilizes the Hb IR spectra.

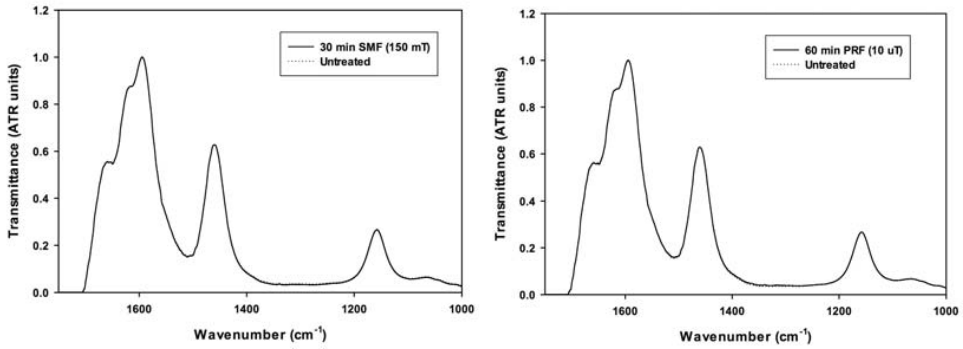

Figure 5. Left: Normalized infrared transmittance spectra of the Amide I–VI region for 30 min SMF exposure of 1 mM Hb in 5M urea and 50 mM Hepes buffer, pH 7.2. No significant differences in transmittance occur throughout the Amide I-IV region ($P > 0.53$, $n = 5$). **Right:** Normalized spectra of 1 mM Hb in 5M urea and 50 mM Hepes buffer, pH 7.2for 1 hr PRF exposure, with the same reagent mixture. Again, no significant differences in transmittance occur throughout the Amide I-IV region ($P > .21$, $n = 5$). Both experiments were repeated with similar results.

Hemoglobin oxygen saturation: Measurements of SO_2 according to the time series described in the Methods section are shown in Figure 6. 95% confidence intervals are shown using dotted lines, and the solid line is a linear regression on the data (Rsqr = .24). The results show that changes in Hb SO_2 due to 10 min SMF exposures were within the variability of the time series examined, as shown in Figure 6, left hand plot. Figure 6, right hand plot shows that changes in SO2 due to removing the chamber/cuvette device from the spectrophotometer were also within the variability of the time series data (Rsqr = .83). However, comparison of the two plots in Figure 6 shows that the effects of mixing were on

the same order of greater than those observed after SMF exposure. As a result of these observations, the choice was made to discontinue these experiments.

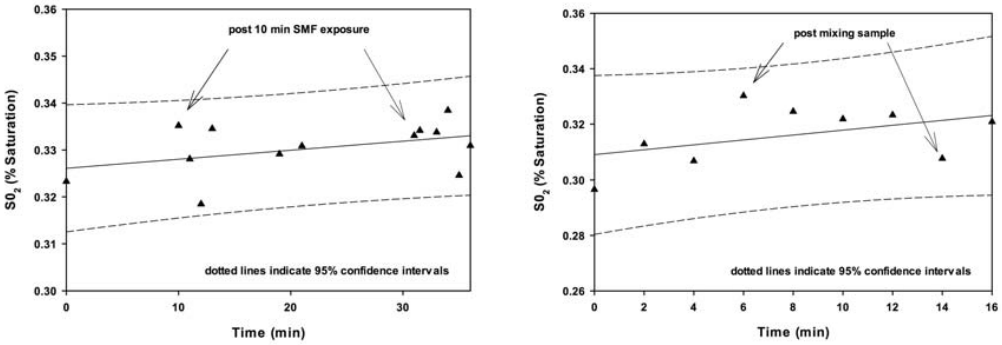

Figure 6. Left: Time series of Hb SO_2 with two 10 min SMF exposures. Changes in SO_2 after SMF exposure are within the variability of the assay. **Right:** Variability of Hb SO_2 assay, with mixing and gentle shaking of sample. Results show that variability due to handling is on the same order as variability due to SMF exposures, and suggest that a more sophisticated apparatus is needed to allow for mixing and the addition/removal of EMF devices.

DISCUSSION AND CONCLUSIONS

The HPT probe was shown to be insensitive to EMF in Tris buffer, suggesting its use for assessment of EMF effects in protein solution. HPT fluorescence spectroscopy showed no effects on Hb in Tris buffer, suggesting that exogenous EMF does not alter the relative amount of mobile and immobile waters on a ns time scale, in solution. Observed EMF effects on Hb deoxygenation could thus be due to an effect on protein internal structure, rather than allosteric mediation of oxy/deoxy conversion by solvation structure. The instability of HPT spectra in hepes suggests that this buffer is not suitable for assessing water structure with

HPT or Gd^{3+}. The short ns-scale relaxation time of water polarization [Royer et al., 1996], and instability of the Gd3+ assay suggests the need to generate EMF exposure directly inside the spectrophotometer. The consistency of the negative results found for the ATR-FTIR experiments suggest that under the conditions employed here, no significant changes in spectra occurred. In the absence of urea, the Hb FTIR spectra showed greater variability than apparent changes due to SMF exposure. Furthermore, the close correspondence of the control and EMF-treated difference and derivative spectra ($P > 0.53$, $n = 5$ for all experiments) in the presence of urea (which greatly enhanced EMF effect on DTT-induced deoxygenation), suggests that ATR-FTIR spectra do not reflect that changes in Hb solution properties that occurred in the presence of DTT. The results clearly obviate the use of deconvolving techniques, whose purpose is to render more information regarding specific frequencies at which significant spectral changes occur [Van deWeert et al., 2005]. Variations in Hb SO_2 after SMF exposure were on the same order as the variability due to mixing in the chamber/cuvette assembly. Because manual mixing is required to stabilize SO_2 after modifying gas pressure, and deoxygenation in the optical cuvette required exposure to the ambient gaseous environment, it is insufficient to expose the Hb in the restricted volume of the optical cuvette. This, suggests the need to develop a specialized device that allows a constant perfusion of the Hb sample through the gaseous environment during EMF exposure.

Although the studies performed here were unable to detect EMF-induced changes in Hb structure and function, further development of the techniques used here may provide insight into the biophysical mechanisms responsible for the EMF effects we observed in DTT/Hb deoxygenation. Because of the short lifetimes of the substates of the Hb T-R transition [Hub et al., 2010], and brief relaxation times of protein conformations and hydration structures [Royer et al., 1996; Juszczak et al., 1999], it is possible if EMF effects occur during field exposure, these are rapidly stabilized upon removal of the field exposure. Thus, the three studies undertaken here collectively suggest the necessity of real-time exposure systems to assess

EMF effects on Hb structure and function. Specialized equipment for single-wavelength excitation and detection of fluorescence and vibronic sideband spectra could be constructed. Non-metallic fiber-optic techniques would allow detection of spectra, while EMF generation occurred during excitation. Similarly, a non-metallic ATR-FTIR device could be constructed to allow real-time assessment of IR spectra during EMF exposure. Indeed, a relatively new technique for providing rapid, noninvasive and reliable in vivo estimation of Hb SO_2, using laser Raman spectroscopy [Torres Filho et al, 2008] may be adaptable to real-time in vivo EMF exposures.

REFERENCES

Barth A. 2007. Infrared spectroscopy of proteins. Biochim Biophys Acta. 1767(9):1073-101.

Bohr C, Hasselbalch KA, Krogh A. Ueber einen in biologischer Beziehung wichtigen Einfluss den die Kohlen-sauerspannung des Blutes aufdessen Sauerstoffbindung ubt. Skand Arch Physiol 1904;15:401–412.

Damian G, Canpean V. 2005. Conformational changes of bovine hemoglobin at different pH values, studied by ATR FT-IR spectroscopy, Romanian J. Biophys. 15:67–72.

Fonseca LC, Corrêa NCR; Da Silva Garrote-Filho M, Da Cunha CC, ; Penha-Silva N. 2006. Effect of the solvent composition on the stability of proteins in aqueous solutions. Quím. Nova vol.29(3):533-548.

Gow AJ, Payson AP, Bonaventura J. 2005. Invertebrate hemoglobins and nitric oxide: how heme pocket structure controls reactivity. J Inorg Biochem. 99(4):903-11.

Guo F, Friedman JM. 2009. Osmolyte-Induced Perturbations of Hydrogen Bonding between Hydration Layer Waters: Correlation with Protein Conformational Changes. J. Phys. Chem. B 113:16632–16642.

Hirsch, R.E. 1994. Front-face fluorescence spectroscopy of hemoglobins. Methods Enzymol. 232, 231–246

Hub JS, Kubitzki MB, de Groot BL. 2010. Spontaneous quaternary and tertiary T-R transitions of human hemoglobin in molecular dynamics simulation. PLoS Comput Biol. 6(5):e1000774.

Jung C. 2000. Insight into protein structure and protein-ligand recognition by Fourier transform infrared spectroscopy. J Mol Recognit. 13(6):325-51.

Juszczak LJ, Friedman JM. 1999. UV resonance raman spectra of ligand binding intermediates of sol-gel encapsulated hemoglobin. J Biol Chem. 274(43):30357-60.

Magazù S, Calabrò E, Campo S. 2010. FTIR spectroscopy studies on the bioprotective effectiveness of trehalose on human hemoglobin aqueous solutions under 50 Hz electromagnetic field exposure. J Phys Chem B. 114(37):12144-9.

Magazù S, Calabrò E. 2011. Studying the electromagnetic-induced changes of the secondary structure of bovine serum albumin and the bioprotective effectiveness of trehalose by Fourier transform infrared spectroscopy. J Phys Chem B. 115(21):6818-26.

Mousavy SJ, Riazi GH, Kamarei M, Aliakbarian H, Sattarahmady N, Sharifizadeh A, Safarian S, Ahmad F, Moosavi-Movahedi AA. 2009. Effects of mobile phone

radiofrequency on the structure and function of the normal human hemoglobin. Int J Bio Macromolecules 44:278–285.

Roche CJ, Guo F, Friedman JM. 2006. Molecular level probing of preferential hydration and its modulation by osmolytes through the use of pyranine complexed to haemoglobin. J Biol Chem. 281(50):38757-68.

Royer WE, Pardanani A, Gibson QH, Peterson ES, Friedman JM. 1996. Ordered water molecules as key allosteric mediators in a cooperative dimeric hemoglobin. PNAS 93(25)14526-14531.

Salvay AG, Grigera JR, Colombo MF. 2003. The role of hydration on the mechanism of allosteric regulation: in situ measurements of the oxygen-linked kinetics of water binding to hemoglobin. Biophys J. 84(1):564-70.

Shigina NA. 2002. Changes in oxygen affinity for hemoglobin during exposure to low frequency magnetic field and low energy laser radiation. Fiziol Cheloveka. 28(5):134-6. (Article in Russian)

Smith BM, Franzen S. 2002. Single-pass attenuated total reflection Fourier transform infrared spectroscopy for the analysis of proteins in H2O solution. Anal Chem. 74(16):4076-80.

Torres Filho IP, Terner J, Pittman RN, Proffitt E, Ward KR. 2008. Measurement of hemoglobin oxygen saturation using Raman microspectroscopy and 532-nm excitation. J Appl Physiol. 104(6):1809-17.

Van de Weert M, Hering JA, Haris PI. 2005. Fourier Transform Infrared Spectroscopy. In: Jiskoot W, Crommelin D, (Eds.) Methods for Structural Analysis of Protein Pharmaceuticals. USA: Springer. pp. 131-166.

Yonetani T, Laberge M. 2008. Protein dynamics explain the allosteric behaviors of hemoglobin. Biochim Biophys Acta. 2008 1784(9):1146-58.

4. THEORETICAL MODELLING

a. LORENTZ MODEL FOR MAGNETIC FIELD BIOEFFECTS: APPLICATION TO BOUND WATERS VIA GIBBS FREE ENERGY AT SURFACE OF A BIOMOLECULE; CORRESPONDENCE TO PREDICTIONS OF ION PARAMETRIC RESONANCE MODEL

INTRODUCTION

The mechanisms by which extremely low frequency (ELF) microTesla-range magnetic fields can directly influence biological processes are now coming under clearer review [Milyaev et al., 2006; Binhi et al., 2007; Machlup, 2007; Muehsam et al., 2009a]. Early speculations that ion and ligand binding may serve as primary transduction pathways for DC and ELF magnetic field effects [Bawin et al., 1975, 1976; Blackman et al., 1982; Smith, 1987; Liboff et al., 1987, 1988, 2003; Lednev, 1991; Chiabrera et al., 1985, 1992; Edmonds, 1993; Muehsam et al., 1994, 1996; Pilla et al, 1997] have been supported by further evidence of well-defined resonance frequencies [Zhadin et al., 1998; Zhadin 1990; Pazur 2004] and supported by additional theoretical modelling [Ramundo-Orlando et al., 2000; Zhadin et al., 2005; Binhi et al., 2007; Muehsam et al., 2009a, 2009b]. Ca^{2+}/CaM binding serves as a model ion binding pathway for the consideration of models for ELF magnetic field effects. In addition to the experimental evidence supporting EMF effects on systems modulated by this pathway [Shuvalova et al., 1991; Bull et al., 1993; Markov et al., 1992, 1993, 1997; Liboff et al., 2003], Ca^{2+}/CaM binding possesses biochemical and biophysical properties that suggest it as a likely EMF-sensitive target. Ca^{2+}/CaM binding is kinetically asymmetrical, i.e., the rate of binding exceeds the rate of dissociation by several orders of magnitude ($k_{on} >> k_{off}$), driving the reaction in the forward direction. Ca^{2+}/CaM binding has been well characterized, with the binding time constant reported to be in the range of 10^{-2}-10^{-3} sec [Blumenthal and Stull, 1982]. In contrast, release of Ca^{2+} from CaM cannot occur until cNOS has converted L-arginine to citrulline and NO,

which takes the better part of a second [Daff, 2003]. Thus, the time scale for binding is too short for effects due to weak, μT-range magnetic fields, which generally require a target lifetime on the order of the Larmor or cyclotron period, measured in hundreds of ms for ELF exposures [Lednev, 1991; Binhi 2002; Muehsam et al., Muehsam et al., 2009a, 2009b]. Thus, the long bound lifetimes on the order of 1 s observed for Ca^{2+} binding to CaM [Cox, 1988; Daff, 2003] suggest a physically reasonable target for weak ELF magnetic field interactions.

One of the challenging aspects of formulating theoretical models for weak ELF magnetic field bioeffects has been the so-called 'kT-Problem' [Binhi et al., 2007; Machlup, 2007]. The 'kT-Problem' refers to the difficulties inherent in the formulation of models for ELF interactions for which the molecular energy of interaction is less than that of the mean thermal noise. In the light of the large and steadily growing body of such nonthermal EMF bioeffects, a number of theoretical models have been developed describing thermal noise limits for EMF interactions [Weaver et al., 1990; Chiabrera et al., 1992; Edmonds, 1993; Muehsam et al., 1994, 1996; Binhi et al., 2003, 2007; Machlup, 2007]. A more detailed description of several of these models for weak ELF magnetic field effects may be found in one of my more recent publications [Muehsam et al., 2009a]. This 'kT-Problem' has also led to some controversy, and even to attempts to argue against the existence weak ELF effects on theoretical grounds [Adair, 1991, 1997], despite the experimental data at hand. However, despite the controversy, there is a large and continually growing body of experimental evidence that weak ELF magnetic fields can cause bioeffects [Bersani, 1999; Binhi, 2002], and the results, taken collectively are difficult to dismiss out of hand. Interestingly, and perhaps not so well-known to scientists in the West, is the more than 130 years of research into bioeffects of static and low-frequency magnetic fields documented in Russia and the former Soviet bloc [Zhadin, 2001].

THE LORENTZ MODEL

In response to the 'kT-Problem,' my earlier publications suggested that, rather than posing an obstacle to EMF detection, thermal noise forces could play an essential role in the detection of magnetic field [Muehsam et al., 1994, 1996; Pilla et al, 1997]. To summarize briefly the basics of the model from Muehsam et al., 2009a, the Lorentz-Langevin equation of motion for a charged species such as an ion or ligand bound in a binding site represented by a harmonic oscillator potential, subject to a DC magnetic field oriented up along the *z*-axis, and in the presence of thermal noise is [Chiabrera et al., 1992]:

$$\frac{d^2r}{dt^2} = -\beta\frac{dr}{dt} + \gamma\left[\frac{dr}{dt} \times B_o\right]k - \omega^2 r + n \qquad \textbf{(1)}$$

Where r is the position vector of the particle; β is the viscous damping coefficient per unit mass (due to molecular collisions in the thermal bath), γ is the target charge-mass ratio; B_o is the magnitude of the magnetic field vector; k is the unit vector along the z-axis; ω is the angular frequency of the oscillator and n is the stochastic thermal noise force vector per unit mass.

A closed form solution to Equation 1 may be found, and adopting the notation of Chiabrera et al., 1992, in the complex plane, the thermal component of the motion *P(t)* is given by:

$$P(t) = e^{-i\omega_L t} Y(t)\,, \qquad \textbf{(2)}$$

and thus undergoes a rotation within the binding site at the Larmor angular frequency $\omega_L = B_o\gamma/2$, bounded by the complex-valued accumulation term *Y(t)*:

$$Y(t) = \frac{e^{-\frac{\beta}{2}t}}{\lambda_2 - \lambda_1}\left[e^{-\frac{\sqrt{\alpha^2-4\omega^2}}{2}t}\int_0^t e^{-\lambda_2\tau}\, n(\tau)\,d\tau - e^{\frac{\sqrt{\alpha^2-4\omega^2}}{2}t}\int_0^t e^{-\lambda_1\tau}\, n(\tau)\,d\tau\right]$$

where

$$\alpha = \beta + B_o\gamma \; ; \; \lambda_{1,2} = \frac{-\alpha \pm \sqrt{\alpha^2 - 4\omega^2}}{2} \, .$$

For the physically relevant case for which the infrared oscillator frequency is much greater than the Larmor frequency, $|\alpha^2| << 4\omega^2$, so that $e^{\pm\frac{\sqrt{\alpha^2-4\omega^2}}{2}t} \rightarrow e^{\pm i\omega t}$, [Edmonds, 1993; Muehsam et al., 1994, 1996], and,

$$P(t) = \frac{-2i}{\lambda_2 - \lambda_1} e^{-\frac{\beta}{2}t} e^{-\frac{iB_o\gamma}{2}t} \left[\int_0^t e^{\frac{+\alpha}{2}\tau} \sin\left(\omega\left(t-\tau\right)\right) n(\tau) d\tau \right]. \qquad \textbf{(3)}$$

Thus, the thermal component of the trajectory maintains the form of a coherent *oscillator* driven by thermal noise, $n(\tau)$, and the trajectory does not devolve into a random walk, as assumed by the model of the particle in a "box" [Adair, 2006]. Physically, this is clear, as oscillator restoring force must be much greater than the thermal noise spectral density in order for the particle to remain bound and undergo oscillations in the infrared region.

From this, the ensemble average of the oscillator amplitude, was derived:

$$\left|P(t)\right|^2 = \frac{kT}{m\omega^2}\left(1 - \frac{\beta^2}{\beta^2 + 4\omega^2}\right)\left(1 - e^{-\beta t}\right). \qquad \textbf{(4)}$$

Note that neither the magnetic field strength nor the charge-mass ratio appears in equation (4). Thus, while the thermal term follows the Larmor trajectory, the time-dependence of the magnetic field contribution to the thermal accumulation disappears for the physically realistic condition $|\alpha^2| << 4\omega^2$, so that the magnetic field does not directly influence the amplitude of the thermal term. The thermal trajectory may then be evaluated from equations (2) and (4):

$$P(t) = x(t) + iy(t) = e^{-i\omega_L t}\left|P(t)\right| = P_o e^{-i\omega_L t}\left(1 - e^{-\beta t}\right)^{\frac{1}{2}}, \quad \textbf{(5)}$$

where

$$P_o = \left[\frac{kT}{m\omega^2}\left(1 - \frac{\beta^2}{\beta^2 + 4\omega^2}\right)\right]^{\frac{1}{2}}. \quad \textbf{(6)}$$

The thermal component *P(t)* of the motion thus follows the Larmor trajectory, rotating in the magnetic field at the Larmor frequency (Larmor frequency $\omega_L = B_o\gamma/2$), bounded by an envelope determined by the ensemble average $\left|P(t)\right|$.

Thus, thermal forces convey the oscillator amplitude towards its equilibrium value, while the trajectory rotates at the magnetic Larmor frequency, so that the magnetic field bioeffect itself is transduced by thermal noise. Because the thermal component *P(t)* itself undergoes Larmor precession, information regarding the magnetic field environment is in effect transduced by thermal forces, an idea first proposed by the late Alessandro Chiabrera [Chiabrera, et al., 1992] and further developed by Mikhail Zhadin [Zhadin, 1998]. In other words, the thermal component *P(t)* contains, in the form of coherent rotation of the oscillator orientation at the Larmor frequency, information regarding the local magnetic field.

CORRESPONDENCE TO PREDICTIONS OF ION PARAMETRIC RESONANCE MODEL

The above summary shows that the rate of angular rotation of the oscillator is independent of thermal forces and physical characteristics of the oscillator, such as the oscillator potential, initial position, initial velocity, etc. Thus, the thermal component follows the Larmor trajectory, regardless of the specific physical

characteristics of the oscillator, in accord with earlier results [Zhadin et al., 1998]. This suggests that it is possible to form a metric for biochemical reactivity that is independent of the MKS values of position and velocity and dependent wholly upon the Larmor frequency and bound lifetime [Muehsam et al., 2009b]. Here, a new metric [Muehsam et al., 2010] for the Lorentz force model is presented that exhibits close correspondence with the results of a meta-analysis of recent experiments [Binhi, 2007] and the Bessel function predictions of the ion parametric resonance (IPR) model [Blackman et al., 1995]. The variance of the projection of the oscillator angular displacement onto the Cartesian axis defined by the initial oscillator orientation measures the range of angles through which the oscillator passes:

$$R(t) = \mathrm{var}\left(\cos \int_0^{t_b} \omega_L(t)\, dt \right) \qquad \textbf{(7)}$$

where $\omega_L = B\gamma/2$ is the Larmor frequency, determined by resultant AC/DC magnetic field, and t_b is the bound lifetime of the system, taken here for $t_b >>$ Larmor period of the DC field. Thus, R(t) provides a simple measure of the reactivity. The magnitude of the ELF effect is proportional to the variability in the angular excursions of the oscillator: greater variability corresponds to the oscillator occupying a wider range of orientations, thus increasing orientations occupied and the likelihood of meeting a preferred orientation. R(t) thus provides a means of computing reactivity for DC, AC, parallel and perpendicular AC/DC magnetic field combinations.

The reactivity measure R(t) provides a geometric measure of the variability of oscillator orientations for combined AC/DC magnetic fields. Figure 1 shows that R(t) yields a characteristic landscape of reactivities for specific values of AC and DC frequencies and amplitudes, shown here for parallel AC/DC field combination for $t_b >>$ 10 Larmor periods . This landscape is an inherent geometrical property of the Larmor frequency itself, and not dependent upon specific characteristics

such as charge/mass ratios, damping coefficients, oscillator frequency. Reactivity is given as a function of AC/DC magnetic field amplitude and the ratio of the AC frequency to fL, to the Larmor frequency of the charged particle in the DC field. Note the prominent peaks occurring when the AC frequency is twice the Larmor frequency = cyclotron frequency. In the same manner as found previously, predictions depend upon bound lifetime (kinetics), and converge rapidly to the results shown in the figure for lifetimes longer than several DC Larmor periods. For such lifetimes, the effects of AC phase averaging are negligible, yielding a metric with no arbitrary parameters [Muehsam et al, 2009b]. Figure 2 shows a comparison of the predictions of R(t) with the Bessel function predictions of the IPR model and data from a metanalysis of seven independent experiments [Binhi, 2007] reporting bioeffects for parallel AC/DC magnetic field combinations. The results show that R(t) provides a slightly better fit to the data than the IPR predictions, particularly in the region where the ratio of AC/DC amplitudes > 5 (here, Binhi uses the magnetic field, H, rather than magnetic induction, B).

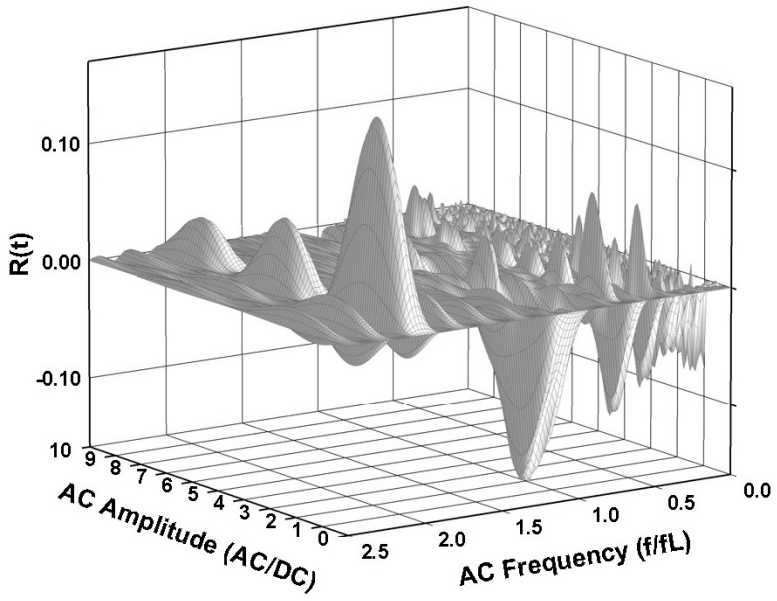

Figure 1: R(t) exhibits maxima and minima in desorption kinetics for bound ion, with prominent regions of enhanced reactivity at the cyclotron frequency and subharmonics, including the Larmor frequency. The reactivity R(t) is uniquely determined by the Larmor frequency, and thus reflects the intrinsic geometry the AC/DC magnetic field combination. This yields a model derived only from the Larmor frequency which employs no additional adjustable parameters to accommodate experimental data.

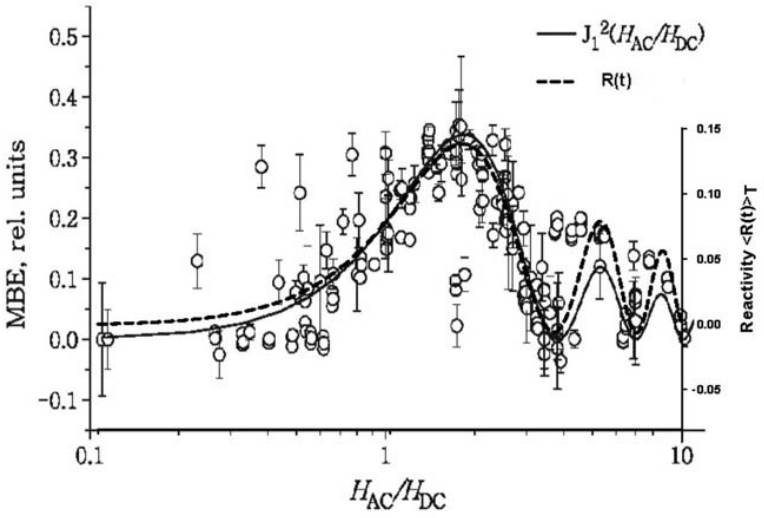

Figure 2:. Comparison of results of Lorentz model with Bessel function solution of ion parametric resonance (IPR) model and metanalysis of seven independent experiments yielding bioeffects in parallel AC/DC magnetic fields. The Lorentz force model fits the data at least as well as the Bessel function solution offered by the IPR model and provides a better fit for $H_{AC}/H_{DC} > 5$. Data shown from Binhi, 2007.

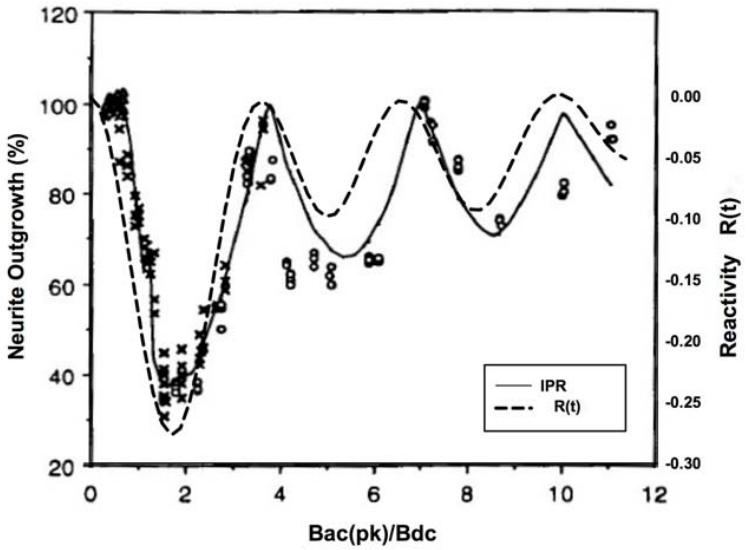

Figure 3: Comparison of results of Lorentz model with Bessel function solution of ion parametric resonance (IPR) model in PC-12 neurite outgrowth model. Lorentz model employs a single Ca^{2+} ion target (dotted line), whereas IPR model requires linear superposition predictions for H^{+}, Mg^{2+} and Li^{+} ions, each over specific frequency ranges, with arbitrary choice of best-fit coefficients for each Bessel function (solid line). Data compared to Blackman et al., 1995.

HYDRATION AND ION BINDING

Because all biochemical reactions occur within the aqueous subcellular matrix, any comprehensive model of EMF bioeffects must take into account the aqueous environment of the target. However, explicit treatment of role of water is presently lacking in models for EMF bioeffects. The dynamics of ion/water interactions play a critical role in ion binding, through the molecular recognition of hydrophobic patches by incoming ligands or drug molecules [Balasubramanian et al., 2003], and water structuring plays a key role in the determination of protein allostery

[Royer, 1996]. Because the passage from interfacial free water to bound water is on the order of a few kT, in order to affect this passage, the magnetic field strength would have to be sufficient to alter bound lifetime, so that magnetic fields below the mT range cannot be expected to affecting this passage directly, as mentioned previously. However, rotational fluctuations within the degrees of freedom available to bound ions are on the order of 0.4 kcal/mole, or just slightly less than kT [Lazaridis et al., 2002]. These rotational fluctuations in potential energy must be distinguished from changes in potential energy due to orientation changes that occur as a direct result of changes in ionic *distance* to hydration. Such changes in energy are greater than kT differ for different ions [Vaslow, 1963; Hyun et al., 1995], and thus could not be induced by LPM. It is interesting to note that changes in energy of hydration due to rotational and translational displacements differ for different ions, resulting in an energetic signature that contributes to the selectivity of ion channels [Laio and Torre, 1999].

In the absence of the magnetic field, the hydration angle between the ion and the net dipole moment of the environment assumes a distribution of available values, $\cos\theta$, with an associated probability of occurrence $P(\cos\theta)$, as shown in figure 4. The specific form of $P(\cos\theta)$ is dependent upon the type of ion and the solvent [Rashin et al., 1994].

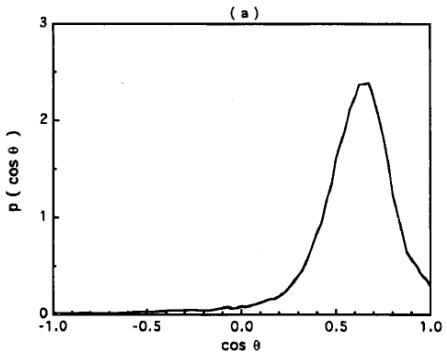

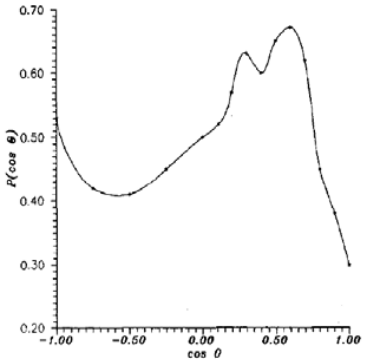

Fig. 11. Relative probabilities of different orientations of water molecule near Ne [13]. θ is the Ne–O–H angle.

Figure 4. Left: Probability of cosθ for the first shell of waters around a chloride ion in the aqueous environment. The angle θ represents the angle between the ionic oscillator and the net dipole moment of the aqueous environment. From [Hyun et al., 1995]. **Right:** Relative probabilities of different orientations of water molecule near an inert gas molecule, Ne. The angle θ represents Ne-O-H angle. Data from [Rashin et al., 1994].

The interaction energy between an ion and its aqueous environment may be described energetically via the angle of hydration between the ion and dipole moments in its vicinity. The principle of superposition allows for the reduction of the interaction with the ion of all waters to that of a single resultant dipole moment, embedded in a continuous medium of known dielectric constant. This is known as the *reduced point dipole* [Hyun et al., 1995], and allows for the definition of a potential energy function for the ion/water system. Thus, change in hydration energy may be taken to first order [Vaslow, 1963; Khalili et al., 2004], so the energy required to orient, e.g. rotate through an angle θ, the relative angle between the dipole field and the ion follows the familiar form:

$$U(r,t,\theta) = -\vec{\mu}\cdot\vec{E} = -\mu E(r)\cos(\theta(t)) \qquad \textbf{(8)}$$

Where the E(r) is the effective electric field felt by the dipole at a distance r from the ion, e.g. the effective dipole electric field due to charges of hydration [Laio et al., 1999]. In the binding site, E(r) is given by the distance between the ion and reduced dipole of the system, a constant for the duration of the bound lifetime [Podgornik et al., 1987; Paul et. al, 2001 ; Teschke et al., 2001] so that

$$E(r) = const. = E(r_o) = \frac{q}{4\pi r \varepsilon(r_o)} \quad \textbf{(9)}$$

where q is the ionic charge and the effective local dielectric constant is given $\varepsilon(r_o)$ is given by:

$$\varepsilon(r_o) = \varepsilon_{\max}\left[1 + (\varepsilon_{\max}/\varepsilon_{\min} - 1)\exp(-r_o/\lambda)\right]^{-1} \quad \textbf{(10)}$$

where $\varepsilon_{\max} = 78$ and $\varepsilon_{\min} = 2.63$, and $\lambda = 1$ Angstrom [Podgornik et al., 1987; Paul et. al, 2001 ; Teschke et al., 2001], and r_o is the distance between the Outer and Inner Helmholtz Planes (IHP) at the protein surface [Kalinin, et al., 1996].

Thus, the contribution ΔG_θ to the change in free energy due to orientation to mean energy of the ion in the dipole field may be written as a function of $\langle \cos(\theta(t)) \rangle$:

$$\Delta G_\theta(t,\theta) = \langle U(t,\theta) \rangle = -\langle \mu E(r_o)\cos(\theta(t)) \rangle = -\mu E(r_o)\langle \cos(\theta(t)) \rangle. \quad \textbf{(11)}$$

In the absence of the magnetic field, to first order in E(r), the mean value of cos(θ), has been shown to assume a constant value [Booth, 1951; Hyun, et al., 1995]:

$$\left\langle \cos(\theta(t)) \right\rangle = \mu E(r) / 3kT = const. \quad \textbf{(12)}$$

Thus, a constant-value baseline exists, for comparison with changes in $\left\langle \cos(\theta(t)) \right\rangle$ due to rotation at the Larmor frequency in order to provide a meaningful measure of the magnetic field induced change in reactivity. Figure 4 shows a typical free energy landscape, from Equation 11, for a parallel AC/DC magnetic field combination where $\left\langle \cos(\theta(t)) \right\rangle$ is computed over 1 period of the DC magnetic field Larmor frequency and phase averaged in the manner described in Muehsam et al., 2009b. Note the prominent resonance occurring at the Larmor frequency when AC/DC amplitude are approximately equal, which is an inherent property of the Larmor frequency for a parallel AC/DC field combination.

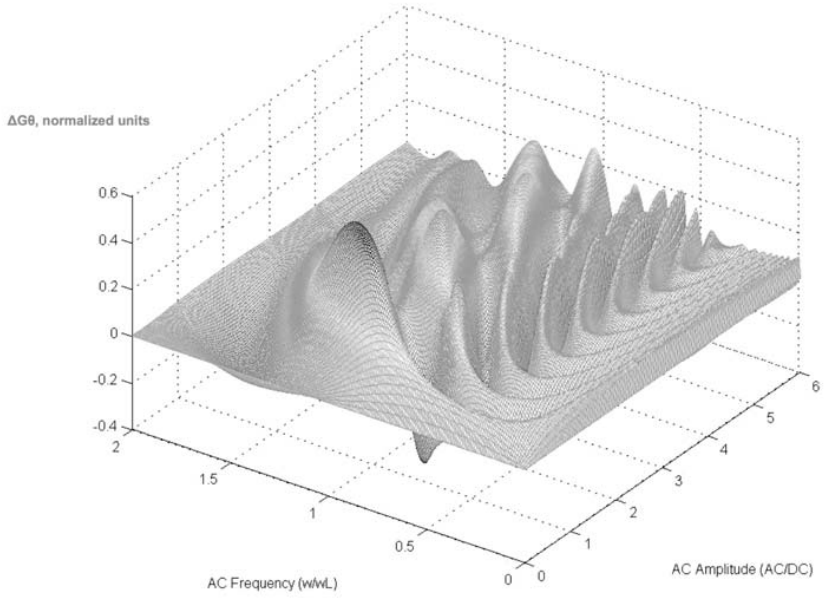

Figure 5. Free energy ΔG_θ for parallel AC/DC magnetic field combination, with DC = 20 μT, employing charge/mass ratio for calcium, in normalized units. Bound lifetime taken here = 1 Larmor period of DC magnetic field, no phase averaging employed. Note that free energy landscape is and inherent property of the Larmor frequency, and thus may be expressed solely in terms of AC/DC magnetic field amplitudes and frequency.

LARMOR ROTATION OF WATERS OF HYDRATION AT PROTEIN SURFACE

The dynamics of ion/water interactions play a critical role in ion binding, through the molecular recognition of hydrophobic patches by incoming ligands or drug molecules [Balasubramanian et al., 2003] and in the allosteric regulation of protein function in macromolecules such as hemoglobin [Royer, 1996]. Because the passage from interfacial free water to protein bound water is on the order of a few kT, protein hydration forms long-lived or semi-permanent hydration layers, and a weak (< 100 μT) magnetic field cannot be expected to affect this passage directly. However, the rotational degrees of freedom of bound waters described above (see Figure 4) offer a means by which ELF magnetic field effects could occur. Here, we analyze in spherical coordinates the effect of the magnetic field on a water molecule bound to a charged interface, subject to an initial thermal motion in the θ-direction, and free to rotate in φ-direction [Rashin et al., 1994; Hyun et al., 1995]. The water molecule is thus modeled as a rigid, charged linkage bound to a surface for a lifetime >> the Larmor period of the magnetic field. Given an initial, thermally activated velocity in the θ – direction,

$$\vec{v} = r\dot{\theta}\hat{\theta}, \tag{13}$$

and a magnetic field up along the z-axis, static or varying slowly relative to the thermal noise [Edmonds, 1993],

$$B = B_o\hat{k} = B_o\left[(\cos\theta)\hat{r} - (\sin\theta)\hat{\theta}\right], \tag{14}$$

the Lorentz force is thus in the φ-direction:

$$ma_\phi = q\left(r\dot{\theta}\hat{\theta}\times B_o\hat{k}\right) = qB_o r\dot{\theta}\left[\hat{\theta}\times\left((\cos\theta)\hat{r} - (\sin\theta)\hat{\theta}\right)\right] = qB_o r\dot{\theta}(\cos\theta). \tag{15}$$

In general, the φ-component of the acceleration is given by

$$a_\phi = r\ddot{\phi}\sin\theta + 2r\dot{\theta}\dot{\phi}\cos\theta + 2\dot{r}\dot{\phi}\sin\theta, \quad \textbf{(16)}$$

but, for the constrained system of a water molecule bound to a charged interface, dr/dt = 0 so that,

$$a_\phi = r\ddot{\phi}\sin\theta + 2r\dot{\theta}\dot{\phi}\cos\theta. \quad \textbf{(17)}$$

From equations (16) and (18)

$$r\ddot{\phi}\sin\theta + 2r\dot{\theta}\dot{\phi}\cos\theta = \frac{qB_o}{m} r\dot{\theta}\cos\theta \quad \textbf{(18)}$$

so that, for small excursions of θ,

$$\dot{\phi} = \frac{qB_o}{2m}. \quad \textbf{(19)}$$

Thus, the application of the magnetic field results in a rotation at the Larmor frequency in the φ-direction. For charged species such a bound water molecules or charged ligands that may be modeled as a constrained linkage, this suggests that the introduction of the magnetic field also introduces a component into the motion that undergoes rotation at the Larmor frequency.

DISCUSSION AND CONCLUSIONS

Future theoretical models for biological EMF transduction will require an explicit treatment of the role of water, which to date has not occurred. As all biological interactions occur within a aqueous medium, any successful attempt at describing

EMF bioeffects must account for interactions with hydration layers around ions, proteins, and ligands. Here, using a reasonable approximation of a water molecule as a linkage bound to a surface, it is shown that the magnetic field may cause rotation at the Larmor frequency in waters of hydration that are tightly bound at a protein aqueous interface. The results may be interpreted from the point of view of reaction kinetics and changes in the electrochemical properties of the aqueous interface at the IHP. Using [L] to represent the concentration of a ligand such as an ion, [R] to represent the receptor molecule or protein surface concentration, the final change reaction in rate constant k_b can be written as a function of the electrostatic potential Ψ at the IHP [Kalinin et al.,1996]:

$$k_b = \frac{[L \cdot R]}{[L][R]} \exp\left(\frac{\delta\rho - e\Psi}{kT}\right), \tag{20}$$

where [L·R] is the concentration of the bound complex, δ is the fraction of available sites filled, ρ is called the tail lateral interaction parameter (negative for attractive interactions), e is the electron charge.

Since the Gibbs free energy defines the final change in reaction rate:

$$k_b \equiv \exp\left(\frac{-\Delta G_\theta}{kT}\right), \tag{21}$$

combining equations (20) and (21), rotation at the Larmor frequency resulting in a change in ΔG_θ may thus be interpreted as a change in effective electrostatic potential at the IHP:

$$\Delta\Psi = \frac{1}{e}\left[-\Delta G_\theta - \delta\rho - kT\ln\left(\frac{[CaCaM]}{[Ca][CaM]}\right)\right], \tag{22}$$

It has been suggested previously that modulation via Larmor precession of ion/water orientation angles could modulate thermal fluctuations in the instantaneous local dielectric constant ε(t) at the binding site and thus the kinetics of binding processes at the Helmholtz planes at electrified interfaces may be [Pilla et al., 1997]. Because a change in free energy ΔG_o can also be interpreted as a change in local effective dielectric constant, rotation at the Larmor frequency may be interpreted as inducing such a change:

$$\Delta G_\theta = -E_o\left[\frac{1}{\varepsilon_2}-\frac{1}{\varepsilon_1}\right] \rightarrow -E_o\left[\frac{1}{\varepsilon(Larmor)}-\frac{1}{\varepsilon_1}\right], \qquad \textbf{(23)}$$

where E_o is the electrostatic interaction energy in the absence of the magnetic field. Physically, as <cos(θ)> increases, the ion/dipole angle decreases towards 0 (or 180º), thus increasing the (negative) potential energy of the system. From this, the local effective dielectric constant is given by:

$$\varepsilon(Larmor) = \frac{1}{\frac{K_o}{\varepsilon_1}-\Delta G} = \frac{1}{\frac{K_o}{\varepsilon_1}+\mu E(r_o)\langle\cos(\theta(t)\rangle}. \qquad \textbf{(24)}$$

Thus, increased variability in the motion due to rotation at the Larmor frequency results in a reduction of the local effective dielectric constant, providing a physical interpretation of the change in binding kinetics due to the magnetic field.

The Lorentz model offers an explanation, and theoretical basis for weak ELF magnetic field effects, based upon the classical dynamics of the bound charged oscillator. Information regarding the AC/DC magnetic field configuration is transferred via the Larmor frequency into the thermal motion of the oscillator. A physically meaningful geometric measure of the dynamics of ion motion predicts resonances in the reactivity of a bound ions or waters of hydration due to weak AC and AC/DC magnetic fields. The underlying mathematics is a straightforward analysis of the classical dynamics of a bound particle in the magnetic field,

subject to thermal noise forces. Here, a new metric based upon the variability of the oscillator position is shown to yield predictions in close agreement with those of the IPR model. The results suggest that desorption kinetics can be significantly accelerated or slowed in a manner dependent upon the ratio of AC/DC field strengths. The model also provides a physically reasonable mechanistic explanation for observed ELF effects including the large body of observed weak 50/60 Hz magnetic field bioeffects. Comparison with experiments shows that, the Lorentz model predicts experimental results equally well as the IPR model, and requires only a single-ion charge-mass ratio. In contrast, in order to fit available data, the IPR model requires of multiple ion superpositions over specific frequency ranges or and the use of linear combinations of Bessel functions with arbitrary coefficients, as used in Blackman et al., 1995 and Binhi, 2007. Perhaps more importantly, the IPR model neglects thermal noise forces, whereas the Lorentz model accounts for these forces and shows that, rather than presenting an obstacle to detection, thermal noise may play an essential role in ELF magnetic field transduction. Thus, the inclusion of thermal noise forces, and the much smaller number of assumptions and variable parameters suggest that Lorentz force model to be a more parsimonious description of the transduction mechanism for weak AC and DC magnetic field bioeffects.

The necessity of a model for EMF effects that accounts for interactions with the aqueous medium is clear. In addition, there exists a substantial and diverse body of reports of EMF-induced changes in the physicochemical properties of water and aqueous solutions, suggesting that EMFs do in fact act directly on the aqueous medium. Extensive research which is likely to have significance to biology has been conducted in physical chemistry and the colloid sciences for more than twenty years. Magnetic treatment of water is now commonly employed to inhibit scaling in industrial heat exchangers and pipes [Busch et al., 1986; Yoon et al., 1994; Koshoridze et al., 2009; Stuyven et al., 2009]. Electric and magnetic field effects have been observed for water surface tension [Amiri et al., 2006], diffusion of ions in solution [Guo et al., 2011], hydrogen bonding structure [Cai et al.,

2009], precipitation of barium oxalate [Berton et al., 1993], $CaCO_3$ and $CaSO_4$ [Beruto et al., 1993; Alimi et al., 2006], electrolytic potential [Otsuka et al., 2006], electrical conductivity [Akopian et al., 2005], evaporation rate [Guo et al., 2012], nucleation and crystal growth rates of diamagnetic inorganic salts [Lundager Madsen, 1995] and suspension stability [Higashitani et al., 1992]. In addition, and perhaps of relevance to our observations of long-lasting EMF effects on human hemoglobin [Muehsam et al., 2013], a variety of EMF effects on aqueous solutions have been observed to persist for up to several days after the removal of applied EMFs. For example, changes in zeta potential and diffusivity of nonmagnetic colloids [Higashitani et al., 1990, 1992], zeta potential of TiO_2 and $CaCO_3$ [Chibowski et. al., 1990, 1994; Holysz, et al., 2002], surface free energy of $CaCO_3$ [Chibowski et al., 1994; Holysz, et al., 1994], Al_2O_3 [Lubomska et al., 2001] and in the nucleation frequency of $CaCO_3$ [Higashitani, K. et. al., 1993]. Changes in UV and IR spectra of water due to exposure to static magnetic fields have also been reported [Usatenko et al., 1977; Fesenko et al., 1995]. Magnetic pretreatment of water has been reported to enhance the yields of plants, livestock and paramecium [Lin et al., 1990], alter cell density, size and nuclear diameter in catfish hepatocytes [Garg et. Al, 1995] and affect the estrus cycles of mice [Pandey et. al., 1996], suggesting that physicochemical changes in the aqueous solutions themselves may be the mediators of some EMF bioeffects.

The above reports of EMF effects directly on aqueous solutions suggests that these physicochemical changes themselves may be relevant to biological EMF transduction. Given the present state of knowledge, a more comprehensive theoretical picture of water and aqueous solutions is needed in order to clearly explain EMF effects on water structure. However, some reasonable speculation has been made regarding magnetic field induced changes in water conformational structure [Susak et al., 2005], and how these may alter biological activity [Rai et al., 1995; Rai, 1997]. Observations of EMF effects on water hydrogen bonding structure [Inaba et al., 2004; Cai et al., 2009] are in accord with molecular dynamics modelling [Chang et al., 2006]. Because hydrogen bonded water

structures are essential factors governing the internal motions of protein molecules [Chou, 1985; Royer et al., 1996], application of the Lorentz model to waters of hydration may suggest a general mechanism for weak ELF magnetic field detection in proteins, and a possible explanation of observed magnetic field effects on human hemoglobin [Muehsam et al., 2013; Mousavy et al., 2009; Magazù et al., 2010; Tao et al., 2011; Sosa et al., 2005; Shalaby et al., 2006; Sakhnini et al., 2001; Iwasaka et al., 2001; Milweski et al., 2006].

REFERENCES

Adair RK. 1991. Constraints on biological effects of weak extremely low frequency electromagnetic fields. Physical Review A 43:1039- 1048.

Adair RK. 1994. Constraints of thermal noise on the effects of weak 60-Hz magnetic fields acting on biological magnetite. Proceedings of the National Academy of Sciences 91:2925-2929.

Adair RK. 2006. Comment: analyses of models of ion actions under the combined action of AC and DC magnetic fields. Bioelectromagnetics 27:332-334.

Akopian SN, Aĭrapetian SN. 2005. A study of specific electrical conductivity of water by the action of constant magnetic field, electromagnetic field, and low-frequency mechanical vibrations. Biofizika. 50(2):265-70.

Alimi F, Tlili M, Ben Amor M, Gabrielli C, Maurin G. 2007. Influence of magnetic field on calcium carbonate precipitation. Desalination. 206(1–3):163-168.

Amiri MC. Dadkhah AA. 2006. On reduction in the surface tension of water due to magnetic treatment. Colloids and Surfaces A: Physicochem. Eng. Aspects 278: 252–255.

Balasubramanian S, Pal S and Bagchi B. 2003. Evidence for bound and free water species in the hydration shell of an aqueous micelle. Current Science. 84(3):428-430.

Bawin S, Adey W. 1976. Sensitivity of calcium binding in cerebral tissue to weak environmental electric fields oscillating at low frequency. In: Proc Natl Acad Sci, USA. pp 1999–2003.

Bawin S, Kaczmarek L, Adey W. 1975. Effects of modulated VHF fields on the central nervous system. Ann NY Acad Sci. 247:74–81.

Bersani F (Ed.), Electricity and Magnetism in Biology and Medicine, Kluwer/Plenum, London, 1999.

Berton R, Beruto D, Bianco B, Chiabrera A, Giordani M. 1993. Effect of ELF electromagnetic exposure on precipitation of barium oxalate. Bioelectrochemistry and Bioenergetics. 30:13-25.

Beruto D, Giordani M. 1993. Calcite and aragonite formation from aqueous calcium hydrogen carbonate solutions: effects of induced electromagnetic field on the activity of CaCO3 precursers. J. Chem. Soc. Faraday Trans. 89:2457-2461.

Binhi V. 2007. A review on theoretical magnetobiology. Preprint submitted to Elsevier. 30 August, 2007.

Binhi VN, and Rubin AB. 2007. Magnetobiology: The kT paradox and possible solutions. Electromagnetic Biology and Medicine 26:45-62.

Binhi VN, and Savin AV. 2003. Effects of weak magnetic fields on biological systems: physical aspects. Physics-Uspekhi 46:259-291.

Binhi VN. 2002. Magnetobiology: Underlying Physical Problems, Academic Press, San Diego.

Blackman CF, Benane SG, Rabinowitz J, House DE, Joines W. 1985. A role of the magnetic field in the radiation induced efflux of calcium ions from brain tissue in vitro. Bioelectromagnetics 6:327–337.

Blackman CF, Blanchard JP, Benane SG, House DE. 1995. The ion parametric resonance model predicts magnetic field parameters that affect nerve cells. FASEB J. 9(7):547-51.

Blumenthal DK, Stull JT. 1982. Effects of pH, ionic strength, and temperature on activation by calmodulin and catalytic activity of myosin light chain kinase. Biochemistry 21:2386-91.

Busch KW, Busch MA, Parker DH, Darling RE, McAtee JL. 1986. Studies of a water treatment device that uses magnetic fields. Corrosion 42:211-221.

Cai R, Yang H, He J, Zhu W. 2009. The effects of magnetic fields on water molecular hydrogen bonds. Journal of Molecular Structure. 938(1–3)15–19.

Chang KT, Weng CI. 2006. The effect of an external magnetic field on the structure of liquid water using molecular dynamics simulation. J. of Applied Phsyics. 100:043917.

Chiabrera A, Bianco B, Caratozzolo F, Giannetti G, Grattarola M, Viviani R. 1985. Electric and magnetic field effects on ligand binding to the cell membrane, in:

A.Chiabrera, C. Nicolini, H.P. Schwan Eds., Interactions Between Electromagnetic Fields and

Chiabrera A, Bianco B, Kaufman JJ, Pilla AA. 1992. Bioelectromagnetic resonance interactions: endogenous field and noise. In "Interaction Mechanisms of Low-level Electromagnetic Fields." Oxford University Press, pp 164-179.

Chibowski E, Gopalakrishnan S, Busch MA, Busch KW. 1990. Residual variations in the zeta potential of TiO2 (Anatase) suspension as a result of exposure to radiofrequency electric fields. Journal of Colloid and Interface Science. 139(1): 43-54.

Chibowski E, Hołysz L, Wójcik W. 1994. Changes in zeta potential and surface free energy of calcium carbonate due to exposure to radiofrequency electric field. Colloids and Surfaces A: Physicochemical and Engineering Aspects. 92(1-2):79-85.

Chou KC. 1985. Low-frequency motions in protein molecules. Beta-sheet and beta-barrel. Biophys J. 48(2):289–297.

Cox JA. 1988. Interactive properties of calmodulin. Biochem. J. 249:621-629.

Daff S. 2003. Calmodulin-dependent regulation of mammalian nitric oxide synthase. Biochem Soc Trans 31(Pt 3):502-5.

Edmonds DT. 1993. Larmor precession as a mechanism for the detection of static and alternating magnetic fields. Bioelectrochemistry and Bioenergetics 30:3-12.

Fesenko E, Gluvstein A. 1995. Changes in the state of water, induced by radiofrequency electromagnetic fields. FEBS Letters 367(1):53-55.

Garg TK, Agarwal N, Rai S. 1995. Effect of magnetically restructured water on the liver of a catfish: clarias batrachus. Electro- and Magnetobiology. 14(2)107-115.

Guo B, Han H, Chai F. 2011. Influence of magnetic field on microstructural and dynamic properties of sodium, magnesium and calcium ions. Transactions of Nonferrous Metals Society of China. 21(2):s494-s498.

Guo YZ, Yin DC, Cao HL, Shi JY, Zhang CY, Liu YM, Huang HH, Liu Y, Wang Y, Guo WH, Qian AR, Shang P. 2012. Evaporation rate of water as a function of a magnetic field and field gradient. Int J Mol Sci. 13(12):16916-28.

Higashitani K, Iseri H, Okuhara K, Kage A, Hatade S. 1990. Magnetic effects on zeta potential and diffusivity of nonmagnetic colloidal particles. Journal of Colloid and Interface Science, 172:383-388.

Higashitani K, Kage A, Katamura S, Imai K, Hatade S. 1993. Effects of a magnetic field on the formation of CaCO3 particles. Journal of Colloid and Interface Science, 156(1):90-95.

Higashitani K, Okuhara K, Hatade S. 1992. Effects of magnetic fields on stability of nonmagnetic ultrafine colloidal particles. Journal of Colloid and Interface Science, 152:125-131.

Holysz L, Chibowski E. 1994. Surface free energy components of calcium carbonate and their changes due to radiofrequency electric field treatment. Journal of Colloid and Interface Science. 164(1):245-251.

Holysz L, Chibowski M, Chibowski E. 2002. Time dependent changes of zeta potential and other parameters of in situ calcium carbonate due to magnetic field treatment. Colloids Surf. A 208:231–240.

Inaba H, Saitou T, Tozaki K, Hayashi H. 2004. Effect of the magnetic field on the melting transition of H2O and D2O measured by a high resolution and supersensitive differential scanning calorimeter. J. Appl. Phys. 96:6127-6133.

Iwasaka M, Miyakoshi J, Ueno S. 2001. Optical absorbance of hemoglobin and red blood cell suspensions under magnetic fields. IEEE Trans Magnetics 37:2906-2908.

J. Hyun and C. S. Babu and T. Ichiye. 1995. Apparent local dielectric response around ions in water: a method for its determination and its applications. J. Phys. Chem. 99:5187–5195.

Kalinin, VV, Radke CJ. 1996. An ion-binding model for ionic surfactant adsorption at aqueous-fluid interfaces. Colloids Surf. A, 114, 337–350.

Khalili M, Saunders JA, Liwo A, Oldziej S and Scheraga HA. 2004. A united residue force-field for calcium–protein interactions. Protein Sci. 13: 2725-2735.

Klassen VI, Zonov'ev YZ. 1967. Influence of magnetic treatment of water on suspension stability. Kolloidnyi Zhurnal. 29:758-762.

Koshoridze SI, Levin YK. 2009. Physical model of scale-formation reduction under magnetic treatment of water in thermal engineering devices. Thermal Engineering. 56(4):338–341.

Laio A and Torre V. 1999, Physical origin of selectivity in ionic channels of biological membranes. Biophysical Journal Vol. 76. pp.129–148.

Lazaridis T, et al., 2002. Contributions to the Binding Free Energy of Ligands to Avidin and Streptavidin. PROTEINS: Structure, Function, and Genetics 47:194–208 (2002).

Lednev VV. 1991. Possible mechanism for the influence of weak magnetic fields on biological systems. Bioelectromagnetics. 12:71-75.

Liboff AR, Cherng S, Jenrow KA, Bull A. 2003. Calmodulin-dependent cyclic nucleotide phosphodiesterase activity is altered by 20 mT magnetostatic fields. Bioelectromagnetics 24:32-38.

Liboff AR, McLeod BR. 1988. Kinetics of channelized membrane ions in magnetic fields. Bioelectromagnetics 9:39–51.

Liboff AR, Smith SD, McLeod BR. 1987. Experimental evidence for ion cyclotron resonance mediation of membrane transport. In: Blank M, Findl E, eds. Mechanistic approaches to interactions of electric and electromagnetic fields with living systems. Plenum Press, pp 281–296.

Lin IJ, Yotvat J. 1990. Exposure of irrigation and drinking water to a magnetic field with controlled power and direction. Journal of Magnetism and Magnetic Materials. 83(1-3)525-526.

Lubomska M, Chibowski E. 2001. Effect of radio frequency electric fields on the surface free energy and zeta potential of Al2O3. Langmuir 17:4181–4188.

Lundager Madsen HE. 1995. Influence of magnetic field on the precipitation of some inorganic salts J. Crystal Growth, 152(1995)94-100.

Machlup S. 2007. Ion Parametric Resonance: Resolving the signal-to-noise-ratio paradox. Electromagnetic Biology and Medicine, 26:251–256.

Magazù S, Calabrò E, Campo S. 2010. FTIR spectroscopy studies on the bioprotective effectiveness of trehalose on human hemoglobin aqueous solutions under 50 Hz electromagnetic field exposure. J Phys Chem. 114:12144-12149.

Markov MS, Pilla AA. 1997. Weak static magnetic field modulation of myosin phosphorylation in a cell-free preparation: calcium dependence, Bioelectrochem Bioenergetics, 43:235-240.

Markov MS, Ryaby JT, Kaufman JJ, Pilla AA. 1992. Extremely weak AC and DC magnetic fields significantly affect myosin phosphorylation. In: Allen MJ, Cleary SF, Sowers AE, Shillady DD (Eds.) Charge and Field effects in biosystems 3, Boston: Birkhauser, pp. 225-230.

Markov MS, Wang S, Pilla AA. 1993. Effects of weak low frequency sinusoidal and DC magnetic fields on myosin phosphorylation in a cell-free preparation. Bioelectrochem Bioenergetics 30:119-125.

Milweski S, Szczepański W. 2006. Effects of electromagnetic fields on the meat performance and wool performance of sheep Arch. Tierz., Dummerstorf 49(Special Issue):219-225.

Milyaev VA, Binhi VN. 2006. On the physical nature of magnetobiological effects. Quantum Electron. 36:691–701.

Mousavy SJ, Riazi GH, Kamarei M, Aliakbarian H, Sattarahmady N, Sharifizadeh A, Safarian S, Ahmad F, Moosavi-Movahedi AA. 2009. Effects of mobile phone

radiofrequency on the structure and function of the normal human hemoglobin. Int J Bio Macromolecules 44:278–285.

Muehsam D, Lalezari P, Lekhraj R, Abruzzo P, Bolotta A, Marini M, Bersani F, Aicardi G, Pilla A, Diana Casper. Non-thermal radio frequency and static magnetic fields increase rate of hemoglobin deoxygenation in a cell-free preparation. Accepted for publication pending revision, Plos One, Feb, 2013.

Muehsam DJ, Pilla AA. 1994. Weak magnetic field modulation of ion dynamics in a potential well: mechanistic and thermal noise considerations. Bioelectrochem Bioenergetics 35:71-79.

Muehsam DJ, Pilla AA. 1996. Lorentz approach to static magnetic field effects on bound ion dynamics and binding kinetics: thermal noise considerations. Bioelectromagnetics 17:89-99.

Muehsam DJ, Pilla AA. 2009a. A Lorentz model for weak magnetic field bioeffects: part I--thermal noise is an essential component of AC/DC effects on bound ion trajectory. Bioelectromagnetics 30:462-75.

Muehsam DJ, Pilla AA. 2009b. A Lorentz model for weak magnetic field bioeffects: part II--secondary transduction mechanisms and measures of reactivity. Bioelectromagnetics 30:476-88.

Muehsam DJ, Pilla AA. 2010. A Lorentz force model for weak AC/DC magnetic field effects predicts observed resonances in desorption kinetics of a bound ion. Proceedings, Bioelectromagnetics Society 32nd Annual Meeting, Seoul, Korea, June 14-18.

Otsuka I, Ozeki S. 2006. Does magnetic treatment of water change its properties? J Phys Chem B. 110(4):1509-12.

Pandey S, Garg TK, Singh KP, Rai S. 1996. Effect of magnetically treated induced water structure on the oestrus cycles of albino female mice mus musculus. Electro- and Magnetobiology. 15(2):133-140.

Paul R, Paddison SJ. 2001. A statistical mechanical model for the calculation of the permittivity of water in hydrated polymer electrolyte membrane pores. J. Chem. Phys. 115, 7762.

Pazur A. 2004. Characterisation of weak magnetic field effects in an aqueous glutamic acid solution by nonlinear dielectric spectroscopy and voltammetry. Biomagn Res Technol. 2(1):8.

Pilla AA, Muehsam DJ, Markov MS. 1997. A dynamical systems/Larmor precession model for weak magnetic field bioeffects: ion binding and orientation of bound water molecules, Bioelectrochemistry and Bioenergetics 43:239-249.

Podgornik R, Cevc G. 1987. Solvent structure effects in the macroscopic theory of Van der Waals forces, J. Chem. Phys. 87 , 5957-5967.

Rai S, Singh NN, Mishra RN. 1995. Magnetic restructuring of water. Medical and Biological Engineering and Computing. 33(4):614-617.

Rai S. 1997. Causes and mechanism (s) of NER bioeffects. Electro Magnetobiology. 16(1): 59-67.

Ramundo-Orlando A, Morbiducci U, Mossa G, and D'Inzeo G. 2000. Effect of low frequency, low amplitude magnetic fields on the permeability of cationic

liposomes entrapping carbonic anhydrase I. Evidence for charged lipid involvement. Bioelectromagnetics. 21:491–498.

Rashin AA, Bukatin MA. 1994. A view of thermodynamics of hydration emerging from continuum studies. Biophysical Chemistry 51. 167-192.

Royer WE Jr, Pardanani A, Gibson QH, Peterson ES, Friedman JM. 1996. Ordered water molecules as key allosteric mediators in a cooperative dimeric hemoglobin. Proc Natl Acad Sci U S A. 93(25): 14526-31.

Sakhnini L, Khuzaie R. 2001. Magnetic behavior of human erythrocytes at different hemoglobin states. Eur Biophys J. 30:467-470.

Shalaby TE, Shawki MM. 2006. Biophysical and biochemical changes in the characteristics of rat blood exposed to combined alternating and static magnetic fields. Rom. J. Biophys. 16:169-180.

Shuvalova LA, Ostrovskaja MV, Sosunov EA, Lednev VV. 1991. Effect of weak magnetic field in the parametric resonance mode on the rate of calmodulin-dependent phosphorylation of myosin in the solution. Doklady Akademii Nauk SSSR (Reports of the Academy of Science of the USSR) 317(1):227-230.

Smith S. 1987. Calcium cyclotron resonance and diatom mobility. Bioelectromagnetics 8:215–227.

Sosa M, Bernal-Alvarado J, Jiménez-Moreno M, Hernández JC, Gutiérrez-Juárez G, Vargas-Luna M, Huerta R, Villagómez-Castro JC, Palomares P. 2005. Magnetic field influence on electrical properties of human blood measured by impedance spectroscopy. Bioelectromagnetics 26:564-570.

Stuyven B, Vanbutsele G, Nuyens J, Vermant J, Martens JA. 2009. Natural suspended particle fragmentation in magnetic scale prevention device. Chemical Engineering Science. 64(8): 1904-1906.

Susak IP, Ponomarev OA, Shigaev AS. 2005. Primary mechanisms of the biological effect of electromagnetic fields. Biofizika. 50(2):367-70.

Tao R, Huang K. 2011. Reducing blood viscosity with magnetic fields. Phys Rev E Stat Nonlin Soft Matter Phys. 84(1):011905.

Teschke O, Ceotto G, de Souza EF. 2001. Interfacial water dielectric-permittivity-profile measurements using atomic force microscopy. Phys. Rev. E 64, 011605.

Usatenko ST et. al., 1977. Effect of magnetic fields on the rotational infrared spectra of water. Colloid Journal. 39(1977)903.

Vaslow F. 1963. The orientation of water molecules in the field of an alkali ion, J. Phys. Chem. 67 p. 2773.

Weaver JC, Astumian RD. 1990. The response of living cells to very weak electric fields: the thermal noise limit. Science. 247:459-462.

Yoon J, Lund D. 1994. Magnetic Treatment of milk and surface treatment of plate heat exchangers: effects on milk fouling. Journal of Food Science. 59:964-969.

Zhadin M, Barnes F. 2005. Frequency and amplitude windows in the combined action of DC and low frequency AC magnetic fields on ion thermal motion in a macromolecule: theoretical analysis. Bioelectromagnetics 26:323-330.

Zhadin MN, Novikov VV, Barnes FS, NF Pergola. 1998. Combined action of static and alternating magnetic fields on ionic current in aqueous glutamic acid solution. Bioelectromagnetics 19:41–45.

Zhadin MN. 1998. Combined action of static and alternating magnetic fields on ion motion in a macromolecule: Theoretical aspects. Bioelectromagnetics 19:279–292.

Zhadin MN. 2005. Review of russian literature on biological action of DC and low-frequency AC magnetic fields. Bioelectromagnetics. 22(1):27-45.

b. MAGNETIC FIELD EFFECTS ON NEURONAL SPIKE TIMING

INTRODUCTION

A variety of electric field effects on neuronal systems have been reported, for applied subthreshold electric field strengths too weak to directly induce action potential firing, including time-dependent modulation of neuronal excitability [Bikson et al., 2004], sensitivity to sub-mV/mm electrical fields in rat hippocampal slices [Francis et al, 2003], increase in Ca^{2+}-activated K^+ channel mean open time in isolated dorsal root ganglia [Marchionni et al., 2006], enhanced expression of voltage-gated Ca^{2+} channels [Grassi et al., 2004], effects on membrane potentials and spike timing [Deans et al., 2007; Radman et al, 2007], gating of ion channels [Kolomytkin et al., 2007], changes in neuronal timing and rate [Reato et al., 2010], neuronal firing and epileptiform activity [Bikson et al., 2004]. Bioeffects due to static (DC) and ELF exposures, for which the induced electric field is negligible, include changes in EEG activity dependent up temporal sequencing of magnetic pulses [Cook et al., 2009], biphasic response in epileptiform spike activity in epileptic patients [Dobson et al., 2000], modulation of inactivation kinetics in K^+ channel currents in trigeminal root ganglion neurons [Shen et al., 2007], changes in action potential shape and spike timing [Wieraszko, 2000; Vargas et al, 2006; Ahmed et al., 2008], modulation of Ca^{2+}-dependent K^+ channel behavior [Azanza et al., 1988; Azanza, 1990], inhibition of neurite outgrowth and reversal of inhibition of Ca^{2+} efflux in PC-12 cells induced by CGS21680, a selective adenosine A2A receptor agonist [Wang et al., 2010], neurite outgrowth [Blackman et al., 1985, 1995; Morgado-Valle et al., 1998], decrease in acetylcholinesterase activity in cerebellum synaptosomal membranes [Ravera et al, 2010], spike timing in cortical neurons [Modolo et al., 2010], spike timing in neuronal ganglia in bees [Schiff, 1991], and modulation of hyperpolarizing K^+ channels [Tonini et al., 2001], resting EEG in human subjects [Cook et al., 2004], neural processing of acute pain [Robertson et al., 2010].

DC MAGNETIC FIELD EFFECTS ON SPIKE TIMING

While the biophysical basis for neuronal electric field effects may be understood by the superposition of the applied electric field with the membrane potential of single cells or cell arrays [Muehsam et al., 1999; Apollonio et al., 2000; Wang et al., 2009], the mechanisms for magnetic field effects remain unclear. Here, in light of experimental observations of magnetic field effects on action potential shape and neuronal spike timing [Azanza et al., 1988; Azanza, 1990; Schiff, 1991; Trabulsi et al., 1996; Wieraszko, 2000; Ahmed et al., 2008; Tonini et al., 2001; Modolo et al., 2010; Vargas et al., 2006], a model is proposed for EMF magnetic field effects on Ca^{2+}-dependent K^{+} channel behavior. Previous models for electric field effects have been offered, based upon Hodgkin-Huxley (HH)-type membrane models [Xia et al., 1998; Apollonia et al., 2000]. An HH-type model adapted to an Izhikevich neuronal model [Izhikevich, 2004] for GSM mobile phone exposures has been suggested [Minelli et al., 2007], also predicting changes in spike timing due to EMF exposure, and another HH model predicts periodic and chaotic dynamics in response to sinusoidal electric field stimulation [Jiang et al., 2009]. A model for microwave frequency electric field effects on a simplified ion channel model has also been offered [Cagni et al., 2007]. Regarding magnetic field effects, a model employing an Izhikevich neuron treated only the electric field induced by a time-varying magnetic field [Modolo et al., 2010]. A Zeeman-Stark model for weak magnetic field effects has been suggested [Bruna et al., 2001], however this model does not account for the presence of thermal noise forces [Bianco et al., 1992]. Also, although the computational simplification achieved by the Izhikevich approximation is desirable, this simplicity comes at the cost of the ability to quantitatively assess changes in biophysical quantities such as channel conductance, time constants, etc. My previous analyses showed that the sensitivity to exogenous EMF of an array of cells with HH-type membranes in gap junction contact is dependent upon the membrane resting potential [Muehsam et al., 1999]. Thus, the model considered here employs an HH-type model to

evaluate the effects ELF magnetic field modulation of Ca^{2+} activity via the Lorentz model on K^+ channel currents and spike timing.

Reports that the magnetic field can act on neuronal cells through Ca^{2+}-dependent pathways include increased Ca^{2+} flux in PC-12 cells [Wang et al., 2010], magnetic field–induced fluctuations in intracellular Ca^{2+} concentration which modulate action potential shape and neuronal spike timing [Trabulsi et al., 1996] (dantrolene, an inhibitor of intracellular Ca^{2+} channels, inhibited these magnetic field effects [Wieraszko, 2000]), EMF modulation of spike timing occurring through changes in intracellular Ca^{2+} concentration which were blocked using nifedipine to block Ca^{2+} channels and apamin to block Ca^{2+}-activated K^+ channels [Tonini et al., 2001], direct modulation of Ca^{2+}-activated K^+ channel activity [Marchionni et al., 2006], and of voltage-gated Ca^{2+} channels [Grassi et al., 2004]. Thus, here we consider a small-conductance Ca^{2+}-dependent K^+-current I_K as a function of the effective free internal Ca^{2+} concentration and membrane voltage V [Engel et al, 1999; Purvis et al., 2005; Wang et al., 2011]:

$$I_K\left(\left[Ca^{2+}\right]_{eff}\right) = \bar{g}_K z_K\left(\left[Ca^{2+}\right]_{eff}\right)\left(V - V_K\right) \tag{1}$$

where and $\bar{g}_K = 37$ mmho/cm^2; $V_K = 12$ mV, and all other parameters governing to K^+, Na^+, and leak conductance relations are given according to [Hodgkin et al., 1952a, 1952b; Fishman et al., 1977; Purvis et al., 2005]. The modulation z_K of the Ca^{2+}-dependent conductance is given by [Engel et al, 1999]

$$z_k\left(\left[Ca^{2+}\right]_{eff}\right) = z_o \frac{\left(\frac{\left[Ca^{2+}\right]_{eff}}{0.0025}\right)^2}{1+\left(\frac{\left[Ca^{2+}\right]_{eff}}{0.0025}\right)^2} \tag{2}$$

where z_o is an arbitrary constant. Ca^{2+} gating of SK channels is mediated by binding of Ca^{2+} to calmodulin (CaM) and subsequent conformational alterations in the channel protein alpha sub-units [Xia et al., 1998; Keen et al., 1999]. Thus, the effect of the magnetic field effect may represented as a modulation of the effective free Ca^{2+} concentration [Muehsam et al., 1996, Muehsam et al, 2009a, 2009b], which considered in detail the effect of the magnetic field on Ca^{2+}/CaM binding. For a static magnetic field B_o, the simplest measure of reactivity is that the effective Ca^{2+} concentration is proportional to the Larmor frequency [Muehsam et al., 1996; Pilla et al., 1997]. For this measure, for example, an increase in the Larmor frequency increases the angular area per unit time spanned by the oscillator, resulting in an increase in effective free [Ca^{2+}], so that

$$\left[Ca^{2+}\right]_{eff} = \gamma_o \Gamma B, \tag{5}$$

where γ_o is an arbitrary constant by magnitude of observed bioeffects in a given magnetic field B and Γ is the target gyromagnetic ratio. For a given choice of γ_o, changes in ELF exposures from baseline may then be assessed. It is important to note that the Lorentz model predicts a change in *effective* Ca^{2+} concentration, interpreted in terms of the change in reaction kinetics, due to increased availability of Ca^{2+} for binding to CaM, rather than an increase due to direct magnetic field effects on ionic currents through the membrane [Muehsam et al., 1996].

The H-H model considered here may be solved via numerical integration using a Runge-Kutta method, and for the conditions employed here the results are stable over changes in step size [Moore et al., 1974; Engel et al, 1999; Stewart et al., 2009]. Matlab code is shown in the Appendix. Adjusting γ_o to yield several mmho/cm^2 sensitivity in the K^+ conductance $\bar{g}_K z_K$ in the μT range, in order to simulate the effects reported by [Tonini et al., 2001; Marchionni et al., 2006], Figure 1 shows the effect of a static magnetic field on single spike shape. The

spiking behavior is is induced here by -10 mV constant current stimulus beginning at t = 10 ms and continuing throughout the simulation. Increasing magnetic field from 25 μT to 250 μT delays spike onset and hastens the return to interspike baseline, thus delaying action potential initiation [Engel et al., 1999]. Because many experiments are carried out in the ambient geomagnetic field, Figure 2 shows action potential response to a 200 μT DC field applied parallel to the 50 μT ambient field, i.e. 250 μT total field strength. Integrating over a 250 ms interval, with a -10 mV constant-voltage stimulus applied from t = 10 ms and continuing throughout the simulation, and, in the absence of applied magnetic fields, i.e. 50 μT geomagnetic field exposure only, the model yields a train of action potential spikes with mean interspike interval (I-I) = 11.9 ms during stimulus, as shown in Figure 2. Addition of a 200 μT DC field increases the I-I to 14.0 ms, as shown in Figure 2, right hand plot. Computing across the range of magnetic field amplitudes from 0-250 μT results in a monotonically increasing mean I-I with increasing magnetic field strength (Figure 3). Carrying the computation out to 500 μT shows that the I-I remains nearly constant with increasing magnetic field after approximately 350 μT, approaching asymptotically a value of I-I = 14.4 ms (data not shown). The results above are in accord with observations that an ELF μT-range magnetic field increased the mean open time of a Ca^{2+}-dependent K^{+} channel [Marchionni et al., 2006].

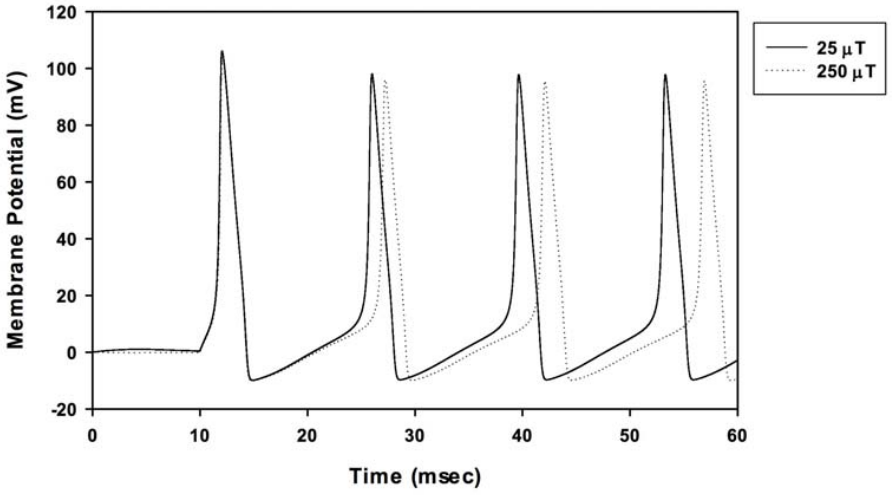

Figure 1: Effect of static magnetic field on spike timing, determined by numerical integration of H-H type model using Runge-Kutta method. Spiking behavior is induced by -10 mV constant current stimulus beginning at t = 10 ms and continuing throughout the simulation. Increasing magnetic field from 25 μT to 250 μT delays spike onset.

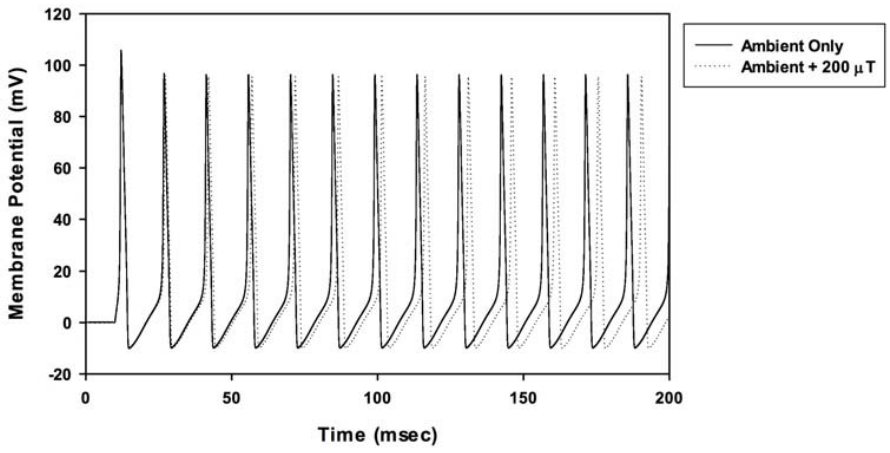

Figure 2: Action potential spike trains in 50 μT ambient geomagnetic field and with added 200 μT static magnetic field. Stimulus commences at t = 10 ms and continues throughout the simulation, producing a regular train of action potential spikes. In ambient field only, mean interspike interval (I-I) = 11.9 ms. Addition of 200 μT static magnetic field oriented parallel to 50 μT geomagnetic field produces train of action potential spikes with mean I-I = 14.4 ms.

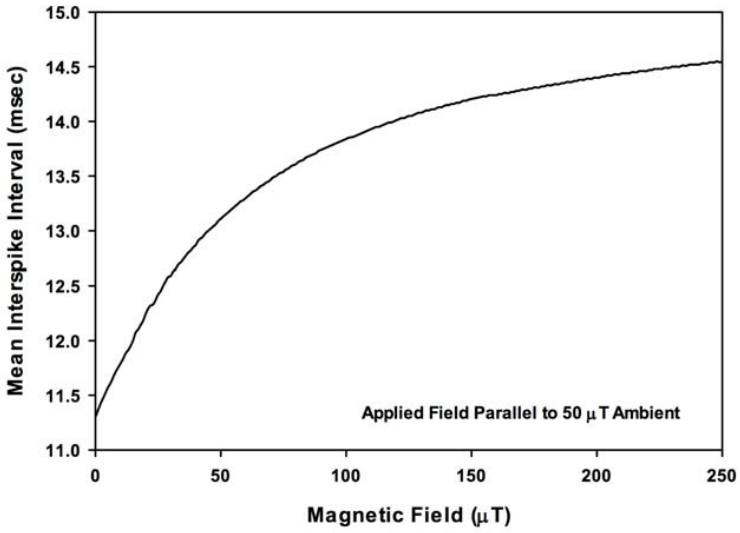

Figure 3: Interspike interval computed across a range of applied magnetic field amplitudes from 0-250 μT, in parallel to 50 μT ambient geomagnetic field. Results show that increasing magnetic field strength reduces the neuronal firing rate. For field strengths from 350-500 μT, I-I remains nearly constant, converging asymptotically to I-I ≈ 14.6 ms at 500 μT (data not shown).

AC AND AC/GEOMAGNETIC COMBINED EXPOSURES

Because the magnetic field acts through modulation of the K^+ conductance, time-varying (AC) magnetic fields will result in a time-dependent modulation of neuronal behavior with. For clarity, the examples shown below are in the absence of the DC geomagnetic component. The effect, via equation 5, of a 200 μT AC magnetic field varying sinusoidally at 50 Hz is shown in Figure 3. The top plot is the AC field amplitude, and the bottom shows the resulting neuronal firing. Here, action potentials were triggered using a constant-voltage -10 mV stimulus beginning at t = 0 ms and continuing throughout the simulation, resulting in a uniformly spaced spike train with mean I-I = 13.6 ms. In contrast, because the precise spike timing is a function of both the baseline I-I and the rate of change of z_K with time, more complex behaviors may be found using various AC frequencies. For example, Figure 4, top plot, shows that for a 5 Hz 200 μT AC sinusoidal magnetic field, the time-dependent K^+ conductance $\bar{g}_K z_K$ varies a twice the AC frequency, due to signal rectification by Equation 2. Thus, the pattern of spikes also repeats at twice the AC frequency, producing a train of action potentials with uneven spike timing. Increased I-I duration occurs while the magnetic field approaches the max/min of the AC cycle as shown in Figure 4, left, bottom plot. These results illustrate a real-time dependence of the spike timing of a Ca^{2+}-dependent K^+ channel. Superposition of parallel 5 Hz 200 μT AC filed with the 50 μT DC geomagnetic field yields the time-varying K^+ conductance $\bar{g}_K z_K$ (see Eqn 1) with periodic maxima every 100 ms shown in Figure 4, right, top plot. Here, the conductance and thus spike patterning repeats at the AC frequency. Figure 4, right, bottom plot, shows the change in spike patterning due to the introduction of the DC geomagnetic field. Note that fewer increases in I-I occur with introduction of geomagnetic field, due to decreased K+ conductance in times for which the AC and DC fields cancel significantly. For example, comparing Figure 4 left and right hand plots, adding the geomagnetic field results in significant cancellation for t = 50 – 150 ms, resulting in reduced conductance and thus and smaller values of I-I during this time period.

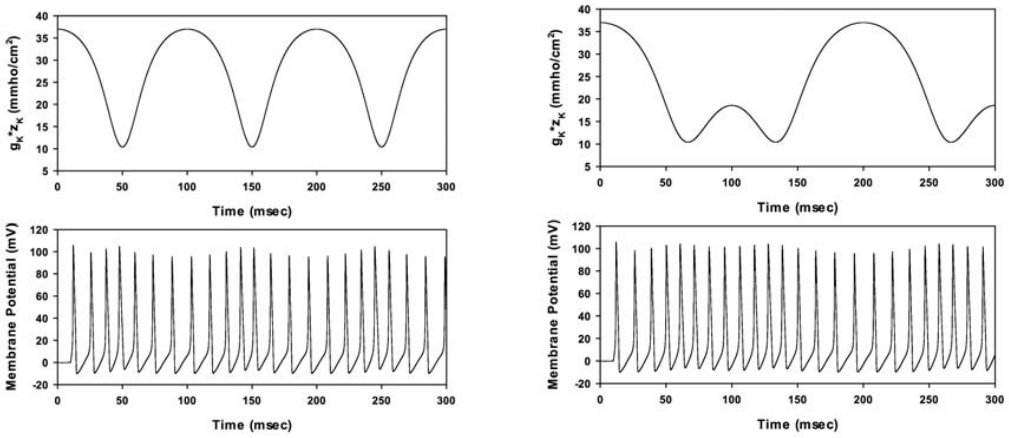

Figure 4: Left: Effect of AC magnetic fields on neuronal spike timing, in absence of geomagnetic field. **Left:** 5 Hz AC magnetic field yields time-varying K^+ conductance $\bar{g}_K z_K$ (top plot) repeating at frequency = 2 X AC frequency, due to signal rectification by Eqn 2. 5 Hz AC field yields a train of action potentials with uneven spike timing (bottom plot), also repeating at 2X AC frequency. Amplitudes employed here = 50-200 μT, using parameters employed above. However, results apply to arbitrary nonthermal amplitudes, due to choice of γ_o in Equation 5. **Right:** Addition of 50 μT ambient geomagnetic field to 5 Hz 200 μT AC magnetic field. Superposition of magnetic fields yields complex time-varying K^+ conductance $\bar{g}_K z_K$ with periodic maxima at AC frequency (top plot). Increase in interspike interval occurs during rising phase of change in conductance (bottom). Results suggest role of geomagnetic field in μT-range bioeffects.

DISCUSSION AND CONCLUSIONS

An H-H type membrane model, when applied to a small-conductance Ca^{2+}-dependent K^+-current channel, predicts an inverse relationship between Ca^{+2} availability and the frequency of action potential firing [Engel et al, 1999; Purvis et al., 2005; Wang et al., 2011]. Application of the Lorentz model for magnetic field bioeffects [Chiabrera et al., 1992; Edmonds, 1993; Zhadin, 1998; Muehsam et al., 1994, 1996, 2009a, 2009b, 2010; Pilla et al. 1997] yields an increase in Ca^{2+} availability, thus increasing the I-I in a neuron undergoing continuous action potential spiking. To my knowledge, this is the first model presented which offers a magnetic field mechanism for effects on spike timing with a distinct molecular target. It is important to note that in this model, the magnetic field does not act directly upon the K^+ current itself, the Ca^{2+} channel currents or the membrane potential itself. Rather, the action of the magnetic field is to modulate Ca^{+2}/CaM activity, thus affecting the conformational states of the K^+ channel protein [Xia et al., 1998; Keen et al;, 1999]. This causes a real-time change in K^+ conductance, resulting in changes in spike train timing. Here, the model is applied to μT-range fields, and the results are in accord with previous observations of μT-range effects on spike timing and action potential shape [Tonini et al., 2001; Marchionni et al., 2006; Wang et al., 2011]. The amplitude sensitivity of the model depends on the choice of the fitting parameter γ_o. Thus, the results shown here may be applied across a wide range of nonthermal magnetic field amplitudes, including observations of mT-range effects [Azanza et al., 1988; Azanza, 1990; Trabulsi et al., 1996; Wieraszko, 2000; Ahmed et al., 2008; Modolo et al., 2010; Ravera et al., 2010]. Further research is required to determine the value of the fitting parameter, and requires experiments wherein spike timing is measured over a range of magnetic field amplitudes. At present, in the absence of more information allowing the value of γ_o to be found empirically, the model only provides information comparing changes from baseline response due to different applied EMFs, rather than providing predictive results for a single magnetic field value. Despite this limitation, H-H models remain useful as they accept direct

input of physiological parameters such as membrane resistance, ionic conductance, time constants for channel behaviors, etc. [Xia et al., 1998; Muehsam et al., 1999; Apollonia et al., 2000; Cagni et al., 2007; Jiang et al., 2009], and thus retain an advantage over the more computationally convenient Izhikevich-type approximations [Izhikevich, 2004; Minelli et al., 2007; Modolo et al., 2010].

Cognitive and physiological neurological effects due to a wide range of subthreshold EMFs have been shown to occur [Cook et al., 2002; 2006] and it is now well-established that many neurons exhibit membrane-potential responses such as changes in spike clustering and timing to subthreshold stimuli [Engel et al., 2008], providing further rationale for understanding bioeffects due to subthreshold EMFs. The spiking neuron model presented here exhibits a real-time sensitivity to changes in magnetic field amplitude. This suggests that bioeffective AC magnetic field frequencies themselves depend upon temporal neuronal activity, rather than being determined only by membrane/channel biophysical properties. Exposure to combined AC and DC fields alters spiking behavior in a time-varying manner, suggesting that signals could be developed to elicit specific changes in spike timing/patterning. The model thus provides a mechanism for understanding and perhaps manipulating neuronal activity using subthreshold ELF signals, and may help to explain observations that specific combinations and temporal sequences of subthreshold EMFs can alter neurological activity [Tsang et al., 2004; Ross et al., 2008; Cook et al., 2009]. Also, for a system with μT-range sensitivity, the addition or removal of the ambient geomagnetic field significantly alters spike timing in a manner dependent upon the AC amplitude and frequency, perhaps supporting observations of neurological bioeffects due to variation with geography, shielding, or removal from the Earth's magnetic field [Schiff et al., 1991; Del Seppia et al., 2000; Choleris et al., 2002; Zhang et al, 2004; Prato et al., 2005; Vargas et al., 2006]. The Lorentz model suggests several metrics for reactivity, based upon ionic targets and effects on hydration layers of proteins and binding sites. All of these metrics are functions of the target Larmor

frequency in the applied magnetic field [Muehsam et al., 2009b, 2010]. Interestingly, for ambient-range magnetic fields, the Larmor frequencies for common ions and oscillating water molecules lie in the same ELF range as the EEG spectrum [Pilla et al., 1997], suggesting that these frequencies might couple directly with neural activity.

REFERENCES

Apollonio F, Liberti M. D'Inzeo G, Tarricone L. 2000. Integrated Models for the Analysis of Biological Effects of EM Fields Used for Mobile Communications. IEEE Transactions on Microwave Theory and Techniques. 48(11): 2082-2094.

Azanza MJ, del Moral A. 1988. Effects of Static Magnetic Field on Isolated Neurons. J. Phys. Colloques 49:C8-2059-C8-2060.

Azanza MJ. 1990. Characterization of neuronal membrane K^+ and Ca^{2+} channels operated under steady magnetic fields exposure. Journal of Magnetism and Magnetic Materials. 83(1–3)527–529.

Bianco B, Chiabrera A. 1992. From the Langevin-Lorentz to the Zeeman model of electromagnetic effects on ligand-receptor binding. J. Electroanalytical Chem. 343(1–2):355-365.

Bikson M, Inoue M, Akiyama H, Deans JK, Fox JE, Miyakawa H, Jefferys JG. 2004. Effects of uniform extracellular DC electric fields on excitability in rat hippocampal slices in vitro. J Physiol. 557(1)175-190.

Bikson M, Inoue M, Akiyama H, Deans JK, Fox JE, Miyakawa H, Jefferys JG. 2004. Effects of uniform extracellular DC electric fields on excitability in rat hippocampal slices in vitro. J Physiol. 557(1):175-90.

Blackman CF, Benane SG, Rabinowitz J, House DE, Joines W. 1985. A role of the magnetic field in the radiation induced efflux of calcium ions from brain tissue in vitro. Bioelectromagnetics 6:327–337.

Blackman CF, Blanchard JP, Benane SG, House DE. 1995. The ion parametric resonance model predicts magnetic field parameters that affect nerve cells. FASEB J. 9(7):547-51.

Cagni E, Remondini D, Mesirca P, Castellani GC, Verondini E, Bersani F. 2007. Effects of exogenous electromagnetic fields on a simplified ion channel model. J Biol Phys. 33(3):183-94.

Chiabrera A, Bianco B, Kaufman JJ, Pilla AA. 1992. Bioelectromagnetic resonance interactions: endogenous field and noise. In "Interaction Mechanisms of Low-level Electromagnetic Fields." Oxford University Press, pp 164-179.

Choleris E, Del Seppia C, Thomas AW, Luschi P, Ghione G, Moran GR, Prato FS. 2002. Shielding, but not zeroing of the ambient magnetic field reduces stress-induced analgesia in mice. Proc Biol Sci. 269(1487):193-201.

Consales C, Merla C, Marino C, Benassi B. 2012. Electromagnetic fields, oxidative stress, and neurodegeneration. Int J Cell Biol. 2012:683897.

Cook CM, Thomas AW, Prato FS. 2002. Human electrophysiological and cognitive effects of exposure to ELF magnetic and ELF modulated RF and microwave fields: a review of recent studies. Bioelectromagnetics. 23(2):144-57.

Cook CM, Thomas AW, Prato FS. 2004. Resting EEG is affected by exposure to a pulsed ELF magnetic field. Bioelectromagnetics. 25(3):196-203.

Cook CM, Saucier DM, Thomas AW, Prato FS. 2006. Exposure to ELF magnetic and ELF-modulated radiofrequency fields: the time course of physiological and

cognitive effects observed in recent studies (2001-2005). Bioelectromagnetics. 27(8):613-27.

Cook CM, Saucier DM, Thomas AW, Prato FS. 2009. Changes in human EEG alpha activity following exposure to two different pulsed magnetic field sequences. Bioelectromagnetics (1)9-20.

Cook CM, Saucier DM, Thomas AW, Prato FS. 2009. Changes in human EEG alpha activity following exposure to two different pulsed magnetic field sequences. Bioelectromagnetics. 30(1):9-20.

D'Inzeo G, Mazzanti M. 2006. Comparison between low-level 50 Hz and 900 MHz electromagnetic stimulation on single channel ionic currents and on firing frequency in dorsal root ganglion isolated neurons. Biochim Biophys Acta. 1758(5):597-605.

Deans JK, Powell AD, Jefferys JG. 2007. Sensitivity of coherent oscillations in rat hippocampus to AC electric fields. J Physiol. 583(2):555-65.

Del Seppia C, Luschi P, Ghione S, Crosio E, Choleris E, Papi F. 2000. Exposure to a hypogeomagnetic field or to oscillating magnetic fields similarly reduce stress-induced analgesia in C57 male mice. Life Sci. 66(14):1299-306.

Dobson J, St Pierre TG, Schultheiss-Grassi PP, Wieser HG, Kuster N. 2000. Analysis of EEG data from weak-field magnetic stimulation of mesial temporal lobe epilepsy patients. Brain Res. 868(2)386-91.

Edmonds DT. 1993. Larmor precession as a mechanism for the detection of static and alternating magnetic fields. Bioelectrochemistry and Bioenergetics 30:3-12.

Grassi C, D'Ascenzo M, Torsello A, Martinotti G, Wolf F, Cittadini A, Azzena GB. 2004. Effects of 50 Hz electromagnetic fields on voltage-gated Ca2+ channels and their role in modulation of neuroendocrine cell proliferation and death. Cell Calcium. 35(4):307-15.

Engel J, Schultens HA, Schild D. 1999. Small conductance potassium channels cause an activity-dependent spike frequency adaptation and make the transfer function of neurons logarithmic. Biophys J. 76(3):1310-9.

Engel TA, Schimansky-Geier L, Herz AV, Schreiber S, Erchova I. 2008. Subthreshold membrane-potential resonances shape spike-train patterns in the entorhinal cortex. J Neurophysiol. 100(3):1576-89.

Fishman HM, Poussart DJ, Moore LE, Siebenga E. 1977. K^+ conduction description from the low frequency impedance and admittance of squid axon. J Membr Biol. 32(3-4):255-90.

Fohlmeister JF, Coleman PA, Miller RF. 1990. Modeling the repetitive firing of retinal ganglion cells. Brain Res. 510(2):343-5.

Francis JT, Gluckman BJ, Schiff SJ. 2003. Sensitivity of neurons to weak electric fields. J Neurosci. 23(19)7255-61.

Kolomytkin OV, Dunn S, Hart FX, Frilot C 2nd, Kolomytkin D, Marino AA. 2007. Glycoproteins bound to ion channels mediate detection of electric fields: a proposed mechanism and supporting evidence. Bioelectromagnetics. (5):379-85.

Hodgkin AL, Huxley AF, Katz B. 1952a. Measurement of current-voltage relations in the membrane of the giant axon of Loligo. J Physiol. 116(4):424-48.

Hodgkin AL, Huxley AF. 1952b. A quantitative description of membrane current and its application to conduction and excitation in nerve. J Physiol. 117(4):500-44.

Izhikevich EM. 2004. Which model to use for cortical spiking neurons? Neural Networks, IEEE Transactions on. 15(5).1063-1070.

Keen JE, Khawaled R, Farrens DL, Neelands T, Rivard A, Bond CT, Janowsky A, Fakler B, Adelman JP, Maylie J. 1999. Domains responsible for constitutive and Ca(2+)-dependent interactions between calmodulin and small conductance Ca(2+)-activated potassium channels. J Neurosci. 19(20):8830-8.

Marchionni I, Paffi A, Pellegrino M, Liberti M, Apollonio F, Abeti R, Fontana F,

Minelli TA, Balduzzo M, Milone FF, Nofrate V. 2007. Modeling cell dynamics under mobile phone radiation. Nonlinear Dynamics Psychol Life Sci. 11(2):197-218.

Modolo J, Legros A, Prato FS, Thomas AW. 2010. Effect of a 1000 μT, 60 Hz magnetic field on spike timing in cortical neurons: a modeling study. Bioelectromagnetics Society 32nd Annual Meeting. Seoul, Korea, June 14-18, 2010.

Moore JW, Ramon F. 1974. On numerical integration of the Hodgkin and Huxley equations for a membrane action potential. J Theor Biol. 45(1):249-73.

Morgado-Valle C, Verdugo-Díaz L, García DE, Morales-Orozco C, Drucker-Colín R. 1998. The role of voltage-gated Ca2+ channels in neurite growth of cultured chromaffin cells induced by extremely low frequency (ELF) magnetic field stimulation. Cell Tissue Res. 291(2):217-30.

Muehsam DJ, Pilla AA. 1994. Weak magnetic field modulation of ion dynamics in a potential well: mechanistic and thermal noise considerations. Bioelectrochem Bioenergetics 35:71-79.

Muehsam DJ, Pilla AA. 1996. Lorentz approach to static magnetic field effects on bound-ion dynamics and binding kinetics: thermal noise considerations. Bioelectromagnetics. 17(2):89-99.

Muehsam DJ, Pilla AA. 1999. The sensitivity of cells and tissues to exogenous fields: effects of target system initial state. Bioelectrochem Bioenerg. 48(1):35-42.

Muehsam DJ, Pilla AA. 2009a. A Lorentz model for weak magnetic field bioeffects: part I--thermal noise is an essential component of AC/DC effects on bound ion trajectory. Bioelectromagnetics 30:462-75.

Muehsam DJ, Pilla AA. 2009b. A Lorentz model for weak magnetic field bioeffects: part II--secondary transduction mechanisms and measures of reactivity. Bioelectromagnetics 30:476-88.

Muehsam DJ, Pilla AA. 2010. A Lorentz force model for weak AC/DC magnetic field effects predicts observed resonances in desorption kinetics of a bound ion. Proceedings, Bioelectromagnetics Society 32nd Annual Meeting, Seoul, Korea, June 14-18.

Pilla A. 2006. Mechanisms and Therapeutic Applications of Time-Varying and Static Magnetic Fields. In Barnes F and Greenebaum B (eds), Biological and Medical Aspects of Electromagnetic Fields. Boca Raton FL: CRC Press. 351-411.

Pilla AA, Muehsam DJ, Markov MS. 1997. A dynamical systems/Larmor precession model for weak magnetic field bioeffects: Ion binding and orientation of bound water molecules. Bioelectrochem Bioenerget. 43(2): 239-249.

Prato FS, Robertson JA, Desjardins D, Hensel J, Thomas AW. 2005. Daily repeated magnetic field shielding induces analgesia in CD-1 mice. Bioelectromagnetics. 26(2):109-17.

Purvis LK, Butera RJ. 2005. Ionic current model of a hypoglossal motoneuron. J. Neurophysiol. 93(2):723-33.

Radman T, Su Y, An JH, Parra LC, Bikson M. 2007. Spike timing amplifies the effect of electric fields on neurons: implications for endogenous field effects. J Neurosci. 27(11):3030-6.

Ravera S, Bianco B, Cugnoli C, Panfoli I, Calzia D, Morelli A, Pepe IM. 2010. Sinusoidal ELF magnetic fields affect acetylcholinesterase activity in cerebellum synaptosomal membranes. Bioelectromagnetics. 31(4):270-6.

Reato D, Rahman A, Bikson M, Parra LC. 2010. Low-intensity electrical stimulation affects network dynamics by modulating population rate and spike timing. J Neurosci. 30(45):15067-79.

Robertson JA, Théberge J, Weller J, Drost DJ, Prato FS, Thomas AW. 2010. Low-frequency pulsed electromagnetic field exposure can alter neuroprocessing in humans. J R Soc Interface. 7(44):467-73.

Ross ML, Koren SA, Persinger MA. 2008. Physiologically patterned weak magnetic fields applied over left frontal lobe increase acceptance of false statements as true. Electromagn Biol Med. 27(4):365-71.

Schiff H. 1991. Modulation of spike frequencies by varying the ambient magnetic field and magnetite candidates in bees (Apis mellifera). Comp Biochem Physiol A Comp Physiol. 100(4):975-85.

Shen JF, Chao YL, Du L. 2007. Effects of static magnetic fields on the voltage-gated potassium channel currents in trigeminal root ganglion neurons. Neurosci Lett. 415(2):164-8.

Stewart RD, Bair W. 2009. Spiking neural network simulation: numerical integration with the Parker-Sochacki method. J Comput Neurosci. 27(1):115-33.

Tonini R, Baroni MD, Masala E, Micheletti M, Ferroni A, Mazzanti M. 2001. Calcium protects differentiating neuroblastoma cells during 50 Hz electromagnetic radiation. Biophys J. 81(5):2580-9.

Trabulsi R, Pawlowski B, Wieraszko A. 1996. The influence of steady magnetic fields on the mouse hippocampal evoked potentials in vitro. Brain Res. 728(1):135-9.

Tsang EW, Koren SA, Persinger MA. 2004. Power increases within the gamma range over the frontal and occipital regions during acute exposures to cerebrally counterclockwise rotating magnetic fields with specific derivatives of change. Int J Neurosci. 114(9):1183-93.

Vargas JP, Siegel JJ, Bingman VP. 2006. The effects of a changing ambient magnetic field on single-unit activity in the homing pigeon hippocampus. Brain Res Bull. 70(2):158-64.

Wang D, Qiao Q, Xie N. 2011. Role of calcium conductance in firing behavior of retinal ganglion cells. Neural Regeneration Research. 6(3):231-235.

Wang J, Che Y-Q, Zhou S-S, Deng B. 2009. Unidirectional synchronization of Hodgkin–Huxley neurons exposed to ELF electric field. Chaos, Solitons & Fractals. 39(3):1335–1345.

Wang J, Che Y, Zhou S, Deng B. 2009. Unidirectional synchronization of Hodgkin–Huxley neurons exposed to ELF electric field. Chaos, Solitons & Fractals. 39(3)1335–1345.

Wang Z, Che PL, Du J, Ha B, Yarema KJ. 2010. Static Magnetic Field Exposure Reproduces Cellular Effects of the Parkinson's Disease Drug Candidate ZM241385. PLoS One 5(11)e13883.

Wieraszko A. 2000. Dantrolene modulates the influence of steady magnetic fields on hippocampal evoked potentials in vitro. Bioelectromagnetics. 21(3)175-82.

Xia XM, Fakler B, Rivard A, Wayman G, Johnson-Pais T, Keen JE, Ishii T, Hirschberg B, Bond CT, Lutsenko S, Maylie J, Adelman JP. 1998. Mechanism of calcium gating in small-conductance calcium-activated potassium channels. Nature. 395(6701):503-7.

Zhadin MN. 1998. Combined action of static and alternating magnetic fields on ion motion in a macromolecule: Theoretical aspects. Bioelectromagnetics 19:279–292.

Zhang B, Lu H, Xi W, Zhou X, Xu S, Zhang K, Jiang J, Li Y, Guo A. 2004. Exposure to hypomagnetic field space for multiple generations causes amnesia in Drosophila melanogaster. Neurosci Lett 371:190–195.

APPENDIX: MATLAB CODE FOR MAGNETIC FIELD EFFECT ON H-H SPIKING NEURON MODEL

```
function HHspikes() % Adapted from HHSimplet.m Summer of Spikes
%Summer Semester, 2009, elec4001 and engg7301, School of Information
%Technology and Electrical Engineering, The University of Queensland,
%Brisbane QLD 4072, Australia.

% HH values
g_K = 37;
g_Na = 120;
g_leak = 0.3;
C_m = 1;
V_K = 12;       % not -12 (H-H original paper has error in it)
V_Na = -115;
V_leak = -10.6;

sim_time = 300;% total simulation time in milliseconds
t_step = 0.01;          % timestep in milliseconds
N = 1 + sim_time/t_step; % total number of timesteps
numb = N;

V = zeros(1,N); n = zeros(1,N); m = zeros(1,N); h = zeros(1,N);

V_rest = 0;
V(1) = V_rest;
n(1) = alpha_n(V_rest)/(alpha_n(V_rest)+beta_n(V_rest));
m(1) = alpha_m(V_rest)/(alpha_m(V_rest)+beta_m(V_rest));
h(1) = alpha_h(V_rest)/(alpha_h(V_rest)+beta_h(V_rest));

time = 0:t_step:sim_time;   % time
```

```
% input current
Iext = zeros(1,N);
Iext(round(10/t_step):round(990/t_step)) = -10;

% adding variable magnetic field quantities
Btot = ones(1,numb); Bfactor  = zeros(1,numb); g_KtimeVar = zeros(1,numb);
Bo = 50e-6*ones(1,numb); %50e-6; %ambient geomagnetic field
B = 100e-6*ones(1,numb); %50e-6*sin(2*pi*50*1e3*time); %applied magnetic
field
Bac = B.*cos(2*pi*5*1e-3*time); Btot = Bo + Bac; Bfactor = Btot; %./Bo; %For
low fields, this is the ratio of total Larmor frequency relative to that of ambient
geomagnetic field.
charge=3.2*10^(-19);mass=7*10^(-26);gamma=charge/(2*mass); wLo =
.5*gamma*Bo; fLo = wLo/(2*pi); wL = .5*gamma*B; fL = wL/(2*pi);%;
tlarm=(4*pi*mass)/(B*charge); %tmax = period of Larmor frequency of DC field

Caconc = 1e6*0.0025*Bfactor; % correct for uT 1e6
Caconc = 0.004*Caconc./max(Caconc);%-2.7e-3; % Engel
%z_K = (1./(1+(0.0025./Caconc).^2)); %Purvis
%z_K = 1.0; % For testing purposes
z_K = ((Caconc./0.0025).^2)./((1+(Caconc./0.0025).^2));% Engel

g_KtimeVar = g_K*z_K;
%g_KtimeVar = 37*((g_KtimeVar)./max(g_KtimeVar));
%g_KtimeVar = 37*((g_KtimeVar+17)./max(g_KtimeVar+17));
%g_Ktime = g_K
max(g_KtimeVar); g_KtimeVar = g_K*z_K+(37-max(g_KtimeVar));

subplot(2,1,1), plot(time,g_KtimeVar); %g_KtimeVar)
set(gca,'ylabel',text(0,0,'gK * zK'))
```

```
set(gca,'xlabel',text(0,-2,'Time (ms)'))

% numerical integration
tic;
for i = 2:N

   %I_K = g_K*n(i-1)^4*(V(i-1)-V_K); %original, time-constant V_K
   %I_K = g_Ktime*n(i-1)^4*(V(i-1)-V_K); %adding variable g_K
   I_K=g_KtimeVar(1,i)*n(i-1)^4*(V(i-1)-V_K);%time-dependent g_K
   %I_K = g_K*n(i-1)^4*(V(i-1)-V_Ktime(i)); % time-dependent V_K
   I_Na = g_Na*m(i-1)^3*h(i-1)*(V(i-1)-V_Na);
   I_leak = g_leak*(V(i-1)-V_leak);

   deriv = (Iext(i) - (I_K + I_Na + I_leak))/C_m;
   V(i) = V(i-1) + deriv*t_step;

   m_deriv = alpha_m(V(i))*(1-m(i-1)) - beta_m(V(i))*m(i-1);
   m(i) = m(i-1) + m_deriv*t_step;
   n_deriv = alpha_n(V(i))*(1-n(i-1)) - beta_n(V(i))*n(i-1);
   n(i) = n(i-1) + n_deriv*t_step;
   h_deriv = alpha_h(V(i))*(1-h(i-1)) - beta_h(V(i))*h(i-1);
   h(i) = h(i-1) + h_deriv*t_step;

%computing interspike interval
%timej = zeros(1,N);
%tempvar = 0;
%for j = 2:N
 %   if -V(j) > 96
  %      timej(1,j) = time(j)-tempvar; %-timej(1,j-1);
   %     tempvar = time(j);
    %    j = j + 100;
```

```
   %end
%end
%interval = max(timej)

end
toc;

subplot(2,1,2),
plot(time,-V)
dis = [time' g_KtimeVar' -V'];
save disdat250.dat dis /ascii

hold on

%plot(time,-Iext-22)
%plot(time,g_Ktime,':')
hold off

set(gca,'ylabel',text(0,0,'Membrane Potential (mV)'))
set(gca,'xlabel',text(0,-2,'Time (ms)'))
%set(gca,'xlim',[9 17])

end

%H-H voltage-dependent quantities here:
function result = alpha_n(V)
   result = 0.01*(V+10)/(exp((V+10)/10)-1);
end

function result = beta_n(V)
   result = 0.125*exp(V/80);
```

```
end

function result = alpha_m(V)
   result = 0.1*(V+25)/(exp((V+25)/10)-1);
end

function result = beta_m(V)
   result = 4*exp(V/18);
end

function result = alpha_h(V)
   result = 0.07*exp(V/20);
end

function result = beta_h(V)
   result = 1/(exp((V+30)/10)+1);
end
```

c. EFFECT OF MAGNETIC FIELDS ON T-R TRANSITION DYNAMICS OF HEMOGLOBIN DEOXYGENATION

INTRODUCTION

Our recent results demonstrating an increase in the rate of human hemoglobin (Hb) deoxygenation due to nonthermal EMF exposures [Muehsam et al., 2013], are in accord with earlier reports of EMF-induced enhanced *in vitro* [Mousavy et al., 2009] and *in vivo* [Milweski et al., 2006] deoxygenation. While the specific transduction site(s) for the magnetic field remain unclear, our results [Muehsam et al., 2013] show that EMF treatment reduces the time to deoxygenate. Although the possible mechanisms of EMF transduction by proteins remains unknown, some speculation has suggested that 'nonthermal' pulsed radiofrequency (PRF) field, for which negligible heating occurs over a low duty cycle, produce transient heating that can alter protein conformation [Laurence et al., 2000] and that protein structural rearrangements not related to temperature [Porcelli et al., 1997] can occur under nonthermal PRF exposure. Regarding magnetic field effects, the para- and dia-magnetic properties of Hb have been known for some time [Pauling et al., 1936; Pauling, 1977], but, as mentioned in a previous Chapter, no clear model currently exists describing magnetic field effects on Hb protein conformation or affinity for oxygen.

Transition from the high O_2 affinity relaxed (R), oxygenated state to the low O_2 affinity tense (T), deoxygenated state occurs as oxygen is delivered by Hb. Although this process is fundamentally dependent upon pH and O_2 saturation, subthermal molecular motions that govern Hb allosteric behaviors have been described using dynamical systems techniques [Yonetani et al., 2008; Eaton et al., 1991, 1999, Frauenfelder et al., 1991, 2003, 2009; Bellelli, 2010, Miele et al., 2012]. Also, the Hb molecule undergoes spontaneous T-->R quaternary transitions of the Hb tetramer [Hub et al., 2010], indicating that these states exist in equilibrium with each other. An example of the potential energy V(rc) as a

function of reaction coordinate rc with subthermal states through which system passes prior to deoxygenation is shown in Figure 1, left hand plot, taken from Frauenfelder et al., 1991. Here, several subthermal states border the final R-T transition, and one transition state corresponding to the R_2 liganded substate. Because experimental results consist of measurement of two states (the oxy-deoxy transition) a two-state model is considered here to describe subthermal oscillations for EMF effects.

MAGNETIC FIELD EFFECTS ON HEMOGLOBIN DEOXYGENATION

Here, the model describes the effects of an static magnetic field (MF) on an ongoing process of Hb deoxygenation (e.g. induced using dithiothreitol, changes in pH, oxygen saturation, etc.) via a modulation of the potential energy function for the R-T transition. Thus, a two-state model is considered to describe the passage between two subthermal protein conformations, one with high oxygen affinity and one with low oxygen affinity. Figure 1, right hand plot, shows V(rc) using a quartic potential to characterize the system as a double-well oscillator with a MF-sensitive subthermal potential energy barrier between two conformational states with different probabilities for the T and R states [Gammaitoni et al., 1989, 1998]:

$$V(r) = a_1 \frac{rc^4}{4} - a_2 \frac{rc^2}{2} + \gamma(EMF) \qquad (1)$$

where a_1 and a_2 are arbitrary constants, and $\gamma(EMF)$is a scalar function of the EMF exposure, yielding a bias in favor of the low-affinity state.

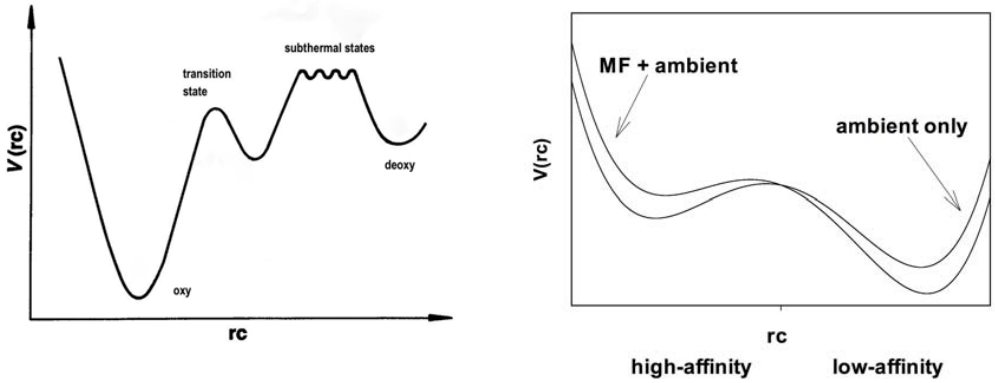

Figure 1. Left: Potential energy landscape for Hb oxy/deoxy transition, showing subthermal conformational states through which system passes en route to deoxygenated state (from Fraunfelder et al., 1991). **Right:** Passage between MF-sensitive subthermal conformations favoring Hb T and R states is described using a dynamical system represented by a bistable quartic oscillator (Eqn 1). Model based upon MF transduction modulation of dynamics of protein hydration governing R-T transitions via Lorentz model (see previous Chapter).

Letting the dynamical motion be driven by thermal noise forces F_n, and subject to viscous damping δ, the equation of motion is thus [Neiman et al., 1994]

$$\frac{d^2 rc}{dt^2} + \delta \frac{drc}{dt} + \frac{dV}{drc} = F_n \,, \tag{2}$$

which may be solved numerically [Gammaitoni et al., 1998].

Simulations were carried out using Matlab software (code shown in Appendix) using appropriate values for physical constants yielding stable solutions in a region free of bifurcations [Pilla et al., 1997]. Following on the results of previous chapters, (MF) here primary MF transduction is describe using the Lorentz model, resulting in a rotation at the Larmor frequency of waters of hydration that determine Hb allosteric behavior, and that the measure of reactivity is dependent upon the hydration orientation angle at the protein surface. Thus $\gamma(EMF)$= $\gamma_o sin(\omega_L t)$ where γ_o is an appropriate constant and ω_L is the Larmor frequency. Because there are several arbitrary constants determining numerical predictions for the model, all results are given as normalized values. Integrating Equation 2, the results yield a chaotic interwell hopping of the reaction coordinate, as shown in Figure 2 for a simulation over 50,000 time units. Figure 2, left, top plot, shows that the reaction coordinate undergoes chaotic interwell hopping between high- and low-affinity states, computed here for MF = 0. Figure 2, left, top plot, shows the phase-plane diagram of these rc dynamics.

Letting the Gibbs free energy for the R-T transition be proportional to the fractional change in the time spent in the low-affinity and high-affinity states,

$$\Delta G = -g_o \left(\frac{t_T - t_R}{t_R} \right) \tag{3}$$

where g_o is an appropriate constant, the rate constant k for the steady-state rate of deoxygenation takes the form:

$$k \equiv \exp\left(\frac{-\Delta G}{kT}\right) = \exp\left(\frac{-\exp^{-g_o\left(\frac{t_T - t_R}{t_R}\right)}}{kT}\right). \quad (4)$$

Deoxygenation as a function of Gibbs free energy from Equations 3 and 4 is shown in Figure 2, right hand plot. The rate constant k is weakly correlated with increasing magnetic field strength, due to a trend towards increasing ratio of t_T/t_R ($r^2 = 0.14$) within the regime for which system dynamics remain chaotic, i.e. no bifurcations occur. Thus, the MF-exposed state exhibits lower oxygen affinity than the ambient only state.

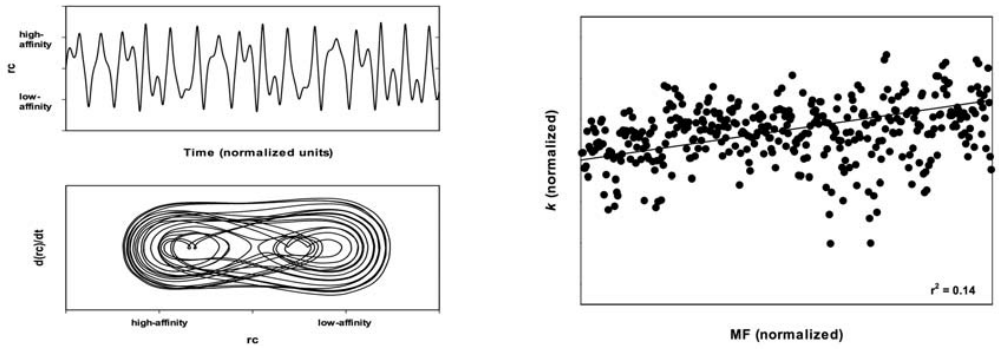

Figure 2. Left, top: Chaotic hopping of the reaction coordinate between high- and low-affinity states. Reaction coordinate rc as a function of time for at MF = 0. **Left, bottom:** Phase plane diagram of rc dynamics, shows that rc undergoes oscillatory motion between high- and low-affinity states. **Right:** Reaction constant via Eqn. 4 determined by Gibbs free energy EMF amplitude for MF exposure. Reaction rate is weakly correlated with increasing MF strength ($r^2 = 0.14$) revealing trend towards more rapid deoxygenation under MF exposure.

DISCUSSION AND CONCLUSIONS

The potential energy function used in Equation 1 has been widely studied in the context of stochastic resonance and bifurcation to/from chaos [Gammaitoni et al., 1989, 1998] and we have previously applied it to MF effects on ion binding processes [Pilla et al., 1997]. However, because it is currently possible to determine the precise values of arbitrary constants that determine the exact location of bifurcations, here the statistics of dynamics are analyzed in a regime with consistent chaotic dynamics. Statistics of the motion are interpreted as a modulation of the Gibbs free energy for deoxygenation, yielding a relationship between steady-state reaction rate and the behavior of the dynamical system. As the MF alters the potential energy function, dynamics are gradually biased towards a more rapid rate of deoxygenation. The model suggests that modulation of known subthermal dynamics of Hb could act to yield recent results found for EMF exposures [Muehsam et al., 2013; Mousavy et al., 2009; Milweski et al., 2006]. While the model presented here produces results generated by the assumptions underlying the MF dependence of the potential energy function, these assumptions do yield some information regarding the stochastic nature of the deoxygenation process. For example, the MF sensitivity shown in Figure 2, right hand plot is indicated by a weakly-correlated trend rather than a deterministic dependence of trajectory upon field strength. As a result, the dynamics may more closely reflect actual process occurring in the supra-quantum regime, where classical approximations to molecular motions may be applied [Binhi et al., 2003]. The chaotic nature of the results also suggests a sensitivity to small changes in initial conditions [Lorenz, 1963], such as those that could occur due to fluctuations in temperature, pH, oxygen saturation, gaseous environment, exposure to UV/visible light, the flapping of butterfly wings [Hilborn, 2004], etc, perhaps shedding light upon the difficulties in independent replication have confounded research into nonthermal EMF bioeffects [Pickard, 1995; Berg, 1999; Gustavsson et al., 1999; Vijayalaxmi et al., 2005].

REFERENCES

Bellelli A. 2010. Hemoglobin and cooperativity: Experiments and theories. Curr Protein Pept Sci. 11(1):2-36.

Berg H. 1999. Problems of weak electromagnetic field effects in cell biology. Bioelectrochem Bioenerg. 48(2):355-60.

Binhi VN, and Savin AV. 2003. Effects of weak magnetic fields on biological systems: physical aspects. Physics-Uspekhi 46:259-291.

Eaton WA, Henry ER, Hofrichter J, Mozzarelli A. 1999. Is cooperative oxygen binding by hemoglobin really understood? Nat Struct Biol. 6(4):351-8.

Eaton WA, Henry ER, Hofrichter J. 1991. Application of linear free energy relations to protein conformational changes: the quaternary structural change of hemoglobin. Proc Natl Acad Sci U S A. 88(10):4472-5.

Frauenfelder H, Chen G, Berendzen J, Fenimore PW, Jansson H, McMahon BH, Stroe IR, Swenson J, Young RD. 2009. A unified model of protein dynamics. Proc Natl Acad Sci USA. 106(13):5129-34.

Frauenfelder H, McMahon BH, Fenimore PW. 2003. Myoglobin: the hydrogen atom of biology and a paradigm of complexity. Proc Natl Acad Sci U S A. 100(15):8615-7.

Frauenfelder H, Sligar SG, Wolynes PG. 1991. The energy landscapes and motions of proteins. Science. 254(5038):1598-603.

Gammaitoni L, Hanggi P, Jung P, Marchesoni F. 1998. Stochastic Resonance. Reviews of Modern Physics, 70:223-287.

Gammaitoni L, Menichella-Saetta E, Santucci S, Marchesoni F, Presilla C. 1989. Periodically time-modulated bistable systems: Stochastic resonance. Phys Rev A. 40(4):2114-2119.

Gustavsson M, Lindgren M, Galt S, Hamnerius Y. 1999. Independently replicated biological effects of ELF electromagnetic fields: a literature study. In Bersani F (Ed.), Electricity and Magnetism in Biology and Medicine, Kluwer/Plenum, London. pp. 979-982.

Hilborn R. 2004. Sea gulls, butterflies and grass shoppers: a brief history of the butterfly effect in nonlinear dynamics. Amer. J. Phys. 72:425-427.

Hub JS, Kubitzki MB, de Groot BL. 2010. Spontaneous quaternary and tertiary T-R transitions of human hemoglobin in molecular dynamics simulation. PLoS Comput Biol. 6(5):e1000774.

Laurence JA, French PW, Lindner RA, Mckenzie DR. 2000. Biological effects of electromagnetic fields--mechanisms for the effects of pulsed microwave radiation on protein conformation. J Theor Biol. 206(2):291-8.

Lorenz E. 1963. Deterministic nonperiodic flow. Journal of the Atmospheric Sciences. 20:130–141.

Miele AE, Bellelli A, Brunori M. 2012. Hemoglobin Allostery: New Views on Old Players. J Mol Biol. pii: S0022-2836(12)00951-5.

Milweski S, Szczepański W. 2006. Effects of electromagnetic fields on the meat performance and wool performance of sheep Arch. Tierz., Dummerstorf 49(Special Issue):219-225.

Mousavy SJ, Riazi GH, Kamarei M, Aliakbarian H, Sattarahmady N, Sharifizadeh A, Safarian S, Ahmad F, Moosavi-Movahedi AA. 2009. Effects of mobile phone radiofrequency on the structure and function of the normal human hemoglobin. Int J Bio Macromolecules 44:278–285.

Neiman A, Schimansky-Geier L. 1994. Stochastic resonance in bistable systems driven by harmonic noise. Phys Rev Lett. 72(19):2988-2991.

Pauling L, Coryell CD. 1936. The Magnetic Properties and Structure of Hemoglobin, Oxyhemoglobin and Carbonmonoxyhemoglobin. Proc Natl Acad Sci U S A. 22(4):210-6.

Pauling L. 1977. Magnetic properties and structure of oxyhemoglobin. Proc Natl Acad Sci U S A. 74(7):2612-3.

Pickard WF. 1996. Where do we go from here? [bioelectromagnetic effects]. Engineering in Medicine and Biology Magazine, IEEE. 15(4):87-90.

Pilla AA, Muehsam DJ, Markov MS. 1997. A dynamical systems/Larmor precession model for weak magnetic field bioeffects: ion binding and orientation of bound water molecules, Bioelectrochemistry and Bioenergetics 43:239-249.

Porcelli M, Cacciapuoti G, Fusco S, Massa R, d'Ambrosio G, Bertoldo C, De Rosa M, Zappia V. 1997. Non-thermal effects of microwaves on proteins: thermophilic enzymes as model system. FEBS Lett. 402(2-3):102-6.

Vijayalaxmi, Obe G. 2005. Controversial cytogenetic observations in mammalian somatic cells exposed to extremely low frequency electromagnetic radiation: a review and future research recommendations. Bioelectromagnetics. 2005 26(5):412-30.

Yonetani T, Laberge M. 2008. Protein dynamics explain the allosteric behaviors of hemoglobin. Biochim Biophys Acta. 1784(9):1146-58.

APPENDIX: MATLAB CODE FOR MAGNETIC FIELD EFFECT ON T-R TRANSITION DYNAMICS OF HEMOGLOBIN DEOXYGENATION

```
load tnoise.dat
global B0 B1 tnoise tf humpf w gammma q;
clear ave time freq reso field crossings G;
gammma=1.1;%1.1 %scaling driving force
w=1;   %AC frequency
%humpsize=  2.0; 2.62
humpsize=.9; %starting oscillator bias
humpf=humpsize;%2.9;

t0=0;   tf=100;

x0=[0 0]; %Initial condition: stationary at oxy setpoint
B0=0;  B1=0;

%top=15;       %ll-loop:

numb=500;

        %j-loop: increasing magnetic field.
        field=zeros(1,numb);  %variation in DC field strength.
        speed=zeros(1,numb);  %holder for velocity data.
        freq=zeros(1,numb);  %variation in AC frequency.
        time=zeros(1,numb);  %time free/bound.
        %loudness=zeros(1,numb);  %variation in gammma (noise).
```

```
        %reso=zeros(numb,top);  %tf/tb for AC peak.
        bias=zeros(1,numb);  %variation in humpf.
%for ll=1:top;ll

for j=1:numb;
%j

options=odeset('AbsTol',1e-2);
[t,x]=ode23('duffing',[t0 tf],x0,options);

        % modulation via field amplitude:
      B0=B0+humpsize/numb;
  %     humpf=humpf-humpsize/numb
  %     humpf=humpf-1.125*humpsize/numb;
      humpf=humpf-1*humpsize/numb;
    %gammma=gammma+5/numb;
     %w=w+0.5*(2*pi)/numb;
humpf
thi=0;tlo=0;

        for k=1:length(t)-1
                if x(k,1)<0
                tlo=tlo+(t(k+1,1)-t(k,1));
                else
                thi=thi+(t(k+1,1)-t(k,1));
                end% (if statement)
        end %(k loop)

%time=thi/tlo
        loudness(j)=gammma;
        time(1,j)=(thi-tlo);%/tlo;
```

```
   G(1,j)=(thi-tlo)/tlo;
   bound(j)=tlo;unbound(j)=thi;
         freq(j)=w/(2*pi);
         field(j)=B0;
         bias(1,j)=humpf;
         speed(1,j)=mean(abs(x(:,2)));

subplot(3,1,1); plot(t,x(:,1))
subplot(3,1,2); plot(x(:,1),x(:,2))
%subplot(2,1,2); plot(t,x(:,1))

Yn=fft(x(:,1),2048); % Fourier spectrum subroutine
nn=length(Yn);
Pyy=abs(Yn);
fr=(0:length(Yn)-1)'*1000/length(Yn);
%semilogx(fr(1:length(Pyy)/2),Pyy(1:length(Pyy)/2))
Pyy=.5*Pyy(1:length(Pyy)/2);
fr=fr(1:length(Pyy)/2);

subplot(3,1,3);
plot(fr(1:length(Pyy)/2),Pyy(1:length(Pyy)/2))
axis([0 200 0 600]);
%plot(x)

%subplot(3,1,3); plot(t,cos(w*t))
pause(.1)
%duffzero
%crossings(j)=q;
end %(j loop)
clf
```

```
%subplot(2,1,1);
plot(field,time)
%subplot(2,1,2); plot(field,-exp(time))
%plot(field,time)
%reso(:,ll)=time';
%end %(ll loop)

duffing.m
function xdot=duffing(t,x)
global B0 B1 tf w gammma tnoise star humpf w;
beta=0;
        %gammma=1;
        %w=15;%1.26;
a1=1;
a2=1;
star=ceil((t/tf)*length(tnoise)+.01); %normalizing noise signal
        if star>length(tnoise)
        star=abs(ceil(.1*randn*(t/tf)*length(tnoise)+.01));
        end
%NOISE=0;
NOISE=gammma*tnoise(star);
        %harrumpf=-humpf*x(1)


xdot=[x(2);-beta*x(2)+a1*x(1)-a2*(x(1).^3)-humpf*cos(w*t)];%adding AC field
%xdot=[x(2);-beta*x(2)+a1*x(1)-a2*(x(1).^3)+NOISE-humpf];%Static
perturbation
%xdot=[x(2);-beta*x(2)+a1*x(1)-a2*(x(1).^3)+NOISE-humpf*cos(w*t)];%Noise
+ AC field

%xdot=[x(2);-beta*x(2)+a1*x(1)-a2*(x(1).^3)+NOISE-humpf*abs(B0)];
```

```
%xdot=[x(2);-beta*x(2)+a1*x(1)-a2*(x(1).^3)-humpf];%Static perturbation no
noise
%
%t/tf
```